Transient and Stationary Properties of the Olami-Feder-Christensen Earthquake Model in One and Two Dimensions

Vom Fachbereich Physik
der Technischen Universität Darmstadt

zur Erlangung des Grades
eines Doktors der Naturwissenschaften
(Dr. rer. nat.)

genehmigte

D i s s e r t a t i o n

von

Dipl.-Phys. Felix Wissel
aus Alzenau i. Ufr.

Referent: Prof. Dr. Barbara Drossel
Korreferent: Prof. Dr. Norbert Grewe

Tag der Einreichung: 30.5.2007
Tag der Prüfung: 4.7.2007

Darmstadt 2007
D17

Abstract

The earthquake model by Olami, Feder, and Christensen (OFC) [Ola92b] is one of the most striking examples of models that are discussed in the context of self-organized criticality. A key feature of self-organized critical systems is the size distribution of avalanche-like events according to a power law, $n(s) \sim s^{-\tau}$.

The OFC model gained its prominent position not at last due to the possibility to tune the degree of dissipation in the system by means of a continuous coupling parameter, α. On the other hand, exactly this lack of a local conservation law led to an ongoing discussion, whether the model displays self-organized critical properties for all values of the coupling, and if so, whether the critical exponent τ is affected by a change in α.

Of equal interest are the transient properties of the OFC model, especially how the transient time behaves as function of the system size L, and whether the dependency can be described by another, possibly universal, critical exponent.

Understanding the limits of small couplings α and large system sizes L is particularly important to answer these questions.

This thesis investigates the transient and stationary properties of the OFC model in one and two dimensions and answers these long-standing questions.

In both cases, $d = 1$ and $d = 2$, the system is driven towards the stationary state by the open boundary conditions and nonlinear terms in the coupling. These two ingredients result in a synchronization effect, which is observed in an adjustment of neighboring lattice sites: a central property of the two-dimensional system is the formation of long-lived patches. In one dimension, only one or two synchronized blocks emerge, which is a result of the reduced geometry.

The transient time, T, is shown to be linear in the system size in one dimension, while it increases in two dimensions as $T(L) \sim L^{\tilde{\mu}}$. The exponent $\tilde{\mu}$ is a rapidly increasing function as the coupling α decreases, and probably diverges for $\alpha \to 0$. The latter is also valid for the transient time as function of α in one dimension, but for not too small couplings up to the conservative case, $T(\alpha)$ shows an exponential decay with increasing α.

In the stationary state, the one-dimensional OFC systems splits into two boundary layers and a synchronized center. The size distribution of avalanches has peaks at avalanche sizes of the order of the system size and a low size regime. While these peaks are independent of the coupling and have a relative weight of the order of $\mathcal{O}(1/L)$, the exact shape of the distributions for small avalanches depends on α, and the weight of avalanches of size 1 eventually reaches unity for $L \to \infty$.

In two dimensions, the size distribution is also dominated by avalanches of size 1. In contrast to the one-dimensional case, $n(s)$ is broad and can be described by a log-normal distribution, $n(s) \sim s^{-\tau-\sigma \ln s}$. The weight of the tail decreases as $1/L$, and both the coefficients in the exponent depend on α.

All these results are obtained by computer simulations and an effective theory based on the patchy structure of the system.

Zusammenfassung

Das Erdbebenmodell von Olami, Feder und Christensen (OFC) [Ola92b] ist eines der bemerkenswertesten Beispiele für diejenigen Modelle, die im Rahmen der Selbstorganisierten Kritikalität diskutiert werden. Eine Schlüsseleigenschaft selbstorganisiert kritischer Systeme ist die Verteilung lawinenartiger Ereignisse gemäß eines Potenzgesetzes $n(s) \sim s^{-\tau}$.

Das OFC-Modell hat seine herausragende Rolle nicht zuletzt deshalb verdient, weil in dem System der Grad der Dissipation durch einen kontinuierlichen Kopplungsparameter α eingestellt werden kann. Andererseits hat gerade das Fehlen eines lokalen Erhaltungssatzes zu einer anhaltenden Diskussion darüber geführt, ob das Modell für alle Werte der Kopplung selbstorganisiert kritische Eigenschaften aufweist, und wenn, ob der kritische Exponent τ von einer Änderung in α betroffen ist oder nicht.

Gleichermaßen interessant sind die transienten Eigenschaften des OFC-Modells, insbesondere, wie sich die transiente Zeit als Funktion der Systemgröße L verhält und ob sich die Abhängigkeit durch einen anderen − möglicherweise universellen − Exponenten beschreiben lässt.

Besonders wichtig um diese Fragen zu beantworten, ist es, die Grenzfälle kleiner Kopplung und großer Systeme zu verstehen.

Diese Doktorarbeit untersucht die transienten und stationären Eigenschaften des OFC-Modells in einer und zwei Dimensionen und beantwortet diese schon lange offenen Fragen. In beiden Fällen $d = 1$ und $d = 2$ wird das System durch die offenen Randbedingungen und nichtlineare Terme in der Kopplung in den stationären Zustand getrieben. Diese beiden Zutaten führen zu einem Synchronisationseffekt, der in einem Sich-Angleichen benachbarter Gitterplätze beobachtet wird: Eine zentrale Eigenschaft des zweidimensionalen Systems ist die Bildung von langlebigen Flecken. In einer Dimension bilden sich nur ein oder zwei synchronisierte Bereiche heraus, was eine Folge der beschränkten Geometrie ist.

Es wird gezeigt, dass die transiente Zeit T in einer Dimension linear mit der Systemgröße anwächst, während sie in zwei Dimensionen wie $T(L) \sim L^{\tilde{\mu}}$ ansteigt. Der Exponent $\tilde{\mu}$ ist eine schnell anwachsende Funktion für fallende Kopplung α und divergiert möglicherweise für $\alpha \to 0$. Letzteres gilt auch für die transiente Zeit als Funktion von α in einer Dimension, aber für nicht zu kleine Kopplungen bis hin zum konservativen Fall zeigt $T(\alpha)$ einen exponentiellen Abfall für ansteigende α.

Im stationären Zustand spaltet sich das eindimensionale OFC-System in zwei Grenzschichten und ein synchronisiertes Zentrum auf. Die Größenverteilung der Lawinen zeigt Spitzen bei Lawinengrößen von der Ordnung der Systemgröße und einen Bereich kleiner Größen. Während diese Spitzen unabhängig von der Kopplung sind und eine relative Gewichtung von der Ordnung $\mathcal{O}(1/L)$ haben, hängt der genaue Verlauf der Verteilung für kleinere Lawinen von α ab und das Gewicht von Lawinen der Größe 1 erreicht schließlich 1 für $L \to \infty$.

In zwei Dimensionen ist die Größenverteilung ebenfalls von Lawinen der Größe 1 dominiert. Im Gegensatz zum eindimensionalen Fall ist $n(s)$ breiter und lässt sich durch eine Log-Normalverteilung $n(s) \sim s^{-\tau-\sigma \ln s}$ beschreiben. Das Gewicht des Ausläufers fällt wie $1/L$ ab und die beiden Koeffizienten im Exponenten hängen von α ab.

Alle Ergebnisse wurden mit Hilfe numerischer Simulationen und durch eine effektive Theorie, die auf der Fleckenstruktur des Systems basiert, gewonnen.

Contents

Abstract **iii**

Zusammenfassung **v**

1 Introduction **1**
1.1 Self-Organized criticality 5
1.1.1 Self-organized vs. critical 5
1.1.2 A closer look at SOC 6
1.2 Earthquake models and related models 10
1.2.1 Precursor models 11
1.2.2 The OFC model 14
1.2.3 Succeeding and related models 19
1.3 Known facts and open questions 21
1.3.1 The literature 22
1.3.2 The questions 28

2 The OFC-model in one dimension **31**
2.1 Small systems 32
2.1.1 A pair of sites 32
2.1.2 Three sites 34
2.1.3 Four sites 36
2.2 Analytical results 41
2.2.1 The matrix method 42
2.2.2 The toppling profile 50
2.3 Numerical results 55
2.3.1 The transient stage 56
2.3.2 The stationary state 64
2.3.3 The avalanche distribution 67
2.4 Summary $d = 1$ 71

3 The OFC-model in two dimensions **73**
3.1 The transient time 75
3.2 Correlation functions and correlation length 87
3.3 The stationary state 93
3.4 Summary $d = 2$ 100

4 Conclusion **103**
4.1 The transient stage in one and two dimensions . . . 103
4.2 The stationary state in one and two dimensions . . . 105
4.3 The relevance of the OFC model . . . 105

A The numerics **107**
A.1 The Grassberger algorithm . . . 108
A.2 The `Box` algorithm . . . 109
A.3 The implementation . . . 110
A.3.1 The `Base` . . . 111
A.3.2 The `Site` . . . 112
A.3.3 The `Box` . . . 112
A.3.4 The `BaseArea` . . . 114

List of figures **117**

List of tables **121**

Bibliography **123**

Acknowledgement **129**

Chapter 1

Introduction

But in science the credit goes to the man who convinces the world, not to the man to whom the idea first occurs.
Sir Francis Darwin

In 1944 Gutenberg and Richter presented an empirical expression that related the cumulative frequency N of earthquakes per year whose magnitude was greater than M:

$$\log N = a + b\,(8 - M) \quad , \tag{1.1}$$

with $a = -2.04 \pm 0.09$ and $b = 0.88 \pm 0.03$ [Gut44]. The magnitude M was measured in terms of the logarithm of the maximum amplitude of a so-called Wood-Anderson seismometer at a given epicentral distance, damping, and magnification [Gut42].

The result (1.1) was based on data taken between 1921 and 1943 in the California-Nevada region. Although only a total of 52 earthquakes of magnitude 5 and higher (in appropriate units and on a given scale, see below) were catalogued during that time, later surveys revealed that this relation holds also for other regions, (for example, for New Zealand with $a = -1.88 \pm 0.05$ and $b = 0.87 \pm 0.04$ [Gut54]).

Already in 1935, Richter had assumed a certain connection between the magnitude of a shock and the seismic moment or the amount of released energy [Ric35]. This connection later led to the now famous Richter-scale.

The special feature of energy magnitude relations for earthquakes are the different ways, in which energy can be set free by different mechanisms. Even for the main mechanism (surface waves or shear waves), different magnitude scales exist, since energy can be distributed by waves within different frequency ranges. The Mercalli-scale, for example, determines the intensity of earthquakes within a range between 1 and 12, where each number corresponds to a predefined amount of destruction. The Mercalli magnitude of an earthquake is estimated by comparing the actual destruction caused by the earthquake with this list [Hes]. In contrast to the Mercalli-scale, the Richter-scale has no upper limit and is frequency-independent due to the special measurement method [NZ].

In a series of papers, Gutenberg and Richter tried to pin down the exact relation between energy and magnitude [Gut41]. Because of the lack of sufficient data, it took some time and several corrections until they published [Gut56]

$$\log E = 11.3 + 1.8M \quad . \tag{1.2}$$

Combining equations (1.1) and (1.2) leads to

$$\log N = c + k \log E \quad , \tag{1.3}$$

or, equivalently,

$$N = CE^k \quad , \tag{1.4}$$

which in the physics related literature is sometimes called the Gutenberg-Richter type scaling. Actually, the real Gutenberg-Richter law as it is used within the seismological context is given in (1.1), and contains the important empirical Gutenberg b-value.

Nevertheless, (1.3) holds for almost all of the hot spots all over the world, up to some minor local deviations in the constants c and k, which depend on the details of the geological composition of the underlying fault structure, as well as on the specific triggering mechanism, the dynamics of the earthquakes, or the regional level of seismicity [Tur92].

Power laws as in equation (1.4) are often found in geophysics or, more generally, in geology. They imply some degree of scale independence. The lack of scale references is known to be connected with the concept of fractal structures. Particularly within the domain of geology, the self-similarity of rock and stone formations on widely different scales is a prominent problem, and this scale invariance is the reason for one of the student's first lessons in geology: an object that defines the scale has to be visible on every photograph taken [Sor00, Tur92]. While many of the concepts and tools associated with fractality and self-similarity have been introduced into the field of geology (leading to, for example, possibly infinite coastlines, depending on the used scale), the origin of the power laws for earthquakes is not a priori given and obvious. (For a review, consult the book by Turcotte [Tur92].)

Though already published in 1956, it took about a decade until the power law nature of the Gutenberg-Richter scaling became subject to theoretical considerations from a physicist's point of view. The first to construct a laboratory as well as a numerical model to explore fault dynamics were Burridge and Knopoff (BK model) [Bur67]. They were mainly interested in the role of friction in the earthquake mechanism. Nevertheless, the BK model already displayed some features that were also found in real earthquakes. Among others, this included the correct statistics of the main shocks (i.e. their size distribution agreed) and the correct after shock behavior. Their original model (and experimental setup) consisted of a linear chain of blocks of a given mass connected by springs on a rough surface. The first block is subjected to a pulling force. Once friction is overcome by the external force, the first block slips and eventually triggers a slippage of its neighbor and so on. The stored potential energy of the chain after each slipping event can be expressed in the coordinates of each block and can be calculated by assuming Hookean elasticity for the springs. Thus, the released energy between the shocks could be determined. For a theoretical treatment, one could solve the system of coupled Newtonian equations for given initial conditions. The experimental and numerical results for the BK model were obtained with a chain of 8 (10) blocks only.

The arrival of high performance computers allowed the simulation of larger and more complex models. Parallel to the rapid evolution of computing power, numerically complicated models became more and more interesting.

Furthermore, Bak, Tang, and Wiesenfeld introduced in 1987 the new concept of self-organized criticality (SOC) [Bak87]. They aimed at two different phenomena, both connected by the appearance of power laws. The first one is the $1/f$, or flicker-noise,

within systems of transported quantities as in ocean currents, traffic flow, electronic devices like transistors, or astronomical radiation effects. In those systems the noise has a frequency power spectrum $\sim 1/f^a$ with a around unity. The second one is the vast amount of empirical data with the same self-similar characteristics as mentioned above for geological surveys. These fractal structures are not only collected in geophysical records, but are also found in magnetic systems, in granular materials, and in spatially extended objects of all kinds, such as star clusters or Internet connections [Li]. For these examples, the power laws are found in the frequency size relations for the entities of concern.

Bak, Tang, and Wiesenfeld proposed the existence of a single, common mechanism for both classes of phenomena. Without any external parameter, systems with many (spatial) degrees of freedom are driven by intrinsic dynamics towards a state that resembles the behavior of statistical mechanics at the critical point. This tuning takes place by avalanche-like propagation of a generalized perturbation, which is specific for each class of systems, and takes the system from one unstable spatial configuration to another one.

In their paper, Bak, Tang and Wiesenfeld created the so-called sandpile model (BTW model) to exemplify self-organized criticality. This model is a discrete cellular automaton acting on integer variables on a square lattice with nearest-neighbor coupling. The integer values can be thought of as grains of sand, hence the name sandpile model. The system is disturbed by randomly adding grains on a random initial configuration. Once some threshold is reached, sites become unstable and avalanches are triggered. The size distribution of avalanches is found to obey

$$n(s) \sim s^{-\tau} \quad , \tag{1.5}$$

with $\tau \approx 2$ being a critical exponent. This paper [Bak87] immediately triggered an ongoing series of publications, all concerned with the nature and origin of SOC (see, for example, [Jen98, Li] and references therein).

Due to the affinity of earthquakes and avalanches, and the similarity of the Gutenberg-Richter scaling and the power law behavior, the Burridge-Knopoff model had a revival as one of the toy models for the further exploration of SOC. In the following years the original train model, where only the first block in a chain is subject to an increase of external tension, as well as several modified versions of the Burridge-Knopoff model (also in two dimensions and/or with uniform input of stress) were investigated [Car89a, Car89b, Nak90, Nak91, Che91, Cri92, dV92]. All of them were subsumed under the label *slip-stick model* or *block-spring model*.

Inspired by those models Olami, Feder, and Christensen introduced their presumably self-organized critical earthquake model in 1992 (OFC model) [Ola92b]. It is a continuous, deterministic, cellular automaton, and equivalent to a two-dimensional Burridge-Knopoff model. In contrast to the BK model, the OFC model is rather easy to simulate numerically. Apart from that, it contains a parameter that controls the amount of dissipation in the system. While for example the Feder-Feder model [Fed91] was also nonconservative, it was a new feature for earthquake models that the degree of dissipation could be changed in the OFC model.

The OFC earthquake model is one of the most prominent in the league of SOC models, not at last due to the variable dissipation. On the other hand, the new freedom concerning the level of conservation also became the basis for a lively ongoing discussion. The questions, whether the OFC model loses its criticality for certain parameter ranges, and whether size distributions for the OFC model obey an expression as (1.5) above, are amongst those to be answered in this thesis.

The following work is divided into four main parts.

Chapter 1 first reviews the basics of self-organized criticality (section 1.1), and locates the OFC model in a list of preceding or following (earthquake) models, attending to both the history and the physics (section 1.2). Naturally, special emphasis is placed on the OFC model. It is introduced with its defining setup and update rules and briefly compared with other models in section 1.2.2. A review of the relevant literature concerning the OFC model is collected in section 1.3, which is closed with a series of open questions.

The second chapter focusses on the OFC model in one dimension. It starts with a discussion of small systems (section 2.1), followed by the presentation of two analytical approaches (section 2.2). The first one allows for a full classification of possible dynamic attractors, the second one deals with the toppling behavior of sites, which turns out to provide useful tools for the more relevant case of two dimensions. Chapter 2 finishes with a numerical survey of the different stages in the time evolution of the model (section 2.3). The transient time and the transient dynamics are discussed, and the properties of the stationary state, including the size distribution of avalanches, are investigated and explained.

The subsequent chapter 3 is similarly organized, but deals with two-dimensional systems. Starting with phenomenological observations, the transient time is determined, and the main mechanisms and effects in the OFC model are named and understood in terms of the system's parameter and intrinsic dynamics (section 3.1). An important feature of the model in two dimensions is the formation of *patches*. They are discussed in detail in section 3.2. Finally, also for two dimensions, the stationary state and its properties are explored in section 3.3.

The last chapter 4 is allocated for a summary of the main results and remarks on the relevance of the OFC model and the findings presented in this thesis.

What might be interesting for computational applications, is the search algorithm, designed to determine the largest site in a square lattice. This algorithm is of minor importance for the scientific statements of the thesis, and presented in Appendix A.

1.1 Self-Organized criticality

This section reviews the basics of self-organized criticality (SOC). Several SOC models are briefly covered as examples, and their dynamic behavior is characterized. The fundamental ingredients for the systems to exhibit SOC are discussed, and models are classified according to their main features. General remarks about the underlying mechanisms of generating SOC, and its special problems, follow.

1.1.1 Self-organized vs. critical

Though the concept of self-organized criticality was already introduced in 1987 [Bak87], and more than 2000 publications were published in the following 10 years until 1997 [Ves98], there exists up to now no general definition of self-organized criticality. Nevertheless, several focal points have emerged throughout the years. The term itself is partly self-explaining.

Self-organization denotes the formation of a complex structure or pattern on a level, which is not accessible to single constituents of the structure. Different mechanisms from biology, social sciences, and information theory are known [Ebe98, Mis94]. Typically, a large number of agents, particles, or individuals are necessary. Though only locally coupled by some dynamic update rule or interaction, they form patterns, which emerge on a larger scale. That these patterns are an attractor of the dynamics, and independent of the initial configuration, is decisive for self-organization.

Criticality refers to a certain state of a system, as it is known from the context of second order phase transitions. It is best described by opposing it to noncritical systems [Jen98]: then the system's response to any (external) perturbation will differ for different regions and times when the system is perturbed. But every response is of the same order and comparable to a certain length scale and a typical relaxation time, both characteristics of the system.

The critical state, however, is characterized by a power law behavior of the order parameter, the capacities, or generalized susceptibilities as a function of some control parameter (for example the temperature) near the critical point. Spatial and temporal correlations are long ranged [Luc, Sor92]. The same perturbation, affecting a critical system at a different space or time might cause a completely different reaction, and is no longer well-described by the average response (in fact, assuming power law distributions, the average might even not exist, but is determined by the largest event observed and thus depends on time).

An important notion connected with critical systems is the concept of *universality classes*. Different models can be classified according to their critical exponents. These are a set of exponents, as they appear in the power laws. Depending on which entity is described, they are denoted with Greek letters (e.g. the order parameter o is a power of the control parameter p, and $o \sim p^{\beta}$ applies). The critical exponents are not independent, but are related to each other (and the dimensionality of the system) via the scaling relations. The universality classes assemble all systems, which have the same critical exponents. The knowledge about the universality class of a given model can thus simplify some of the calculations. The deeper reason for this kind of universality lies in the independence of the system's global behavior from the microscopic details (it might depend on the symmetries and the number of the degrees of freedom, though). This is also valid for SOC, since the nature of criticality in self-organized criticality is the same as in usual criticality.

The difference between SOC and ordinary criticality lies in the missing control

parameter. The SOC system is driven to the critical point by intrinsic dynamics without the need to fine-tune any external parameter [Bak96, Bot95]. Sometimes the mere existence of power laws is misleadingly denoted self-organized criticality. But many different mechanisms for generating power laws are known, mostly of a purely mathematical nature, and they lack any connection to self-organization [Sor00].

While only a few models exist, that definitely deserve the label SOC, examples of systems exhibiting power laws are far beyond the range and scale of all the ones named in the introduction. They reach from such small things as grains of rice [Fre96, MS99], over water droplets [Plo93] up to star like objects on an astronomical scale [Gai06]. In fact, power laws in physics and nature in general seem to be as universal as exponential functions, and the universe itself might have a fractal dimension, as far as the clustering of galaxies is concerned [Che89]. Examples more down-to-earth can be found in social sciences or in economics [Bak96, New04].

In the late eighties and in the beginning of the nineties, people hoped that SOC might be the universal mechanism to explain the ubiquitous power laws, as suggested by Bak and colleagues. Later research revised that point of view, and by now SOC is only one mechanism amongst others and not capable of accounting for every occurrence of power laws [Sor00].

1.1.2 A closer look at SOC

1.1.2.1 A first classification

The different models displaying SOC behavior can be divided into two main groups, and their important features are described below. Both share the generic description of some cellular automaton, defined on a generalized topology, such as a certain kind of lattice, a tree, or a network. Sites can take on different values, either from a discrete set like integers or states, or from a continuous interval.

In a very general fashion the SOC systems operate in a stationary state far from equilibrium. This out-of-equilibrium feature is governed by external driving and internal relaxation [Jen98]. The stationarity is found in the statistical properties obtained by averaging over long periods of time. In the original BTW model and in comparable sandpile models, the external input consists of grains of sand, one by one dropped on a randomly chosen site. The BTW model is a prototype of this class. Other models define a uniform global increase in some continuous variable, which can be thought of as stress or energy. We will come back to this difference, when we discuss the threshold behavior below.

Note that there is also a third type of model, which is referred to as *extremal* models [Pac96]. Examples are an evolutionary model by Bak and Sneppen (BS) [Sne93] or the invasion percolation model [Wil83]. In these models, thresholds are assigned to each site (a resistance against pressure for pores or a species' fitness in the BS model). In each time step, the site with the lowest threshold is updated. Its threshold value (and possibly that of its neighbors) is chosen anew from some distribution. Power laws are not found in event distributions (by definition there is only one update per time step), but in the local distance between successive updates. The extremal models are quite similar to the coherent-noise models [New96]. The latter offer a robust mechanism for generating power laws, but are not SOC: they lack the coupling between the participating elements, and the interaction is replaced by an external stress, affecting many elements at once [Sor00]. If the meaning of the threshold value as the fitness of species is reinterpreted as a barrier distribution against rupture over a fault line, the

BS model can also be thought of as a model for earthquakes [Kei95].

1.1.2.2 The role of conservation

As a basic feature, it is necessary for the systems to be open in some way. Otherwise, the stationarity by constant input cannot be maintained. In strictly conservative systems, a SOC state is only possible, if a spatial inhomogeneity is introduced [Gri90]. This "openness" can be realized in two ways: either by open boundary conditions (grains of sand are lost at the border) or dissipation is introduced in burst events. For those , the term *avalanche* is commonly used throughout the different models, despite the fact that the bursts model an earthquake or a forest fire. For some models a combination of both features seems to be necessary to obtain a SOC state. A prominent example for the ongoing discussion is the OFC model. The interplay between local dissipation and the influence of the boundaries is addressed in section 1.3 and, of course, in the main chapters of the thesis. Note that an avalanche in the sandpile models is only a redistribution of grains. Thus, sand must leave the system in order to prevent an ever-ongoing avalanche.

Nevertheless, at least a local conservation law was argued to be important to obtain a SOC state [Gri90], and the BTW model is no longer critical, once the local particle conservation is violated [Man90]. In [Hwa89], it was mentioned that the simple redistribution of sand actually resembles a dissipative system all the same, as far as the gravitational energy is concerned. Up to now, the general role of conservation is not yet clearly understood. Some models are known to behave self-organized critical with the presence of dissipation [Jen90, Fii93] or only in the conservative case [Cha97, Man90]. Sometimes both is claimed for the same model [Lis96, Bro97]. Others, as in the class of forest fire models [Che90, Bak90a, Dro92], have an inherent dissipation mechanism (fire), without which they actually make no sense. This illustrates the relevance of the OFC model, since it was the first one, where dissipation could be switched on and tuned continuously (more about this in chapter 1.2.2).

1.1.2.3 The effect of geometry

Although system-wide correlations are one of the hallmarks of SOC, this does not necessarily require a spatial structure. From the above examples, one might have gained the impression that a certain geometry as a lattice must be involved [1]. There are models, which completely neglect the spatial coordination of participating sites. One of them is the class of random-neighbor models for sandpiles, where neighbors are randomly assigned to each site. Either a new topology is chosen after each avalanche with a fixed number of neighbors per site (this is called the annealed random-neighbor model), or a fixed network of interacting sites is spanned once. The latter model is referred to as the quenched random-neighbor model. In order to obtain a critical state, it is necessary to have a varying number of neighbors for at least some sites in the system. In both types of models, depending on certain constraints, power laws in the avalanche distributions were found (see for instance [Chr92a, Bro97, Kin99]). Models of this kind can be considered as mean-field versions of the more fundamental models.

Another point where the extension of the systems becomes decisive is the limited geometry. Simulations or experiments can only be performed for finite sizes of the

[1] Of course, correlations are also found in purely temporal samples as time series of, say, heartbeats. They also do not involve a spatial extension. Here, the emphasis is on correlations between components that are affected by avalanches, which is a genuine spatial effect

samples. Power laws can therefore only be observed over a specific range, up to an upper cutoff. The reduced system size is handled by suitable scaling functions $G(x)$. They are constant unity for small arguments and fall off to zero for large x. Distributions, for example, are then of the form $n_L(s) = s^{-\tau}G(s/L^D)$, where D is a critical exponent, like τ, and event sizes are measured relative to an accessible system size L. Using such scaling functions allows a comparison of observed quantities for different system sizes, and a so-called finite-size scaling probably allows for statements on thermodynamic limits. For the detection of small events there might also be a lower cutoff, either due to the experimental situation or a smallest unit is defined numerically (i.e. the precision).

1.1.2.4 SOC, branching processes, and percolation

SOC is closely connected with the idea of critical branching processes, which in turn is related to the percolation theory [Als88, Sor00, Kim06]. An avalanche in the sandpile model can be thought of as a path, possibly containing loops. The starting site relaxes and causes now unstable neighbors to relax as well. This reaction happens with a certain probability, depending on the current state of the neighbors (this description seems to be specific for the BTW model, but it is rather generic. Exactly the same notion holds for the forest fire and other models). The path is recognized as the spanning tree between relaxed sites.

A branching process also begins with a single starting point. In each time step, a single node can spawn new nodes with a defined branching probability. Such a series is called critical, if each site on average generates one child. For a collection of such families of nodes, family sizes are distributed according to a power law. In higher dimensions, the avalanche loops become less and less important, and above an upper critical dimension they can be neglected. In this case, the branching process yields a mean-field theory for the avalanche process, which allows the determination of upper critical exponents [Als88].

1.1.2.5 The separation of timescales

Further defining features of SOC are the threshold dynamics and the separation of timescales, which are intertwined. One timescale is set by the slow external feeding. Measured on that scale, avalanches happen instantaneously. This is easily implemented for numerical models, the external drive is simply halted during the simulation of an avalanche. For laboratory systems some experimental effort has to be done to achieve such a clear separation [Hel90] or it is not possible at all [Plo93].

On the other hand, main shocks of real earthquakes have a temporal duration of several seconds up to several minutes - which is still negligible compared to the time it takes for the stress to establish (this time can be of the order of centuries). Furthermore, the average annual shift between tectonic plates is in the range of centimeters, while during an earthquake, slips of several meters are recorded [Sor00], leading to velocities of $\sim cm/yr$ compared to $\sim m/s$. Thus, as far as numerical simulations and the dynamics of the earth's crust is concerned, the onset of an avalanche is abrupt and hence nonlinear on the slow timescale.

As already addressed above, the relaxation threshold can be reached in two ways: First, the external drive is of random nature and divided in many small portions, yielding a stochastic system. Second, the input is global, and uniform, and the same

for all components. This type of driving results in deterministic models, where the only randomness in the system arises from the initial configuration.

Actually, as different as these two groups seemingly are, there exists a connection between them.

First, stochastically driven sandpiles can be related to continuous models with uniform increase in the limit of vanishing input. This limit is either achieved by a large value of the integer threshold, together with unit drive, or by infinitesimal growth and a continuous state variable. As long as the ratio between external drive and the threshold is very small, each single component receives the same mean amount of input in-between successive instances of avalanches. The statistical properties of such a locally driven system with small growth units are the same as for the deterministic earthquake model [Chr92a] (see also section 1.2.1.3).

Secondly, the completely stochastic forest fire model [Dro92] can be mapped into a deterministic one, again, sharing the same statistical behavior. This mapping is done in two steps [SR00]: The random ignition of trees (corresponding to a flash in the original model) is to be replaced with an deterministic triggering of avalanches. This so-called auto-ignition model (still with stochastic growth) is then recast into a completely deterministic one by eliminating the random creation of new trees.

Thus, as far as the threshold dynamics is concerned, the only important point seems to be a sudden, nonlinear response of the system to however the external drive is added. This nonlinear response, in turn, corresponds to a separation of the two different timescales.

1.1.2.6 The implicit tuning

This is a crucial point. Soon after the concept of SOC was introduced [Bak87], it was argued that the necessity of two timescales actually corresponds to the tuning of their ratio to some small value [Man90]. A second parameter was later identified to be also implicitly tuned to a critical value of unity in [Soc93], at least for two models of slip-stick processes and forest fires, which lose their criticality, if this parameter has a value different than unity. Recently, the criticality in the BK model (and also for the OFC model) was suspected to depend on implicit assumptions about friction [Cla05]. These assumptions correspond to some tuning as well. Taken together, it might be tempting to discard the notion of self-organization within the context of SOC.

However, except for the separation of timescales, this implicit tuning was only found in some models with only a limited range of applicability. Additionally, it might be questioned, whether the earth's crust or other natural examples can be regarded to be tuned. Thus, the perception about self-organization is still well reasoned in its own right.

Nevertheless, the underlying mechanism for how this self-organization comes about needs some more explanation. A possible scenario was proposed in [Sor95]. The authors recommended a non-linear feedback process of the order parameter on the control parameter, such that the critical value of the control parameter becomes attractive. This idea was applied in [Zap95]. The avalanche dynamics of the BTW sandpile was mapped on a so-called self-organized branching process. For a self-organized branching process the branching probability of each node (the control parameter) is a dynamic quantity, and depends on the current flux of grains leaving the system (the order parameter). If the net flux totals zero, the probability stays fixed at the critical value. For increasing flux, the branching probability decreases and vice versa. This feedback mechanism ensures that the system is always near the critical point. A possible de-

viation from the critical point is overcome by the attraction imposed by the feedback mechanism.

The idea of a feedback process was picked up in [Kin99], where a more general framework was formulated. The observed self-organization in SOC systems is traced back to the existence of an appropriate parameter that controlled the avalanche process. In contrast to standard percolation, but similar to the feedback mechanism above, this parameter is not fixed *a priori*. Instead, it is subject to a time evolution. The flow of this parameter in the parameter space is coupled to the current state of the system (just as the branching probability is coupled to the number of grains in the system above). As the system evolves into a stationary state, this parameter also evolves towards its asymptotic value. For systems that end up in the same steady state for any initial configuration, this asymptotic value will be unique. If it equals unity, the system is said to be critical.

If the value of unity is approached only for a special choice of parameters, this point in parameter space is recognized as a dynamic stability against external perturbations, as it is known for example in relaxation processes in equilibrium. However, if there exists a finite parameter regime, for which the system is critical, not only a mere point, one finds a structural stability. The latter was termed *generic* SOC.

Systems can also reach a state near criticality for a large range of parameters, which was coined *almost critical*. Being *almost critical* is defined in terms of the above control parameter, which approaches unity, but does not exactly equal 1. Important for this scheme to work out properly is a suitable choice of this control parameter. Its asymptotic value must be reached during the time evolution, and its initial value should reflect the (random) initial configurations of the system. In other words, an appropriately defined quantity, which depends on the considered model, can be regarded as a measure for the degree of criticality of this model. For the OFC model, the quantities to determine the type of criticality are layer branching rates. They are presented in detail in section 1.3.1.

I believe that models, where an implicit tuning is responsible for the observed criticality, behave according to such a feedback mechanism and belong to the class of almost critical systems. In the case of the sandpile model, the exact tuning to the critical point by the conservation of sand grains seems the rather natural choice, since sand does not disappear, as it was stated in [Kin99].

1.2 Earthquake models and related models

This section presents the definitions of some, and the features of a few, of the earthquake models which were studied in the physical literature so far, and which contributed to the development of the OFC model. The overview is given in chronological order (1.2.1). Those models, which followed the OFC model, are also discussed (1.2.3). In between these two sections, the OFC model is sketched (1.2.2). Thus, the evolution of the OFC model will be understood, and further developments are related to the history of models.

Some of the models explained below have already been covered in part by the introduction. They are listed for completeness.

1.2.1 Precursor models

1.2.1.1 The Bak-Tang-Wiesenfeld sandpile

The BTW model [Bak87] may be considered the mother of all SOC models.

Defined on a square lattice of linear size L, each stable site can take on integer values between zero and three. The system is initially empty, and in each time step a randomly chosen site is increased by one. This setup, of course, models a pile of sand, fed from an external source, a single grain at a time. If, at any moment in time, a site's value is larger than three, this site becomes unstable and is diminished by four grains. These four units are distributed to the nearest neighbors, one grain per site. Boundary sites have less neighbors, resulting in a loss of sand at the border and keeping the overall dynamics stationary. Governed with these rules, the BTW sandpile constitutes an Abelian and discrete cellular automaton.

In one dimension, the stable values for each site are 0 and 1, and two particles at a site trigger an avalanche. The final state is rather trivial, each site contains exactly one grain and each avalanche runs through the entire system [Bak90b].

The BTW model was was both subject and origin of an almost uncountable number of research projects and became the foundation of a whole new branch of physics. A lot more could be said about the BTW model, but that is best found elsewhere, for example in [Tan88, Kad89, Dha89, Man90].

1.2.1.2 The Burridge-Knopoff model

As explained in the introduction, this model was the first to discuss some generic features of earthquakes. It was incorporated into the context of SOC soon after the BTW model. Just like the BTW model for sandpiles, the BK model serves as a prototype for almost all earthquake models that were presented in the last 15 years and it is the canonical example for the so-called *slip-stick* models. Originally, it was defined in one dimension [Bur67], and Burridge and Knopoff considered an analytical model as well as a laboratory system. Later on, the model was extended to two dimensions, and other modifications were studied [Car89a, Car89b, Nak90, Nak91, Che91, Cri92, dV92].

In the experimental setup, L blocks of mass m are ordered linearly, each connected to its nearest neighbors via springs with elastic constants k_i. The schematic setup is shown in figure 1.1. For $x_{i,m}$ being the position of the i-th block after the m-th avalanche, and l_i being the length of the relaxed spring, the potential energy of the system right after the m-th avalanche is given by

$$E_{p,m} = \frac{1}{2}k_1 \left(x_0 - x_{1,m} - l_1\right)^2 + \sum_{i=2}^{N} \frac{1}{2}k_i \left(x_{n-1,m} - x_{n,m} - l_i\right)^2 \quad . \tag{1.6}$$

x_0 is the position of the first block, which is the only block subject to an external pulling force F_p, and hence x_0 is not a constant in-between the avalanches. An avalanche comprises a number of slipping events of adjacent blocks, which occur within a short time interval. The shift in x_0 is proportional to the time, and avalanches are defined from the second block on.

F_1 is the force, which is exerted from the block positioned at x_0 on the second block via the spring k_1. As soon as this force is bigger than the static friction, the second block begins to slip, possibly triggering its neighbor to slip, and so on. After each avalanche, the change in the potential energy can be calculated using equation (1.6).

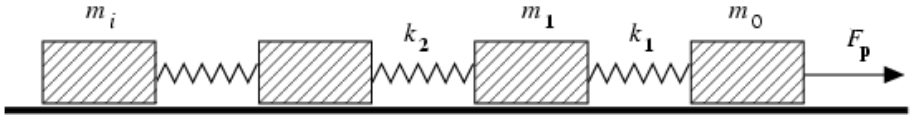

Figure 1.1: Schematic setup of the Burridge-Knopoff *train* model. In the original publication, all the blocks have the same mass m and springs with elastic constants k. Later work studied individual masses and springs.

Thus, the amount of energy released in a collective slippage process is determined. For many avalanches, the energy release is distributed according to a power law.

On the other hand, one can solve the equation of motion for each block:

$$m\ddot{x}_i = k_{i+1}(x_{i+1} - x_i) + k_i(x_{i-1} - x_i) - F_f(\dot{x}_i) \quad , \tag{1.7}$$

where $F_f(\dot{x}_i)$ is a friction force, which depends only on the block's velocity. This system is a set of N coupled equations. In the above described setup, the BK model is called the *train* model, since the pulling force is only imposed on the first block (see also figure 1.1).

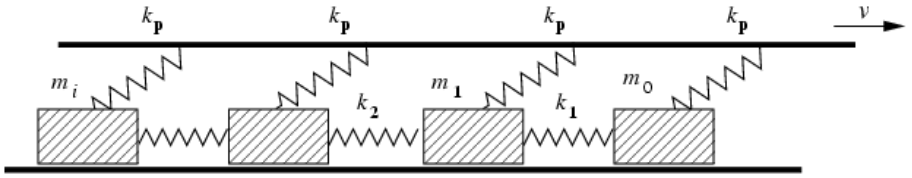

Figure 1.2: Schematic setup of the Burridge-Knopoff *chain* model. All blocks are drawn along by the movement of the upper plate.

For a more realistic modelling one allows all the blocks being driven. This feature is implemented by an extra term $F_e(x_i)$ in equation (1.7). This external force $F_e(x_i) = k_p(x_i - vt)$ corresponds to a third spring attached to each block and fixed at a plate, which moves with a constant velocity, v, parallel to the chain of blocks. This setup is called the *chain* model (figure 1.2). The equation of motion now reads

$$m\ddot{x}_i = k_{i+1}(x_{i+1} - x_i) + k_i(x_{i-1} - x_i) - F_f(\dot{x}_i) - F_e(x_i) \quad . \tag{1.8}$$

The force F_f, which turns up in equations (1.7) and (1.8) and which describes the friction between the blocks and the surface, is modelled differently for different versions of the BK model. In [Bur67] it was assumed to contain two parts. The first part combines viscous and frictional effects, while the second one - proportional to $\dot{x}_i$ - collects radiation effects. Carlson and Langer, for example, chose a form [Car89a]

$$F_f(\dot{x}_i) = \mathrm{sgn}(\dot{x}_i)F_0/(1 + |\dot{x}_i|) \quad . \tag{1.9}$$

Sets of equations as (1.7) or (1.8) are treated by a transformation onto dimensionless variables and performing numerical simulations, or they are studied analytically: numerically, the size distributions are comparable to the Gutenberg-Richter scaling [Bur67, Car89b]. Crisanti et al. surveyed the BK model from a dynamic system's point of view. They found deterministic chaos and that the generalized Lyapunov exponents diverged [Cri92]. The same holds already for a two block system as examined in [dV99].

Nakanishi [Nak90, Nak91] mapped the BK model onto a cellular automaton, which resembles features of the later Feder-Feder model (section 1.2.1.4) and inspired the OFC model. He considered the *total* force acting on block i as in the above Newtonian equations (1.7,1.8) and defined a threshold force F_{th}. The springs between the blocks are assumed to be homogeneous with a spring constant k_c, while the plate spring has a constant k_p. All the forces increase uniformly, until the first one reaches the threshold. It is then decreased by an amount δF, a part of which is equally distributed amongst its neighbors:

$$\begin{aligned} F_i \rightarrow F_i &= F_i - \delta F \\ F_{i\pm1} &\rightarrow F_{i\pm1} + \frac{1}{2}\Delta_N \delta F \end{aligned} \tag{1.10}$$

The ratio Δ_N is given by $2k_c/(k_p+2k_c)$. Neighboring forces, which temporarily exceed F_{th}, are handled similarly, resulting in avalanches. Nakanishi also found that size distributions are consistent with the Gutenberg-Richter scaling, but slightly different than in the BK model.

Note that for non vanishing k_p the Nakanishi version of the BK model actually is nonconservative. This dissipation effect was not recognized, either by the author (who termed the ratio of k_c/k_p the *stiffness* of the system) or anyone else, until this kind of mapping was picked up again by Olami, Feder, and Christensen.

1.2.1.3 The Zhang model

The Zhang model [Zha89] was actually meant as a modified sandpile model, and turned out to be a first earthquake model. In fact, for an infinitesimal external driving, it is equivalent to the conservative OFC model.

The BTW integer sites are replaced with continuous state variables $z_{i(jk\ldots)}$ (the *energy*, instead of the interpretation as grains of sand), on a d-dimensional hyper cube. Initial values are taken from the interval $(0, z_c)$, and the boundaries are open. A randomly chosen site is incremented with a small energy input δz, and becomes unstable when its value is greater than or equal to the threshold, $z_u \geq z_c$: each of the $2d$ nearest neighbors receives an extra energy input Δ_Z, which is determined by the current value of the unstable site divided be the number of neighbors ($\Delta_Z = z_u/2d$). The unstable site z_u is reset to zero, and the avalanche continues for any neighboring site,which is above the threshold. The Zhang model is trivial in one dimension, just as the BTW model [Bla00]. In higher dimensions, the size distribution, $n(s)$, of avalanches obeys $n(s) \sim s^{-\tau}$. This result was not taken from numerical simulations, but derived by analytical considerations.

A remarkable feature of the Zhang model is found in the distribution of energy values, averaged over all the sites in the system. This distribution shows $2d$ many peaks with finite width at multiples of a pseudo quantum, which is slightly larger than $1/2d$ (the first peak is at $E = 0$ and is rather sharp). These peaks can be thought of as smeared particles, and mirror the fact that energy can only be transferred in multiples of the pseudo quantum. A similar behavior is recovered in the OFC model (see below).

1.2.1.4 The Feder-Feder model

Although originally formulated in the language of the integer sandpile models, the sites in the Feder-Feder model [Fed91] can take on continuous values. Again, sites are located on a square lattice, and the threshold for the energy variables is 4. The system

is globally driven, and open boundary conditions are used. Each site being at or above the threshold is set to zero during an avalanche, and the nearest neighbors are increased by a fixed amount of one unit of energy. Later on, these rules were reformulated and generalized (to match the other continuous models like the Zhang model), such that the threshold is unity and each neighbor receives an extra input of $\Delta_F = 1/2d$ for a hypercube in d dimensions [Cor95].

The FF model was the first, for which the transported quantity (sand or energy) is not conserved. If two or more unstable neighbors each contribute an energy amount of Δ_F, sites can temporarily be far above the threshold, They are decreased to zero, while their neighbors only receive a total energy amount of $2d\Delta_F = 1$, which corresponds to a net loss of energy. Nevertheless, the distribution of avalanches obeys a power law, although the exponents differ from those of conservative models.

1.2.2 The OFC model

The Olami-Feder-Christensen earthquake model was first proposed in 1992 [Ola92b], discussed in a series of papers [Chr92b, Chr92c, Chr92d, Ola92a], and intensively studied in [Chr92a]. The following sections define the dynamic update rules of the OFC model in detail, and compares them to the models described above. A summary over the insights obtained is presented in a later section (1.3.1), after those models, which are extensions or modifications of the original OFC model are specified (1.2.3).

1.2.2.1 The OFC rules

The OFC earthquake model is defined on a square lattice of linear size L with open boundary conditions. To each of the L^2 sites, a continuous variable $z_{ij} \in [0, 1]$ is assigned and initialized with a random value taken from a flat distribution. In one dimension this changes to a single linear chain of size L with sites z_i. The interpretation of the z_{ij} is that of stress between sites, or an amount of potential energy stored at that site (actually it is the amount of force a site sustains, see below).

Such a system, once initialized, is then subject to a uniform growth process. Each site is increased by the same value, which is determined by the largest site in the system, until that particular site reaches the critical threshold $z_c = 1$. The exact value of the threshold need not be unity, but the overall behavior of the model is independent of the choice of z_c, and the value 1 has proven useful for the numerical simulations.

Sites, for which z_{ij} is equal to or larger than the threshold, are unstable. They relax according to the update rule

$$\begin{aligned} z_{nn} &\rightarrow z_{nn} + \alpha z_{ij} \\ z_{ij} &\rightarrow z_{ij} = 0 \quad . \end{aligned} \tag{1.11}$$

For such a relaxation process, the term *toppling* has been coined and is used in the following. The indices nn denote the nearest neighbors of the unstable site, and α is the coupling between the sites. It is also a measure for the dissipation in the system and can be chosen from the interval $[0, 0.25]$ where the upper bound, $\alpha = 0.25$, corresponds to the conservative case (the interval of allowed values increases to $[0, 0.5]$ in one dimension with a conservative coupling $\alpha = 0.5$, respectively). Beside the system size L, the coupling α is the only parameter in the OFC model.

The toppling of one site can cause its neighbors to become unstable as well. A series of topplings defines an avalanche. Single avalanches are separated from another

by the growth process, which is assumed to be infinitesimally slow on the timescale of the topplings (or, the other way round, the avalanches occur instantaneously on the timescale of driving). The importance of these two timescales has been discussed in section 1.1.2.

Except for the randomness in the initial configuration, the OFC model is deterministic. Nevertheless, the system is highly non linear. Thus, the state of the system cannot be predicted over large timescales, but has to be determined from the current state by calculating each intermediate configuration.

1.2.2.2 The relation to the BK model

The above formulation is similar to that from the Zhang model (1.2.1.3) or the FF model (1.2.1.4), but hides the relation to the BK model (1.2.1.2), from which the OFC model actually originated. In fact, the globally driven BK model (the chain model in $d = 2$) can be mapped directly onto the OFC model, which is presented in the following.

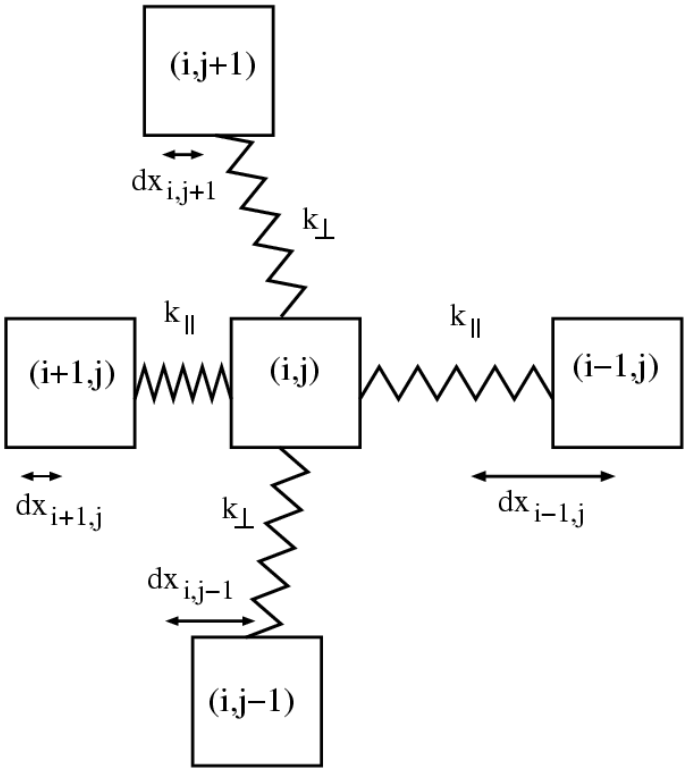

Figure 1.3: Detailed view of the block located at (i, j) and the surrounding blocks with their displacements, $d_{i\pm1,j\pm1}$, against the equilibrium position.

In the two-dimensional BK model, the total spring force, which acts on a block with coordinates (i, j) being at rest, can be expressed as (compare to equation (1.8))

$$\begin{aligned} F_{i,j} = &- k_{\parallel} \left(\mathrm{d}x_{i+1,j} - 2\mathrm{d}x_{i,j} + \mathrm{d}x_{i-1,j}\right) \\ &- k_{\perp} \left(\mathrm{d}x_{i,j+1} - 2\mathrm{d}x_{i,j} + \mathrm{d}x_{i,j-1}\right) + k_p \mathrm{d}x_{i,j} \quad . \end{aligned} \tag{1.12}$$

Note that the site is at rest and hence the friction force F_f just cancels that tension. $\mathrm{d}x_{i,j}$ is the replacement of block (i,j) relative to its equilibrium position in the lattice defined by the movement of the external plate.

This plate is connected to each block with springs of elastic constant k_p. The springs between the blocks are assumed to be homogeneous, but one allows for different spring constants $k_\parallel$ and $k_\perp$ in the two directions parallel and perpendicular to the movement of the plate. Similar to the cellular automaton proposed by Nakanishi (in equation 1.10), a single slipping event is governed by a change in the forces:

$$\begin{aligned} F_{i\pm1,j} &\to F_{i\pm1,j} + \delta F_{i\pm1,j} \\ F_{i,j\pm1} &\to F_{i,j\pm1} + \delta F_{i,j\pm1} \\ F_{i,j} &\to F_{i,j} = 0 \quad , \end{aligned} \tag{1.13}$$

and the changes δF in the neighbors' forces are calculated as:

$$\begin{aligned} \delta F_{i\pm1,j} &= \frac{k_\parallel}{2k_\parallel + 2k_\perp + k_p} F_{i,j} = \alpha_\parallel F_{i,j} \\ \delta F_{i,j\pm1} &= \frac{k_\perp}{2k_\parallel + 2k_\perp + k_p} F_{i,j} = \alpha_\perp F_{i,j} \quad . \end{aligned} \tag{1.14}$$

For $k_\perp = k_\parallel = k$, these expression reduce to

$$\delta F_{nn} = (4 + k_p/k)^{-1} F_{i,j} = \alpha F_{i,j} \quad , \tag{1.15}$$

and we recover the toppling rule (1.11). Now the values z_{ij} of the OFC model can directly be interpreted as the modulus of the net force exerted on site (i,j) (the vector character of the forces and the directions are neglected in the above derivation). Furthermore, the stress imposed from the moving plate via k_p is related to the degree of dissipation in the OFC model. For $k_p = 0$, one obtains the conservative case. From now on, we concentrate on the homogeneous case $\alpha_\perp = \alpha_\parallel = \alpha$.

The energy packages that could be transferred between neighboring sites have a lower limit α and are bounded from above by a maximal possible package,

$$p_{\max} = \frac{\alpha}{1-\alpha} \quad . \tag{1.16}$$

The value of $p_{\max}$ can be derived by assuming all the sites in the system being at the threshold. Then the first toppling site adds a package of α to its neighbors, lifts these neighbors to $1+\alpha$, which results in a package of size $\alpha(1+\alpha)$ for the neighbor's topplings, and so on. Equation (1.16) is obtained by summing up the generated geometric series in α.

1.2.2.3 The models in comparison

All the above listed models are similar to some extent, but it should have become clear there are major differences. The models are related to each other and compared with the data found for real earthquakes in table 1.1. After all, a model should mirror some natural features, though these models were not meant to establish a theory of quakes in the first place, but are more or less toy models for the exploration of SOC. This statement is not true for the BK model, which actually *was* built to examine the fault-friction interplay. Therefore and for a better comparability, the BK model is

model	driving	toppling	exponent τ (from $n(s) \sim s^{-\tau}$)
BTW $2d$	local (one grain at a time)	$z_u - 1$ $z_{nn} + 0.25$	1.98
BK $1d$ (Nakanishi)	global	$z_u - \delta z$ $z_{nn} + 0.5\Delta_N \delta z$	~ 2
Zhang $2d$	local (fixed δz per time step)	$z_u = 0$ $z_{nn} + 0.25 z_u$	2 (analytically)
FF $2d$	global	$z_u = 0$ $z_{nn} + 0.25$	~ 1.5
OFC $2d$	global	$z_u = 0$ $z_{nn} + \alpha z_u$	1.91 for $\alpha = 0.2$

Table 1.1: Comparison between different (earthquake-) models. Data taken from [Bak87, Nak91, Zha89, Fed91, Ola92b].

represented by the cellular automaton of Nakanishi in one dimension. Also, the integer valued BTW model, for which stable sites are $\in [0, 3]$ with the threshold at $z_c = 4$, is mapped onto the interval $[0, 0.75]$ accompanied by setting $z_c = 1$. This redefinition eases the comparison.

In every case, z_u denotes the current unstable site, whether its value is continuous or discrete, and the z_{nn} are the nearest neighbors. δz in the Zhang model and in the model of Nakanishi are parameters, as well as Δ_N, which is determined by the elastic constants. A single grain in the mapped version of the BTW model corresponds to a value of 0.25. The characteristic exponent, τ, as it is found in the size distributions, is to be compared with the exponent of the real earthquake distribution, $\tau_{GR} \sim 2$. Note that the Gutenberg-Richter b-value is around unity and not near 2. Actually, both values are equivalent to each other due to the following reason:

One can determine the *probability* of an earthquake larger than any given reference, or one works with the *density* of quakes. The first is the cumulative sum or integral of the second, and hence the exponents differ by one. Of course, the same holds for the power laws obtained by numerical simulations, and one has to be careful when comparing publications, and to watch, which quantity is used. The size distribution of avalanches, $n(s)$, in this work measures the frequency of events, and thus describe densities in the above sense.

The exponent in the Nakanishi model was reported to be around 2, but was slightly different for different parameters of the system.

As presented in the next section (1.3.1), there is no universal exponent for the OFC model, but it depends on the degree of dissipation. The exponent given in table 1.1 is the one, which is claimed to match the real situation the best, and is obtained for $\alpha = 0.2$ [Ola92b].

While unstable sites in the BTW model and in the Nakanishi model are diminished by a constant value, possibly resulting in a rest energy at that site, the energy of a

toppled site is strictly zero in the other three models. The only difference between the Zhang model and the conservative OFC model is in the driving (stochastic versus uniform). The FF model differs from the OFC model such that the redistributed energy is not proportional to the value of the toppled site.

The fact that the dissipation can be tuned to different values is the great advantage of the OFC model. The FF model is nonconservative as well, but in a more rigid and limited way. The sandpile models lose their criticality, for any dissipation introduced, as remarked in section 1.1.2. With the OFC model one had a simple toy model at hand to test the statements on the role of dissipation, and to examine the interplay between conservation and spatial inhomogeneities for SOC systems as discussed above.

1.2.2.4 The measures

Before modified models of the OFC type are presented, the questions on how to determine the size of an avalanche and how to measure the time is discussed. As far as the first question is concerned, there are in principle 4 possibilities to quantify an avalanche. They turn out to be equivalent to each other, because they fulfill scaling relations as explained below.

If the size of an avalanche is counted by the number of participating sites, the question arises, whether secondary topplings of the same site should be counted twice or not. Regarding only the total number of distinct sites corresponds to determining the *area* (a) of an avalanche. Counting each individual toppling, including several discharges of the same site, gives the *size* (s) of the avalanche, which is the measure used in this work. Actually, there exists a threshold value α_c for the coupling in each dimension, below which secondary topplings are not possible. Thus, at least for these cases, the size s and the area a are interchangeable. The results presented in chapters 2 and 3 are obtained for $\alpha < \alpha_c$, except when explicitly stated otherwise.

One can also measure the maximal distance between the site, which triggered the avalanche, and all other sites, which relaxed during that avalanche. This measure is called the *radius* (r) of the avalanche (sometimes denoted as the *radius of gyration*).

The fourth possibility is the *life-time* (l) of an avalanche, which counts the distinct number of necessary time steps during the simulation. A time step is defined by the synchronized update of all unstable sites at a given moment. For example, the toppling of the first site constitutes a time step. Whether all neighboring sites or only a single neighbor is lifted above the threshold, the relaxing of all these sites belongs to the second time step. By repeating this consideration, the lattice decomposes into two sub lattices equivalent to the black and white fields of a checkerboard. Only sites within the same sub lattice can be updated in the same time step.

The different measures are related to each other by scaling laws, similar to the critical exponents. For any measures x, y, z of the set $\{a, s, r, l\}$, the relation $\langle x \rangle \sim y^{\gamma_{xy}}$ is valid, and the exponents fulfill $\gamma_{xz} = \gamma_{xy}\gamma_{yz}$ [Sor00].

As for the size of an avalanche, there are several possible ways to measure the time. One can sum up the amount of energy put into the system from the outside. In each time step [2], this is a well defined entity, the difference between the largest site in the system and the critical threshold value. This measure yields a continuous time. A discrete measure is given by counting time as the number of distinct topplings (the size of an avalanche).

[2] after each avalanche, not in the above sense of subsequent updates. Remember, avalanches are instantaneous on the slow timescale.

However, time is only an interesting quantity for the transient stage. The steady state of the system should by definition be stationary and as such independent of time. In the context of numerical simulations in the literature, time is sometimes denoted as the total number of avalanches, when given as a quality measure for the obtained statistics.

For the examination and determination of the transient times in one and two dimensions (sections 2.3.1 and 3.1), time is measured in terms of topplings per site, which is the total number of topplings in the system after random initialization, divided by the number of sites, L^2.

1.2.3 Succeeding and related models

The models described in this section are very similar to the OFC model and could just as well be included in the forthcoming section 1.3, where the results for the OFC model in the literature are summarized. However, the modifications are stronger than, for instance, simply adding noise. The connection to other fields of research also justifies an own section beyond the fact that the below addressed models constitute a different type of model.

1.2.3.1 The Integrate-and-fire model

This model was first thoroughly discussed in the context of neurobiology [Tuk88]. The rules given below for this model can also be applied to describe flashing fireflies [Mir90] or, for small lattices, the dynamics of cardiac pacemakers [Pes75]. The model is sometimes also referred to as IOF model (integrate-and-fire oscillators).

Each site of the lattice represents a neuron, which fires a signal to neighboring neurons, if its axon potential is above some threshold value. The signal in turn excites other neurons, possibly leading to a synchronized pulse in the system. If a signal does not trigger a neuron to fire, a corresponding value is added to the current potential (hence the name integrate and fire, IAF). For no excited neurons in the system, each neuron is fed from external sources. Of course, this description just resembles the dynamics of the OFC model. However, there is a small, but important difference.

Formulated in the language of the SOC community, this model was introduced in [Cor95] and further discussed in [Cor97]. While a toppled site is reset to zero as in the OFC model, the growth process in the IAF model is governed by the following differential equation instead of a uniform external driving

$$\frac{\mathrm{d}z_{ij}}{\mathrm{d}t} = S - \gamma z_{ij} \quad , \tag{1.17}$$

with a positive γ, describing a saturation term. For $\gamma = 0$, this corresponds to the usual global input. For finite γ and with a threshold at $z_c = 1$, the period of each site would be given by

$$T_{\mathrm{IAF}} = \frac{1}{\gamma} \ln\left(\frac{S}{S-\gamma}\right) \quad , \tag{1.18}$$

if there was no coupling between the sites. The coupling is either modelled to be of the Feder-Feder type, i.e. a site receives a constant extra input from relaxing neighbors, or the input is proportional to the toppling site as in the OFC model.

For the FF coupling, no SOC is found for any value of α and any (global) value of γ. Depending on the exact value of γ, avalanches are either of all sizes, but not power

law distributed, or the system fully synchronizes, with only avalanches of size L^2. If one allows for different γ at each site, uniformly distributed around a mean, power laws can be obtained for suitable combinations of the parameter.

More interesting is the OFC coupling. In [Cor95] a phase diagram is presented in the $\alpha - \gamma$ plane, which distinguishes 3 clearly separated phases. For small α and intermediate to large γ, the whole lattice synchronizes. A single diamond shaped front propagates through the system, starting at the same site at each step and reaching all neurons in the system. This phase is realized for α being smaller than some threshold, a polynomial-like expression in S/γ, which is proven analytically. For α above this threshold, a periodic behavior is found, where avalanches of only a few different sizes alternate. This state is very sensitive to the initial conditions. For even larger α, close to the conservative case, power law distributed avalanche sizes with an exponential cutoff are observed. This finding still holds for large γ, but for γ being above a threshold value, a peak of the order of $\mathcal{O}(L^2)$, but smaller than the system size L^2, superposes the exponential cutoff. If power laws are observed, the critical exponents are continuous functions of the parameter α and γ.

1.2.3.2 The Random-Neighbor OFC model

The Random-Neighbor OFC model (RN-OFC) was proposed in [Lis96] and can be thought of as a mean-field version of the OFC model, because the spatial structure of the lattice is completely ignored, except for the effect of the open boundaries. These are important for exhibiting SOC, as it was addressed in the section about SOC (1.1.2) and will be discussed in detail for the OFC model below (1.3.1). The RN-OFC update rules for driving and toppling are the same as in the original OFC model, but the 4 sites to receive the energy packages are chosen anew randomly for each toppled site (annealed randomness). For toppling sites at the border (corner), energy is redistributed only amongst 3 (2) sites somewhere in the lattice.

Lise and Jensen [Lis96] found characteristics of criticality even for nonconservative α above a critical $\alpha_c = 2/9$, though the data did not scale with the system size. These findings were shown in [Cha97] to rely on wrong assumptions about the energy distribution per site. There, the authors presented a self-consistent theory to determine the correct distribution. SOC behavior is then only observed for conservative α.

In [Bro97] the energy distribution was deduced analytically, and no criticality was found for any $\alpha < 0.25$. This result was confirmed by Pinho et al. [Pin98], who also examined lattices in three dimensions (i.e. bulk sites have 6 random neighbors, surface, edge and corner sites less, accordingly).

For hard wired couplings between random sites (quenched randomness), power laws are observed as long as there are at least two sites in the system with a lesser coordination number than the rest of the lattice [Lis02b]. This SOC behavior is reported to break down below $\alpha_c \sim 0.1$.

1.2.3.3 The Socolar-Grinstein-Jayakaprash model

The now described model has no specific name in the literature so far. I refer to it as the SGJ model, because it was proposed by Socolar, Grinstein, and Jayakaprash [Soc93]. They used the same setup as for the OFC model, but changed the update rule for sites neighboring the unstable site. The energy input for those sites does not only depend on the current value of the toppling site z_u, but also on the current state of the receiving site itself, thus resembling a kind of auto-feedback mechanism. To be

precise, the toppling is defined by

$$z_{nn} \rightarrow \gamma z_{nn} + \alpha z_u \quad , \tag{1.19}$$

and is interpreted to model any deviation from the linear elasticity in the springs between the blocks in the original BK model. The resetting of the toppling site to zero is not changed. By allowing values of $\gamma \neq 1$, any possible degeneracy in the system, stemming from two or more unstable sites relaxing in the same time step and having simultaneously a $z_{ij} = 0$, is effectively removed. The authors claim that such a degeneracy should not be considered generic for the formation of SOC.

The essential point of the paper is a discussion of the implicit tuning in SOC systems. A modified forest-fire model is also discussed, beside the modified OFC model. The latter is mainly examined within periodic boundary conditions. Basically, no SOC behavior is found for all γ (negative γ are not considered, for being non-physical).

The authors also present some results for open boundary conditions and find localized avalanches with $s_{\max} \sim 10$ independent of the system size for $\gamma < 0.9$. For larger γ, the tail in the distribution increases, and the distributions appear to be power laws for γ near unity, but a different non-SOC behavior is not completely ruled out by further analysis of, for example, the Lyapunov exponents.

1.2.3.4 The Manna model

This model did actually not inherit any feature of the OFC model (in fact, it was proposed in 1991), nor is it related to it, if not for being another sandpile model, which displays SOC behavior. However, it is a rather prominent example of SOC systems and should be mentioned, at least as a representative of those other models, which deserve to be listed, but are not of significant importance for the present work.

The Manna model [Man91a] is a reduction of the BTW sandpile model and allows only for two states at each site of a square lattice with open boundaries. A site can be empty or occupied. Grains are added randomly. If the chosen site is empty, it will be occupied. If it was already occupied, both particles are redistributed randomly to another nearest neighbor each and so on. The avalanches are driven by this hard core repulsion and are of a genuine stochastic nature. This feature is in contrast to the original sandpile, where the avalanche dynamic is deterministic. Nevertheless, the Manna model can be tracked analytically [Dha99], and some exact results are known for the recurrent states or the minimal and maximal number of particles in the system.

The Manna model gave rise to two more sandpile-like models, which are known as the critical slope model (CSM) and the critical laplacian model (CLM). In those models, the threshold is not defined for the actual number of grains per site, but in the height difference of neighboring sites (CSM) or in the second derivative (CLM) [Man91b].

1.3 Known facts and open questions

Right in the very first papers, where the model had been proposed, several features of the model were already discussed, and numerous results were already reported [Ola92b, Chr92b, Chr92c, Chr92d, Ola92a]. This section is concerned with those results that were obtained in research so far. A catalogue of the known facts about the OFC model is compiled, and the arguments, which were discussed in the literature, are also repeated. The section concludes with a collection of open questions, which are to be answered in the main chapters of this thesis.

1.3.1 The literature

1.3.1.1 The size distribution of avalanches

Power laws in the size distribution of avalanches were found for all α, down to a critical $\alpha_c = 0.05$, below which the distributions were of an exponential type, and avalanches became localized. The critical exponent τ was found to depend on α, and thus to be non universal, but different distributions, seen as functions of the system size for the same value of α obeyed finite-size scaling [Ola92b]. The cutoff in the distributions (as it appears in the scaling function $G(s/L^D)$) was claimed to scale as $L^{2.2}$. This finding was soon after questioned, because scaling relations are violated. In two dimensions, the critical exponent D in the scaling function must be less than or at most equal to 2.

Klein and Rundle estimated for which system sizes this scaling leads to a contradiction [Kle93]. If the scaling was right, the probability for an avalanche of size $s = L^{2.2}$ would not vanish. Since the total stored energy in the system can be L^2 at most (each site just below the threshold), and since the total energy removed from the system during one avalanche is bounded from below by $(1 - 4\alpha)$ times the number of topplings, the inequality

$$(1 - 4\alpha)L^{2.2} \leq L^2 \tag{1.20}$$

cannot be maintained for sufficiently large L. However, that contradiction sets in for system sizes far beyond the computable limits. Up to now, the biggest lattice sizes simulated are $L = 2048$ [Hel04], and the critical size is $L_c = 3125$ for a coupling of $\alpha = 0.2$. The same paper [Kle93] argued that statements on criticality in nonconservative systems have to be handled with caution, as long as system sizes are too small.

In a reply [Chr93], the overestimated scaling was related to secondary topplings (i.e. a site receives enough energy from its neighbors to topple a second time, after having triggered the toppling of the neighbors itself in the first place). For $\alpha \leq 0.2$ no secondary topplings are possible, which was shown analytically. In [Bot97] the threshold value of the coupling, for which no secondary topplings are observed, was numerically determined to $\alpha_c = 0.24$. Nevertheless, even for α below 0.2, the cutoff appears to scale as $L^{2.2}$. Using more realistic assumptions about the distribution of energy in the system, it was also shown in [Chr93] that a contradiction similar to (1.20) sets in for system sizes $L \sim 760\,000$, and conclusions about the criticality are claimed to be still valid. The "wrong" scaling with $D = 2.2$ is still observed numerically, as for example in a recent work by Ramos et al. [Ram06].

Grassberger [Gra94] found no specific transition at $\alpha_c = 0.05$ (the lower bound in [Ola92b]), but avalanches were power law distributed only for small L and large α. In [Cor95] the breakdown of power law distributions is reported to occur at $\alpha_c = 0.16$, while Lise et al. observed a convergence towards criticality (and hence power laws in the size distributions) with increasing system size, and an universal critical exponent was claimed to be $\tau = 1.8$ for all values of α [Lis01a]. The latter was confirmed by an examination of subsystems placed at the corner, at the boundaries, and in the center of a larger system [Lis01b]. Irrespective of where the subsystems were located, the corresponding distributions were reported to obey finite-size scaling and the exponent τ appeared rather robust.

Later publications concerned with the question about the criticality of the OFC model did not concentrate on the size distribution of avalanches, but considered other techniques. Their results are presented below.

1.3.1.2 The energy distribution

The first investigation of the energy distribution in the OFC model was presented in [Ján93]. There, the mean energy in the system was surveyed as a function of time and for various degrees of dissipation. Of course, for $\alpha = 0$, the sites decouple, and the mean energy oscillates with a frequency of unity, measured in terms of the external driving. For nonvanishing couplings, the oscillations are preserved, but the overall amplitude decreases, and the frequency increases for larger values of α.

The mean energy in the system was assumed to equal 1 by Klein and Rundle for their construction of a contradiction discussed above [Kle93]. In [Chr93], the mean was shown to be about 0.54 for $z_c = 1$.

Grassberger also explored the energy distribution of the sites [Gra94], but he did not consider the mean energy. Instead, he focused on the distribution in the interval $[0, z_c]$. For periodic boundaries and conservative coupling, this distribution has five delta peaks at multiples of $\alpha = 0.25$ (from 0 to 1). Smaller α result in a softening of these peaks. This feature was further examined in [Dro02], and the results are discussed in the next section concerned with the influence of the boundary conditions.

For open boundaries, the energy *difference* between neighboring sites is also peaked at multiples of α, but the peaks are superposed by an uniform background. This finding is similar to the results for the Zhang model (section 1.2.1.3). The actual distribution within the unit interval does not show any apparent ordering [Gra94]. This result might be due to fact that the systems did not reach their stationary state yet, see the discussion in section 3.1.

A thorough investigation in [Mil03a] confirmed the peaks at multiples of the coupling, at least for $\alpha < 0.2$, but several peaks not at multiples of some other unit are also observed. For larger values of α, peaks are found at multiples of a quasi-unit, which is larger than the actual coupling.

The results indicate that sites are mostly lifted just at the threshold before they topple, or only slightly above. Only for larger α, most of the topplings are imposed by a toppled neighbor, which lifts its neighbors far above the threshold (for conservative $\alpha = 0.25$, the quasi-unit is at about 0.31).

1.3.1.3 The boundary conditions

It was known that SOC systems have to be "open" in some sense, in order to avoid never-ending avalanches (see also section 1.1.1). Since the intrinsic dissipation in the OFC model already ensures finite avalanche sizes, it is not necessary to use open boundaries as for the sandpile model.

In [Chr92b] *open* and *free* boundary conditions were discussed. For open boundaries, all the sites are coupled to their neighbor by the same α and energy is lost at the border due to the missing neighbors. Free boundaries are defined such that border sites are coupled to the interior of the system with a renormalized $\alpha_{bs} = \alpha/(1-\alpha)$ and in the same manner for corner sites with $\alpha_{co} = \alpha/(1-2\alpha)$. The authors also mention the *reflecting* boundaries with $\alpha_{bs} = 1/3$, but no further results are presented. For free boundaries, the exponents are reported to be smaller than those for open boundaries and the onset of the localization of avalanches (mirrored in exponentially decaying size distributions) starts for larger α at around 0.1 (instead of $\alpha_c = 0.05$ for open boundaries).

The first attempt to study periodic boundaries was in [Soc93], but a slightly modified version of the OFC model was considered (see section 1.2.3.3). For the relevant

combination of parameters, which resembles the usual OFC model, a periodic final state is found for all α.

The effect of the boundary conditions was also studied by Grassberger [Gra94]. For periodic boundaries, the system settles in a strictly periodic state after a short transient time for $\alpha \leq 0.18$. This periodic attractor is defined either by the number of the topplings, which is L^2, or by the amount of energy per site that has to be put into the system per cycle, $1-4\alpha$. The steady state is characterized by single topplings only, and each site has a distance of at least α to its neighbors. Every site topples for itself, without lifting any other site above the threshold, and receives in turn 4 packages of each neighbor of size α without being activated. The loss in each cycle is just absorbed by the external driving. This attractor is not unique and marginally stable against perturbation.

In [Dro02] it was shown that for infinite numerical precision this periodic attractor is the only surviving state of the system, even for $\alpha > 0.18$, and that the sites of a given configuration (a snapshot of the current state) can be classified into 4 groups. These groups differ from each other by the necessary number of neighbors to topple (1,2,3,4), before the specific site topples. Size distributions for different *finite* precisions have approximately the same slope, but for higher precision, the weight of the distributions $n(s > 1)$ is diminished. For infinite precision one would obtain single topplings only.

Open boundary conditions are found to result in power law distributions for almost all α and for small lattices, even for α below 0.05 [Gra94] (the lower limit in [Ola92b]). The inner part of the system settles in a quasi-stationary state, which is similar to the one found for periodic boundaries. The open boundaries are recognized to prevent the ordering of that inner system. Every once in a while, a larger avalanche is triggered at the boundary and intrudes into the interior, forcing these sites to reorganize in another quasi-stationary state. Evidence for this scenario is found in a sharp peak at $n(s = 1)$ in the size distribution, while the relative weight of the power law tail decreases as $1/L$. For larger systems, these results are hard to verify, because of the long transient times, and the asymptotic behavior is only assumed to be the same. Nevertheless, the proposed finite-size scaling in [Ola92b] should break down for large L, though Grassberger, too, states a dependence of the cutoff on the system size as $\sim L^D$ with $D > 2$.

Even for open boundary conditions, one can obtain a quasi-periodic behavior in the OFC model, if one switches from the continuous driving to a discrete energy input combined with dynamic random thresholds (annealed disorder, see also the discussion of noise in the OFC model below); In [Ram06] the external input was not chosen infinitesimally, but in discrete steps of size 10^{-4} (measured in units of the threshold value $z_c = 1$). Still, the growth was applied globally and uniformly, but the thresholds were Gaussian distributed with a standard deviation σ. Thus, the largest site is not lifted exactly to the threshold, but can be slightly larger than unity, before triggering an avalanche. The quasi-periodic behavior is observed in the avalanche time series, and the period length is proportional to the degree of dissipation in the system. The periodicity vanishes for small σ.

As we have seen, the open boundaries have a specific impact on the observed behavior. They are decisive for destroying the systems' tendency to desynchronize (such that each site decouples from its neighbors). A periodic ordering of the system is no longer possible, once the boundary conditions break the spatial symmetry. For a system not to end up in a periodic state as within periodic boundaries, the slightest perturbation of a single defect site in a periodic lattice suffices [Cev98].

In the following, and in the main chapters of this thesis, I will focus on OFC systems with open boundaries.

1.3.1.4 The influence of noise

Also discussed in [Ola92b] was the influence of noise in the OFC system. For $\alpha = 0.2$, noise of zero mean and a variance of up to 0.25 (measured in units of the threshold) was added to each toppling site without any observed change in the exponents or in the cutoff. [Ján93] introduced disorder in the thresholds. They were chosen locally as $z_c(i,j) = z_c + \zeta(i,j)$ with $\zeta(i,j)$ being uniformly distributed with zero mean. As a result, the critical behavior is destroyed, and one obtains exponential size distributions. It was concluded that disorder introduces a second length scale in the system, apart from the system size L.

Another way of implementing quenched noise was presented in [Mou96]. There, the noise was imposed in the redistribution of energy via $\alpha(i,j) = \alpha + \zeta(i,j)$ (again taken from a flat distribution with $\zeta(i,j) \in [-\zeta, \zeta]$). For small ζ, the SOC state survives, but for larger noise, the system synchronizes such that only large avalanches of the order of the system size and single topplings are observed. The author claims to find a region of re-entrance into criticality and even a fourth phase for rather large disorder and small α, where distributions decay exponentially. All the above findings were summarized in a phase diagram in the $\alpha - \zeta$ plane.

Our recent work has shown that these different phases are actually not real phases, but show up as artefacts of a crossover behavior of different length scales, induced by disorder and coupled to the system size [Bac05].

A similar approach of adding disorder was discussed in [Cev95, Cev98], where the stability against small perturbations was studied. Instead of adding global noise, one allows for lattice defects. A different but fixed $\alpha_d < \alpha$ was assigned to certain sites, either randomly or along straight lines of at most one 10th of the (linear) system size. The α values for the other sites were kept constant. For not too many defects (up to 5% of the system) the criticality is preserved. The obtained power laws in the size distributions interpolate between the corresponding undisturbed systems. The cutoff in the distributions is also affected by the introduction of defects, it decreases for increasing disorder. For a fixed fraction of defects, the cutoff varies as a function of the system size, but the small avalanche regime does not change. For larger α, the systems are less perturbed by adding defects. If the disorder is above 5%, the SOC behavior breaks down.

The latter work [Cev98] also addresses the stationarity of the system by comparing distributions, which were taken at different times. The systems are claimed to reach their equilibrium state rather quickly, and the exponent τ appears to be universal for large L. The large avalanches are found to be triggered mainly at the boundaries of the system.

1.3.1.5 The transient stage

The question about the stationarity of the OFC model arose rather soon. In [Gra94], Grassberger indicated the extremely long transient times and realized that earlier findings have to be adjusted. The system sizes surveyed so far were simply too small, and observation times were too short to assert the steady state of the systems.

Grassberger also introduced a fast algorithm for the numerical simulations. Most of the time during the simulation is spent in the search of the site with the largest

energy. For a two-dimensional array of linear size L, this time is of the order of $\mathcal{O}(L^2)$. Through a clever way of book-keeping, where only the largest sites are stored in an extra register, this time can be reduced drastically to be of the order of $\mathcal{O}(L)$ (see also appendix A.1).

The missing neighbors at the borders induce a different period of the boundary sites of $(1-3\alpha)$ in contrast to the period of the interior of the system, which is $(1-4\alpha)$ (both in units of the input). This connection was first mentioned in [Mid95], where Middleton and Tang observed the influence of the boundary region on the system. They found a boundary-driven synchronization between neighboring sites. Such synchronized sites form *patches* that were called *self-organized regions* and can be characterized by the following properties: sites within a patch have approximately the same energy value. They are stable over many cycles (the period of the inner part of the system, $1-4\alpha$) [Bot97, Dro02], and sites within the same patch have the same toppling behavior, e.g. they topple in the same sequence and most of the time one by one. For different α values, the patches differ in their size (increasing patch size for increasing α), but for each α, the patches grow with distance from the boundary [Dro02].

During the evolution of the system, the patches invade the system. After a short transient time, the center of the system behaves similarly to a periodic system, i.e. one finds only single toppling events. The boundaries start to develop the patches and form an invasion front (except for the patchy structure, this mechanism was already pointed out in [Gra94]).

This invasion was observed to obey a power law $y(t) \sim t^{\beta(\alpha)}$, where $y(t)$ measured the intrusion depth as a function of the time t [Mid95]. The exponent β depended on α, just as the exponent τ for the size distribution of avalanches. Grassberger conjectured that the intrusion stops below a critical α value [Gra94].

[Lis02a] examined this intrusion by defining subsystems of a large lattice and comparing statistical quantities as the average earthquake size of such subsystems placed in the corner, at the border, or centered within the large system. These quantities were observed until they reached a stationary value. Both the exponents, τ and what was called a dynamic critical exponent, which is the counterpart to the above β, are found to be universal and independent of α.

The missing neighbors at the boundaries are equivalent to a less effective driving rate of the sites next to the boundary. The effect of unequally driven sites was also studied in [Mid95]. The authors presented a Poincaré map for a system of two sites (see also section 2.1.1 for a detailed analysis) and found a continuous interval of stable configurations, when both sites are grown homogeneously.

On the other hand, if one site was driven with a slower rate $(1+\epsilon)^{-1}$, compared to the unit drive of the faster site, the system has only one fixed point. This attractor is characterized by an avalanche of size 2. The slower site always topples first (yielding a package of size α) and triggers a subsequent toppling of the faster site, lifting it above the threshold and receiving in turn a package bigger than α. Thus, it keeps up with the faster driven site and this fixed point can be maintained. Middleton and Tang called this a *phase-locked* state and deduced that such an inhomogeneity propagates from the border of the system into the center and is responsible for the long-range correlations. A similar return map was shown in [Soc93]. However, the authors did not focus on the consequence of different driving rates, but studied a modified OFC model. Their results were discussed above in section 1.2.3.3.

1.3.1.6 The criticality of the OFC model

This section discusses the criticality in the OFC model beyond the observation of power laws and their scaling behavior. In a sequence of publications and replies, deCarvalho and Prado [deC00, deC01], and Christensen and coworkers [Chr01] exchanged arguments concerning the criticality in connection with branching rate techniques.

The branching rate for the OFC model is defined as the renormalized avalanche size minus the triggering site[3]. The renormalization is necessary due to the different number of neighbors for boundary (corner) sites compared to bulk sites. Thus, the real number of descendants is divided in each branching step by the coordination number of the ancestor site.

It is known that this branching rate has to be unity in order to describe a critical process [Har63]. deCarvalho and Prado found the branching rate of the nonconservative OFC model to be less than unity. Therefore, they concluded, the OFC model is not critical for $\alpha < 0.25$ [deC00].

In [Chr01] it was noted that for *correlated* processes (as the OFC systems are), the branching rate can also be expressed as function of the mean size of events as $\sim 1 - 1/\bar{s}$ [Fel57]. Only when $\bar{s}$ as a function of the system size L approaches a constant for $L \to \infty$, the OFC model would be not critical. The authors claimed that the data presented in [deC00] could not rule out the possibility of a genuinely critical model, even for nonconservative $\alpha < 0.25$.

[deC01] then justified some of the results of the first paper and proposed that the OFC model would fall into the class of almost critical systems [Kin99], and hence the branching rate would be near unity, but not exactly one.

Miller and Boulter [Mil02] extended these ideas and defined *layer* branching rates for each layer perpendicular to the border, thus coping with the boundary effects. Layers deep within the system should mimic the true behavior of infinite L. In a $1/L$ plot for various system sizes they confirmed the results in [deC01] and by extrapolation they found only the conservative case to be critical with the corresponding branching rate equal to unity. Nonconservative systems are disposed of as almost critical.

1.3.1.7 The connection to real earthquakes

As a last point, the properties of the OFC model common to or important for real earthquakes are mentioned.

Pepke and Carlson were the first to compare different models, as far as the predictability of large events are concerned (which is of prime interest, at least for real quakes). In [Pep94] they considered the BTW model, the OFC model, the (uniform) BK model, and a model by Chen, Bak, and Obukhov [Che91]. The latter is a uniformly driven lattice model, but thresholds are randomly assigned anew to any toppling site from the interval $[0, 1]$, and energy is not only transferred to nearest neighbors. Instead, it is redistributed between sites according to a power law in the distance, thus introducing long-range correlations.

The authors applied several forecasting algorithms as they are used for real earthquakes. In this comparison, the OFC model was the most predictable, having a 90% success in predicting large events within an alarm time of 20% (measured in some appropriate units; for totally uncorrelated events one would obtain a ratio of 1 between correct forecasts and the alarm time percentage).

[3] In the terminology of branching processes, the branching rate is the mean number of successors, and hence the subtraction.

An astonishing finding for real earthquakes is formulated in Omori's law [Omo94]. It states that the frequency of foreshocks (R_f) before or aftershocks (R_a) after a large event at a time t_m obeys a power law

$$\begin{aligned} R_f &\sim (t_m - t)^{-q} \\ R_a &\sim (t - t_m)^{-p} \quad , \end{aligned} \tag{1.21}$$

where the rates R_i are simply counting the shocks, independent of their size and both the exponents are around unity. The first law in (1.21) is sometimes referred to as the *inverse* Omori's law.

In [Her02], main events in the OFC model were defined to be avalanches with at least 1000 toppling sites in a system with $L = 512$. The time was discretized into small steps of $\delta t = 10^{-4}$ (in units of the external energy input) and an avalanche was considered as a main event at t_m, if there was no larger avalanche in the interval $[t_m - \delta t, t_m + \delta t]$. The system was then monitored and statistics were averaged over 10^6 main shocks. The authors found a behavior in agreement with the phenomenological Omori's law for different α, but the best conformance was reached for $\alpha \sim 0.17$. The total foreshock activity was about one order of magnitude smaller than the one for after shocks, which is also observed in seismicity. However, the exponents differed from unity, $p \sim 0.76$ and $q \sim 0.7$ are reported for the best matching α.

The idea of comparing real life data with the statistics of the OFC model was picked up in [Hel04]. The authors examined not only the shock activity before and after a large avalanche, but extended the comparison to a set of phenomenologically known relations. For instance, the total occurrence of aftershocks, N_a, depends on the magnitude m of the main shock as $N_a \sim 10^{km}$, where k is found in the range $0.5 - 1$ [Hel03]. The average distance, D_a, between aftershocks and the epicenter of the main event has a similar dependence on m, $D_a \sim 10^{0.5m}$. Helmstetter et al. generated an artificial earthquake catalogue from the OFC dynamics and found almost all of the observed relations of real seismicity at least qualitatively reproduced in the OFC model. Especially, they confirmed the accordance with Omori's law and recovered the connection between main-shock magnitude and aftershock behavior. They also observed an equivalent relation between the large avalanche and the foreshocks, which is not yet recorded for real quakes, but increases the predictability of the OFC model and might be useful for further research in seismology.

[Pei04a] constructed a network from sites, which triggered an avalanche, and this network is analyzed for its degree distribution. Graphs generated by the sequence of epicenters of real quakes are known to be scale free [Abe04] as introduced by Barabasi and Albert [Bar99, Alb02]. The same is found for the topology of the OFC networks, but only for the nonconservative case. $\alpha = 0.25$ results in networks that have the characteristics of random graphs.

1.3.2 The questions

In the last section it has become clear that the OFC model is not yet fully understood and there are still some riddles to be solved.

We already encountered the different and contradictory statements on the exponent in the size distributions of avalanches. Some authors find a universal τ [Cev98, Lis01a, Lis01b], while others find power laws, but with an exponent depending on the degree of dissipation [Mid95, Bot97]. Even authors, who find an α independent exponent, do not agree on the exact value of τ (1.8 in [Lis01b], or 1.63 in [Cev98]). A third group finds

power laws, but they are claimed to break down below some critical value of α, and again, there is no agreement about that critical value ($\alpha_c = 0.05, 0.07, 0.16, 0.18, 0.23$ are reported in [Chr92b, Ola92b, Cor95, Gra94, Chr01]). Most importantly, some authors disagree completely with the criticality of the dissipative OFC system and pin the critical α_c to 0.25 [deC00, Mil02].

The broad avalanche size distributions, which are found numerically without any doubt, are explained either by finite computer precision [Gra94, Dro02], with a new feature of being almost critical [deC00, Mil03b], or by a third possibility, where the superposition of many different mechanisms are said to be responsible for so-called *dirty* power laws [Dro02].

In the limit $L \to \infty$, the criticality of the OFC model is claimed to be at least almost conserved [Mil03a], or only the small avalanche regime is said to have non vanishing weight [Gra94, Dro02], while still others support the SOC thesis, and hence claim that the SOC state is the one to be realized for infinite system sizes. [Lis01b].

The above-mentioned arguments were all aiming at the steady state of the OFC systems. The statements on the transient behavior in the literature are contradictory, too. In one case, the transient time is said to be independent of the coupling [Lis02a], while it is found to be faster with increasing α in [Mid95]. On the other hand, it is not clear, how to decide, whether a system is stationary at all. Many of the scientists involved are aware of this problem, and claim to be working with system configurations that had a time evolution long enough to reach the stationary state, but they do not give a reasonable proof or present evidence for this statement.

Furthermore, it is obvious that $\alpha = 0$ corresponds to a rather uninteresting system of uncoupled oscillators. Due to the extremely slow time evolution of the OFC model for small α, no one studied the behavior of the system in that regime up to now, nor examined the limit $\alpha \to 0$.

Also, the OFC model was only studied on a two-dimensional lattice or in higher dimensions [4]. If not on a lattice or hypercube, spatial extensions were ignored all together as in the RN OFC models (section 1.2.3.2), or were incorporated in the form of special graphs with a certain topology [Lis02b]. Even if the model in one dimension might not be relevant for the seismology, what are the features of the OFC sites along a chain? So, in short, the questions that should be addressed in this work are the following:

- what are the characteristics of the OFC system in *one* dimension?
- what can be said about the evolution towards the stationary state, both, in $d = 1$ and $d = 2$, and does the transient time depend on α or not? And if it does, how?
- what actually *is* the stationary state and what are its properties?
- can the OFC model be maintained in the club of SOC models? Is it almost critical or not critical at all?
- what is the thermodynamic limit of infinite system sizes? How do the system's features change in the limit of vanishing α?

The following chapters examine these questions and shed some light on the discussions above.

[4] except for the explorations of the $1d$ BK model, which is similar to the OFC model [Nak90, Nak91], and a short consideration in [Chr92b], where a phase diagram was presented in the $\alpha_\perp - \alpha_\parallel$ plane, including $\alpha_\perp = 0$.

In view of the long transient times already mentioned several times, an important tool for my work was a new algorithm to determine the largest site in the system. With this new implementation I could explore those parameter regimes that were not accessible for the other scientists a decade ago, beyond the possibilities of faster computers I could rely on. The algorithm is a generalized, iterated bisection of the system combined with a hierarchy of recursive meta levels, which allowed a search of the order of $\mathcal{O}(\ln L)$ (instead of $\mathcal{O}(L)$ of the Grassberger algorithm). A detailed description is given in appendix A.

Chapter 2

The OFC-model in one dimension

> *Everything you've learned in school as "obvious" becomes less and less obvious as you begin to study the universe. For example, [...] there are no straight lines.*
>
> *R. Buckminster Fuller*

This chapter concentrates on the OFC model with the sites arranged along a one-dimensional chain. First, the focus is on small systems, up to 4 sites in a row. Minute systems (2 and 3 sites only) can be tracked analytically by means of Poincaré cuts or return maps as introduced by Middleton and Tang [Mid95] and Socolar et al. [Soc93] for the OFC model.

Systems having 4 sites are already too extended to cope with in the same manner, and one has to resort to numerical methods. Nevertheless, we encounter a specific behavior and properties that are also found in systems with large L.

For even larger systems, and in particular for the thermodynamic limit $L \to \infty$, another analytical approach is introduced, where the current configuration of a system is represented by a generalized state vector and avalanches constitute linear operators acting on that vector. This approach allows for a detailed classification of dynamic attractors in the OFC model, as well as for a discussion of the stability of these orbits.

Local balance equations, which couple the toppling and therefore the loss of energy at each site with the global growth of the system are also used. In addition, a mean-field-like solution for the toppling profile is derived. This result is generalized and turns out to be very useful for the discussion of two-dimensional systems in chapter 3.

Later sections deal with a complete numerical survey of the transient behavior, including the determination of the transient times as a function of the coupling and the system size, and with a characterization of the stationary state and its properties. The chapter finishes with a summary of the findings in $d = 1$.

Before small system sizes are investigated, the definition of the OFC model and its update rules, modified for the case of one dimension, are shortly repeated:

L sites are ordered linearly, each site i takes on values $z_i \in [0, 1]$. Initialized with a random z_i from a uniform distribution, each z_i is increased at a constant rate. The interpretation of the z values as an energy or a force still applies. The site with

the largest (initial) value reaches the threshold $z_c = 1$ first, becomes unstable, and possibly triggers an avalanche. α times the current energy of any unstable site z_u is redistributed to the right and left neighbor. In $d = 1$, α can be chosen from the interval $(0, 0.5)$, in contrast to the OFC model in two dimensions. The conservative case is given for $\alpha = 0.5$. Throughout the following chapter, the results are presented for open boundaries, where energy is lost at the borders. As in $d = 2$, within periodic boundary conditions, the system settles in a periodic state of length L, when measured in the number of topplings, or of period $1 - 2\alpha$ in units of the external driving (as opposed to $1 - 4\alpha$ in two dimensions). This attractor consists of single topplings only.

A peculiarity of the one-dimensional system is that the left and the right branch of an avalanche (moving to the left and the right border of the system) are independent of each other and do not cross each other.

There is only a single possibility for an avalanche to occur at a certain site twice: when the sites on either side of the first unstable site simultaneously receive enough energy to topple, as well as transfer enough energy to the now empty site in the middle to allow for a second avalanche starting at the same site. This is not possible for any other configuration, because a single branch of an avalanche leaves a row of relaxed sites behind, all having an energy value $z_i \in [\alpha, p_{\max}]$, where $p_{\max} = \frac{\alpha}{1-\alpha}$, as shown in the derivation of equation (1.16).

For $\alpha < \alpha_c = (\sqrt{3}-1)/2 \sim 0.366$, no secondary topplings are possible, even if both neighbors of the triggering site are just below the threshold. Then, they are lifted to $1 + \alpha$ each and deliver twice the energy package of $\alpha(1 + \alpha)$. α_c is the solution for the inequality $2\alpha(1 + \alpha) < 1$. In the following, $\alpha < \alpha_c$ is used, besides where stated otherwise.

2.1 Small systems

2.1.1 A pair of sites

As already mentioned, the system of two sites was studied in [Soc93, Mid95] and the results are summarized as a preparation for the system of three sites.

Let the two sites have values z_1 and z_2. A return map is constructed by determining the value $z_2(n + 1)$ as a function of the value $z_2(n)$, where $z_2(n)$ is the second site's value right after the n-th toppling of z_1. For recurrent configurations, possible values of $z_2(n)$ are all in the interval $(\alpha, 1)$. Nevertheless, for random initial configurations, transient states can also show up where z_2 is larger than 1. The return map explicitly reads

$$z_2(n+1) = \begin{cases} z_2(n) & \text{for} \quad \alpha \le z_2(n) < 1 \\ 1 + \alpha - \alpha z_2(n) & \text{for} \quad 1 \le z_2(n) < 1/\alpha \\ \alpha^2 z_2(n) & \text{for} \quad z_2(n) > 1/\alpha \end{cases} , \tag{2.1}$$

and is visualized in figure 2.1. The system has a continuous set of periodic states for $z_2^* \in [\alpha, 1]$. The period length is two topplings or $1 - \alpha$ in terms of the external input. Both sites topple alternately, each site delivering a package α without triggering the other site to topple.

The situation changes if one site, z_1, is driven slower with a driving rate $(1 + \epsilon)^{-1}$,

compared to the unit drive of the fast site z_2. The return map is then given by

$$z_2(n+1) = \begin{cases} z_2(n) + \epsilon(1-\alpha) & \text{for} \quad \alpha \leq z_2(n) < 1 \\ 1 + \alpha + \epsilon - \alpha(1+\epsilon) z_2(n) & \text{for} \quad 1 \leq z_2(n) < 1/\alpha \\ \alpha^2 z_2(n) & \text{for} \quad z_2(n) > 1/\alpha \end{cases} , \qquad (2.2)$$

and the dynamics of the system end up in a single fixed point $z_2^* = 1 + \epsilon \frac{1-\alpha}{1+\alpha} > z_c$ (see figure 2.2 below). This state was termed *phase-locked*, because the two sites are no longer independent of each other, but are synchronized. The single avalanche consists of two toppling events, where the slow site z_1 always lifts the fast site z_2 over the threshold z_c, and receives a package larger than α, thus coping with the lesser input from the outside.

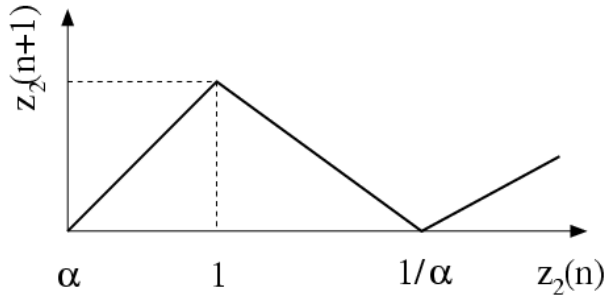

Figure 2.1: Return map for the uniformly driven system of two sites. Depending on the initial values, the system settles somewhere on the diagonal line of fixed points in the dashed square.

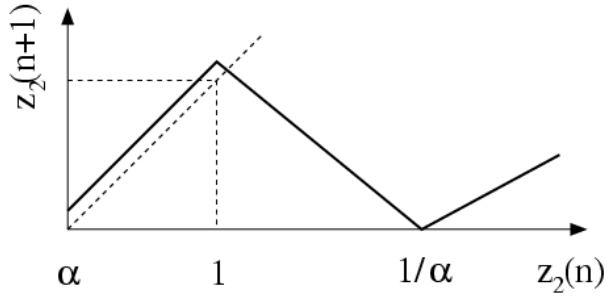

Figure 2.2: Return map for the system of two sites, where one site is driven slower than the other. The dashed diagonal line denotes the line of possible fixed points, cutting the graph at $z_2^* = 1 + \epsilon(1-\alpha)/(1+\alpha)$.

It is this synchronization that causes the instability with respect to small perturbations of the periodic state within periodic boundaries as discussed in section 1.3.1, even in the limit of infinite L. Due to the different driving rates, a single source or sink in the lattice cannot maintain the desynchronization with its surrounding sites, and sooner or later the fast (slow) site will be triggered by (triggers) a subsequent toppling. Since this implied toppling, in general, will yield a package larger than α, this toppling

in turn corresponds to another different effective driving rate with respect to one of the neighbors. Thus, the single defect site is the seed for an ever-increasing perturbation. We will encounter this mechanism again when discussing the patch-like structure of the lattice in two dimensions in chapter 3.

2.1.2 Three sites

For the system of three sites, a similar approach is applied, which was inspired by the return map in the case $L = 2$. The three sites are labeled z_l, z_m, and z_r for the left, middle and right site, respectively. This system is the smallest possible with nontrivial dynamics, since the different sites are no longer homogeneous. For $L = 2$, the inhomogeneity had to be put in by hand to find a coupled state.

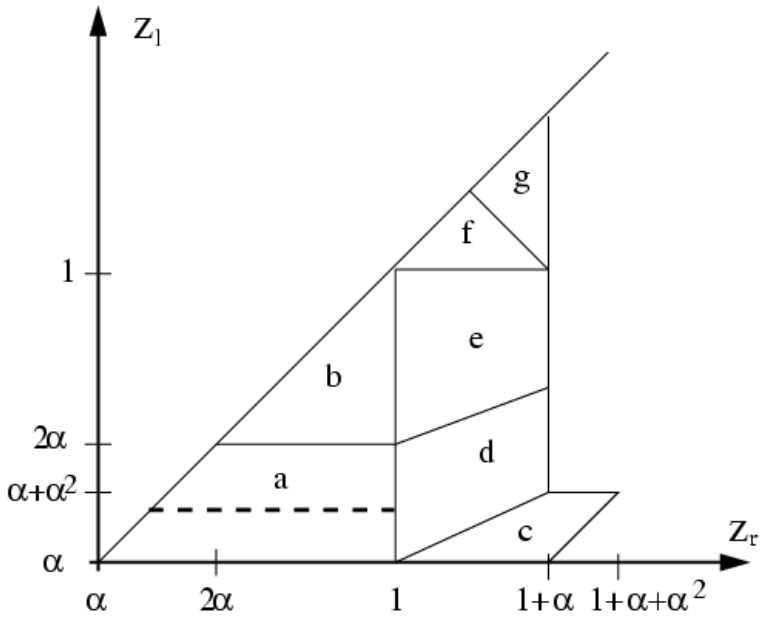

Figure 2.3: Poincaré map in the $z_l - z_r$ plane for the system of three sites and $z_m = 0$. Only the part for which $z_l \leq z_r$ is shown. The different regions with a specific sequence of topplings and phases of intermediate growth are separated and labeled from a to g. These regions are listed in detail in table 2.1. The fixed point line as derived below in equation (2.3) is indicated by a dashed line.

The system is examined by following the dynamic path in the z_l-z_r plane for $z_m = 0$; A Poincaré map in the configuration space is constructed whenever the center site topples. Possible values of the two border sites are $\in [\alpha, 1 + \alpha + \alpha^2]$. The lower value is realized when a boundary site just toppled itself and lifted the center site directly to the threshold. The upper limit occurs only, if all the sites were at the threshold before (it is necessary for one of the outer sites to be infinitesimal larger than the other two, thus triggering the toppling of the center site). Note that the Poincaré map is observed whenever $z_m = 0$, and not at a specific periodic moment in time. This can also happen directly at the occurrence of an avalanche, thus dealing with unstable configurations.

All the possible configurations can be classified by the different scenarios of top-

pling events and growth phases, where the external driving adds energy to the system. There exists a total of 14 different scenarios but due to the symmetry between the two boundary sites, only the case $z_l < z_r$ has to be considered, which reduces the number of scenarios to be calculated to seven.

G, T_r, G, T_l, T_m a	$\alpha \leq z_l < \min(2\alpha, z_r)$ $\alpha \leq z_r < 1$	$z_l' = \alpha(1+2\alpha) - \alpha z_l$ $z_r' = \alpha(1+2\alpha) + z_r$ $-(1+\alpha)z_l$	$\in [\alpha, \alpha(1+\alpha)]$ $\in [\alpha, 1+\alpha^2]$
G, T_r, G, T_l, G, T_m b	$2\alpha \leq z_l < 1$ $2\alpha \leq z_r < 1$	$z_l' = z_l - \alpha$ $z_r' = z_r - \alpha$	$\in [\alpha, 1-\alpha]$ $\in [\alpha, 1-\alpha]$
T_r, G, T_m c	$\alpha \leq z_l < \alpha z_r$ $1 \leq z_r \leq 1+\alpha+\alpha^2$	$z_l' = 1 + \alpha + z_l - \alpha z_r$ $z_r' = 1 + \alpha - \alpha z_r$	$\in [1+\alpha-\alpha^2-\alpha^3, 1+\alpha]$ $\in [1-\alpha^2-\alpha^3, 1]$
T_r, G, T_l, T_m d	$\alpha z_r \leq z_l < \alpha + \alpha z_r$ $1 \leq z_r < 1+\alpha$	$z_l' = \alpha(1+\alpha) + \alpha^2 z_r - \alpha z_l$ $z_r' = 1+\alpha+\alpha^2(1+z_r) - (1+\alpha)z_l$	$\in [\alpha, \alpha+\alpha^2]$ $\in [1-\alpha-\alpha^2-\alpha^3, 1+\alpha^2]$
T_r, G, T_l, G, T_m e	$\alpha + \alpha z_r \leq z_l < 1$ $1 \leq z_r \leq 1+\alpha$	$z_l' = z_l - \alpha z_r$ $z_r' = 1 - \alpha z_r$	$\in [\alpha, 1-\alpha]$ $\in [1-\alpha-\alpha^2, 1-\alpha]$
T_r, T_l, G, T_m f	$1 \leq z_i \leq 1+\alpha$ $\alpha(z_l+z_r) < 1$	$z_l' = 1 + \alpha - \alpha(z_l+z_r)$ $z_r' = 1 + \alpha - \alpha(z_l+z_r)$	$\in [\alpha, 1-\alpha]$ $\in [\alpha, 1-\alpha]$
T_r, T_l, T_m g	$1 \leq z_i \leq 1+\alpha$ $\alpha(z_l+z_r) \geq 1$	$z_l' = \alpha^2(z_l+z_r)$ $z_l' = \alpha^2(z_l+z_r)$	$\in [\alpha, 2\alpha^2(1+\alpha)]$ $\in [\alpha, 2\alpha^2(1+\alpha)]$

Table 2.1: Scenarios in the Poincaré map, sorted by their toppling and growth sequences. The first column shows the different scenarios $(a-g)$, presented in figure 2.3. Second column: range of configurations in state space for which each scenario is realized. Third column: resulting states after the second toppling of the center site and the ranges for the new z values.

The classification is proceeded by the following scheme: the growth phase between the avalanches is denoted by G, which, of course, is global and independent of the sites. Each toppling event is described by an expression T_i, where the index $i \in \{l, m, r\}$ denotes the site that topples. A scenario is then classified according to the sequence of events of the set $\{G, T_i\}$. For instance, the scenario (T_r, G, T_l, T_m) describes a situation where the right site is lifted above the threshold by the toppling of the center site. It relaxes (T_r), the whole system is fed from the outside (G), and the toppling of the left site (T_l) triggers the middle site to topple as well (T_m).

For each scenario, the configuration is evaluated when the center site has toppled again. Table 2.1 lists all scenarios $(a-g)$ according to their sequential representation, together with a range of possible values for the resulting states (i.e. possible z values of the boundary sites).

We are interested in possible fixed points of the map. By comparing initial and final z_i values for the different regions, one recognizes region a as the only possible candidate to have an overlap in the ranges of the z_i's before and after the evaluation of the characteristic sequence for all values of α. The fixed points are calculated by setting

$$\begin{aligned} z_l^*(n+1) &= \alpha(1+2\alpha) - \alpha z_l^*(n) \\ z_r^*(n+1) &= \alpha(1+2\alpha) + z_r^*(n) - (1+\alpha) z_l^*(n) \quad , \end{aligned} \tag{2.3}$$

and demanding that $z_i^*(n+1) = z_i^*(n)$, or in a vector notation, which allows for an easy stability analysis,

$$\underline{z}^* = \alpha(1+2\alpha)\underline{\underline{1}} + \underline{\underline{M}}\ \underline{z}^* \quad . \tag{2.4}$$

$\underline{\underline{1}}$ denotes the unit matrix in two dimensions, and

$$\underline{\underline{M}} = \begin{pmatrix} -\alpha & 0 \\ -(1+\alpha) & 1 \end{pmatrix} \quad . \tag{2.5}$$

The first equation in (2.3) is solved by

$$z^* := z_l^* = \frac{\alpha(1+2\alpha)}{1+\alpha} \quad . \tag{2.6}$$

The second equation in (2.3) is then trivially fulfilled, resulting in a continuous fixed point line for $z_r \in [z*, 1]$.

There exist two such lines, the second one being obtained by interchanging the two sites. These fixed point lines are attractive (eigenvalues of $\underline{\underline{M}}$ are $-\alpha$ and 1) and are marginally stable against shifts in the larger component. The resulting attractor is a sequence of two avalanches, written as (G, T_i, G, T_j, T_M), where T_i is the toppling of the larger site, and T_j denotes the toppling of the site with $z_j = z^*$. Thus, the site at the fixed point triggers the center site to relax.

A special attractor is found for both sites at the fixed point value. Then, both boundary sites topple simultaneously, lift the center site above the threshold, and receive a package of the size z^*, written as $(T_{r,l}, G, T_m)$ in the above notation. In contrast to the asymmetric case, this orbit consists of a single avalanche of size 3, instead of two avalanches with size 1 and 2 for boundary sites with different z values.

2.1.3 Four sites

We now turn to a chain of 4 sites. This system is already too extended to apply an examination, such as in the case $L = 3$, even if one exploits the symmetry between sites. Although the configuration space is quite large [1], characteristics of the periodic orbits, the number of different attractors, and their length could be determined as a function of the coupling parameter α.

[1] For the continuous system with 4 sites, the configuration space is $\mathbb{R}^4$. The statement on the size of the configuration space applies for the discretized version, for which 2^{p4} different states exist.

The continuous unit interval between zero and the threshold is discretized by switching from continuous state variables to integer valued z_i. The precision, the influence of which was also examined, could then be chosen by setting the threshold value z_c to different powers of 2, i.e. $z_c = 1024$ corresponds to a precision of 2^{-10}, and $z_c = 1048576$ corresponds to 2^{-20}. α was still a float variable and special care was taken to avoid rounding errors in the numerical simulations.

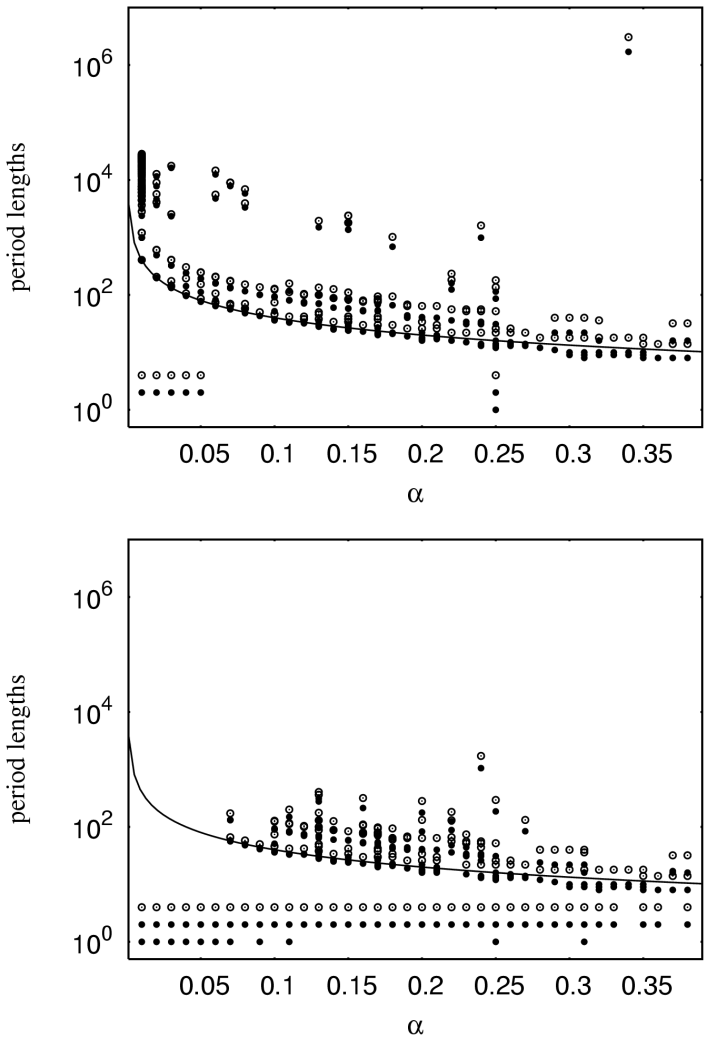

Figure 2.4: Period lengths for a system of 4 sites as a function of the coupling α, counted in two different measures: the number of topplings within a cycle (circles) and the number of avalanches (dots). Upper figure for a precision of 2^{-20}, lower figure for a precision of 2^{-10}. The solid line in both figures corresponds to $f(\alpha) = 4/\alpha$.

Since the 4 sites are all in the range of integers $[0, z_c]$, the total state space for stable configurations is finite, and every initial configuration sooner or later ends up in a recurrent state. The search for periodic orbits was done via a complete scan over 128^4

initial states in the case of higher precision and over 32^4 initial states for lower precision. Each of these states was initialized consecutively, and following configurations were calculated numerically. Thereby, every state was stored, and each forthcoming configuration was compared against the states in the memory until a known state was found again. Thus, the length of each attractor, and their relative weight could be determined, in the case of several attractors for the same value of α.

To speed up the search, the toppling sequence was also stored in an integer list (with entries from 1 to 4), and this list was first checked against possible matches. Whenever the toppling sequence was identical and periodic for a certain regime, the sequence of states was investigated afterwards as a final affirmation.

Due to this double-checked search, a beat-like effect was found: Toppling sequences can be periodic over many cycles, but the corresponding states are not recurrent and have a much longer period length. For example, states at the beginning of each toppling period are identical in three of the four sites, but the fourth site is slowly increasing (or decreasing) until the recurrent toppling sequence is disturbed, and the system settles in another (toppling) cycle. This second cycle then persists only for a limited time until it finally turns back into the first orbit (or into a third one and so on).

The coupling α was chosen between 0.01 and 0.38, in discrete steps of 0.01. The results are presented in figure 2.4. The length of the attractors was measured once in the number of avalanches, represented as dots and once in the number of topplings, marked with circles.

There exists a smallest possible attractor of 4 topplings. These topplings can all happen in a single avalanche, or are split in a sequence of two avalanches. Using the notation of the previous section (2.1.2), the two possible realizations are described as

$$\begin{aligned} P_1 =& (T_1, T_2, T_3, T_4, G) \qquad \text{and} \\ P_2 =& (T_1, T_2, G, T_4, T_3, G) \quad . \end{aligned} \tag{2.7}$$

The associated states of the orbits just before the external growth phase are calculated to

$$\begin{aligned} \underline{z}_1 =& (\alpha + \alpha^2, \alpha + \alpha^2, \alpha, 0)^T \qquad \text{and} \\ \underline{z}_2 =& (\tilde{z}, \tilde{z}, 0, \alpha + \alpha^2)^T \quad . \end{aligned} \tag{2.8}$$

$\tilde{z}$ is an arbitrary value $\in [\alpha + \alpha^2, 1]$. The realization of these attractors depends on the details of the numerical implementation of the dynamic update rules, since the two sites z_1 and z_2 are degenerate in both realizations $\underline{z}_1$ and $\underline{z}_2$. Note that all occurring avalanches are triggered at the boundaries else the attractors cannot be maintained This feature is also found for larger systems (up to some exceptions).

Both orbits are symmetric with respect to the two half systems of sites $(1, 2)$ and $(3, 4)$, but the manifestation of the symmetry is slightly different. In the case of a single avalanche, $(P_1, \underline{z}_1)$, the same site always triggers the avalanche, which then affects all other sites. The same type of toppling sequence is obtained when the site indices and values are interchanged according to $z_1 \leftrightarrow z_4$ and $z_2 \leftrightarrow z_3$.

The second period, $(P_2, \underline{z}_2)$, consists of two avalanches of size 2. Both avalanches only reach half the system, and the two subsystems decouple, which is also observed in the corresponding configuration. The symmetry is found in the alternate triggering of avalanches, which are separated by two in general different growth phases. Interchanging of sites $(1, 2)$ and $(3, 4)$ is equivalent to a shift in time, and a reset of the beginning and the end of the cycle.

# of topplings	# of avalanches	absolute occurrence	relative weight
4	1	29	0.003%
4	2	1025730	97.8%
50	41	2070	0.2%
50	43	20747	1.98%

precision = 2^{-10}

# of topplings	# of avalanches	absolute occurrence	relative weight
50	43	1.96367×10^7	7.31%
136	100	4.82264×10^6	1.79%
136	101	2.43976×10^8	90.90%

precision = 2^{-20}

Table 2.2: Observed periods and their lengths measured in topplings and avalanches for $\alpha = 0.09$ and two different precisions, 2^{-10} (upper table) and 2^{-20} (lower table). Periods can be degenerate in the sense that the same number of topplings is split into different numbers of avalanches. The higher the precision, the more preferred are the long attractors.

Both attractors are affected by the computing precision, which determines the size of the state space. For less precision, the number of possible configurations is smaller, and states, which are close to each other for higher precision, are now taken as identical configurations. This feature also explains the large number of attractors with a long period for better computational precision: the longer the period, the more diverse states are reached, and the larger the number of configurations within an attractor, the more likely are adjacent states to occur. These different states overlap and cannot be resolved as being different for low precision.

The smallest period of 4 topplings is realized for almost all α in the case of low precision for the z-values, while only for small α for better precision ($\alpha = 0.25$ is an exception explained below).

For lower precision, the period of two avalanches seems to be the natural one, it occurs more often and it has the larger weight (see table 2.2). This finding holds for all α except for $\alpha = 0.34$, but then the period with all topplings in a single avalanche also does not appear. Additionally, the attractor with a single avalanche is only realized for two specific configurations, the one given in (2.8) and the corresponding mirrored state. On the other hand, the second orbit of two avalanches is realized over a whole range of configurations, because $\tilde{z}$ can take on many different values. This feature is affirmed in the weight of the attractors, but not to be mistaken with the basins of attraction. For small α, the two orbits with 4 topplings are the only attractors, and their weights add to unity, as the data suggest, but I did not do a survey of *all* possible

initial states, and other rare attractors cannot be ruled out.

For better precision, small attractors are only observed for small α, and only the orbit with two avalanches is found. $\alpha = 0.25$ is the single instance, where both the small periods coexist for better precision, and it is somewhat isolated from the other data points.

These findings can be explained with an integer effect: The dynamics of the OFC systems typically involve expressions of the form

$$\sum_n c_n \alpha^n \quad . \tag{2.9}$$

They appear either in transferred packages of energy, in the energy variables themselves, or in the external feeding. The coefficients c_n are unity or of the order of $\mathcal{O}(1)$), and n is finite. Since the total range of possible z-values is a power of 2, and because this range is a representation of the unit interval $[0, 1]$, these sums can exactly be matched by integer values for certain values of α. Especially $\alpha = 0.25$ corresponds to a negative power of 2, and $0.25 \times z_c$ yields an exact energy package of 2^{p-2}, where $p = 10, 20$ is the precision.

The same holds for the other points along the α axis, for which the orbit $(P_1, \underline{z}_1)$ is found ($\alpha = 0.31$ is near $0.3125 = 2^{-2} + 2^{-4}$, $\alpha = 0.09$ is approximated by $0.09375 = 2^{-4} + 2^{-5}$. The exact match is only possible for lower precision, since $2^{-10} \sim 10^{-3}$ corresponds to the third decimal position). Generally, the smaller the values of α, the better the approximation by finite[2] polynomials of the above form (2.9). Small periods are preferably found for small α, due to this integer effect, even for better precision.

The degeneracy of attractors in the sense of splitting the same number of topplings into a different number of avalanches, is not only found for short orbits. Nevertheless, the short period of 4 topplings is a somewhat special case, since the two corresponding attractors are of a different type. The general case is obtained for longer periods, and there exist two mechanisms for the degeneracy. For both, the resulting period depends on the exact initial configuration:

First, if a site is lifted exactly to the threshold, it might topple within that avalanche or the avalanche stops, and a second avalanche is triggered at that site. Thus, the toppling sequence, and even the transferred packages of energy, are exactly the same (within relevant precision), but more or less avalanches are recorded for each instance. This mechanism can in principle be ruled out by the details of the numerics. However, it is also very sensitive to the precision of the simulation.

The second explanation is the inherent mechanism of the OFC system to create degenerate sites whenever an avalanche is triggered somewhere in the center of the chain. Then, the two sites, which are the endpoints of the same avalanche, both have a $z_i = 0$. Again, the implementation of the update rule determines, which site relaxes first (after the growth phase or intermediate topplings). Sites in the middle of the two former endpoints possibly relax only after having received packages of both the temporarily synchronized sites. The total size of the avalanche will be determined by which of the sites triggered the middle-site toppling.

One also recognizes the gap between short attractors of size 4 (topplings) and the larger attractors. This gap increases for decreasing α approximately as $f(\alpha) = 4/\alpha$ (the solid line in figure 2.4), and vanishes for lower precision and small α, because there

[2] Of course, infinite series would always be exact.

are no larger orbits, as discussed above. However, if the resolution is good enough, the period lengths for the long attractors diverge for $\alpha \to 0$.

This behavior proportional to $\sim 1/\alpha$ can be explained as a boundary effect. Since boundary sites have only one neighboring site, they only receive a package of the order of $\mathcal{O}(\alpha)$ per unit cycle, while the sites in the middle are loaded from two sites, and therefore receive $\sim 2\alpha$. For a given distance in variable space between the center site and a site at the border, it takes around $1/\alpha$ many cycles to obtain the same distance again. Since not only these two sites, but all four must have the same energy value (and therefore the same distance between all sites), for a configuration to be on a periodic orbit, the period length diverges as $1/\alpha$.

Another feature is the so-called persistence of attractors for certain ranges of α values. The same attractor with the same toppling sequence can be reached, if α is changed very slowly, such that the system can follow adiabatically. At some point, packages are too large (or too small) to maintain the same avalanche sequence. Further topplings are then triggered (or missed), and the attractor changes and settles in another periodic orbit. The new orbit can have the same number of total topplings and the same periodicity in the toppling sequence, resulting in the discussed degeneracy. It can also have another different toppling sequence, which is seen in the step-like slope of the orbits for different α.

A last point is the diversity of the periodic attractors. There are not only very long periods for a certain value of the coupling (the points around 10^6 avalanches for $\alpha = 0.34$ are valid data points with non vanishing weight of about 10%). There are also very different periods for the same α. Most are found for small α and, of course, better precision (e.g. up to 40 different attractors between 406 and 28410 topplings for $\alpha = 0.01$, not counting the small periods of 4 toppling). Generally, most of the periods are distributed along two bands, which correspond to $f(\alpha) = 4/\alpha$ and $f(\alpha) = 12/\alpha$. Responsible for these long attractors is the beat effect, which was mentioned in the discussion on the implementation of the search algorithm for the periods.

We will now leave the small systems and concentrate on larger chains. Some of the points just discussed will turn up again, so for a clearer presentation they are reiterated here:

(Large) avalanches are mainly triggered at the boundaries. Those initialized somewhere in the center result in two degenerate sites with the same z value. The better the precision, the larger the total state space and the longer the possible periodic attractors. The chains have a tendency to decouple into a left and a right subsystem, both with its own boundary layer. The size of the subsystems is about half the system size L.

2.2 Analytical results

This section discusses some analytical approaches to the OFC systems in one dimension. First, an operator technique is presented to explain the diverse attractors, which can, in principle, exist in the one-dimensional OFC model.

The second part of the section deals with the derivation of the toppling profile of the sites in the stationary state. This profile is very useful for the understanding of

the OFC model, and a similar setup is used for two-dimensional systems in section 3.1. For this reason, the approach is presented in detail.

2.2.1 The matrix method

The representation of a system's current configuration as a state vector was already used in the discussion of small chains, i.e., when the periodic states were found in equation (2.4) and (2.8). This representation is rather intuitive, and it was not necessary to define the state vector explicitly, since it is simply a suitable notation where the ordering of the sites is naturally implemented.

Different states of a system can be grouped into certain universality classes. This grouping is possible due to the external feeding of the system. Such a class is represented by the configuration that is obtained right after the growth phase. The external energy input adds exactly the same amount of energy to all the sites. If we split that amount of energy into several portions, and added them one by one, but uniformly on every site, any temporary state would belong to the same universality class. To get rid of that ambiguity, a new representation of the system's state is introduced. Instead of using a vector $\underline{z}$ with entries that correspond to the actual values of the sites, a reduced vector, or difference vector, $\underline{x}$, is considered, which has entries of the form $x_i = z_{i+1} - z_i$.

Formally, a reduction operator, $\underline{\underline{R}}$, is applied, which is given by

$$\underline{\underline{R}} = \begin{pmatrix} -1 & 1 & 0 & \dots & 0 \\ 0 & -1 & 1 & & \vdots \\ \vdots & & \ddots & & \\ 0 & & \dots & -1 & 1 \\ 0 & 0 & \dots & 0 & 0 \end{pmatrix} \quad . \tag{2.10}$$

The last row contains zero entries only, reflecting the fact that the different sites are not independent from another. $\underline{\underline{R}}$ diminishes the rank of the state vector $\underline{z}$ by 1, denoted by the indices L and $L-1$:

$$\underline{x}_{L-1} = \underline{\underline{R}}_{L\times L}\underline{z}_L \quad . \tag{2.11}$$

The last entry in $\underline{x}$ equals zero. We cancel that entry, and we also drop the index, but bear in mind that a reduced vector of size $(L-1)$ describes a system of size L.

For the proper chain, $\underline{z}$, a single toppling of site i would be described by an operator that resembles the unit matrix everywhere except for a 3×3 block located on the diagonal around the i-th column and row:

$$\underline{\underline{T}}(i) = \begin{pmatrix} 1 & 0 & \dots & & & & \\ 0 & \ddots & & & & & \\ & & 1 & \alpha & 0 & & \\ & & 0 & 0 & 0 & & \\ & & 0 & \alpha & 1 & & \\ & & & & & \ddots & 0 \\ & & & & \dots & 0 & 1 \end{pmatrix} \quad . \tag{2.12}$$

An avalanche, for instance running from site j to site k, is accordingly simply the product of such toppling operators, $\underline{\underline{A}}(j,k) = \prod_{i=j}^{k} \underline{\underline{T}}(i)$.

$\underline{\underline{R}}$ has no inverse, and one cannot calculate the effect of avalanches or topplings on a reduced state vector $\underline{x}$ by applying a scheme like defining a $\underline{\underline{\tilde{T}}}(i) = \underline{\underline{R}}^{-1}\underline{\underline{T}}(i)\underline{\underline{R}}$ and solving for the new state $\underline{x}'$ after the toppling.

Nevertheless, the effect of an isolated toppling (or the first toppling in an avalanche) can easily be determined. The site, which topples first and potentially triggers an avalanche, is reset from the threshold value to zero. That is, it is reduced by one. The neighbors are increased by an amount of α. Thus, the difference to the toppled site changes by $(1+\alpha)$ for each neighbor, but with opposite signs. Furthermore, a toppling, which in the original representation affects only the triggering site and the two neighbors, now also influences the differences with respect to the next nearest neighbors. With other words, a single (isolated) toppling is described by adding a vector of the form

$$(0, \ldots, 0, -\alpha, 1+\alpha, -(1+\alpha), \alpha, 0, \ldots, 0)^T \tag{2.13}$$

to the reduced state vector, with the 4 non vanishing entries at the appropriate places (from $i-2$ to $i+1$ for a toppling of site i). Such isolated topplings differ only in the position of the non-zero elements, but they do not contain any nonlinear effect of the state on the following configuration.

This nonlinearity is found in subsequent topplings, i.e. in any avalanche larger than 1. Now, the change in the difference vector depends on the former values of the sites, due to the coupling with α and higher powers in α [3]. Any of these subsequent topplings can be written as a matrix operator acting on the reduced state vector. Since the natural order of the sites is somewhat mixed up in the difference vector, one has explicitly to take the direction of the avalanche into account (the proper toppling as represented by the expression (2.12) neither discerns between the first and subsequent topplings, nor whether the avalanches spreads to the left or the right [4]). Thus, there exist two different matrices that (could) follow the triggering of an avalanche at site i:

$$\underline{\underline{M}}_l^{i-1} = \begin{pmatrix} 1 & 0 & \ldots & & & & & 0 \\ 0 & \ddots & & & & & & \vdots \\ \vdots & & 1 & 0 & -\alpha & 0 & & \\ & & 0 & 1 & 1+\alpha & 0 & & \\ & & 0 & 0 & -\alpha & 0 & & \\ & & 0 & 0 & \alpha & 1 & & \\ & & & & & & \ddots & 0 \\ 0 & \ldots & & & & & 0 & 1 \end{pmatrix} \tag{2.14}$$

describes the effect on the reduced state vector of an imposed toppling of site $i-1$ to the left of the first toppling, while a subsequent toppling of site $i+1$ to the right of

[3] The first hint on the typical OFC mechanism. It is this nonlinearity in α that drives the OFC systems. We will recover this behavior again.

[4] A note on the directions. When the states are represented as vectors, the avalanches are rather moving upwards or downwards. Left and right applies when figuring the system as moving blocks on a surface, i.e., the transposed vector is considered as the true configuration.

the toppled site i, is given by

$$\underline{\underline{M}}_r^{i+1} = \begin{pmatrix} 1 & 0 & \dots & & & & 0 \\ 0 & \ddots & & & & & \vdots \\ \vdots & & 1 & \alpha & 0 & 0 & \\ & & 0 & -\alpha & 0 & 0 & \\ & & 0 & 1+\alpha & 1 & 0 & \\ & & 0 & -\alpha & 0 & 1 & \\ & & & & & \ddots & 0 \\ 0 & \dots & & & & 0 & 1 \end{pmatrix} \quad . \tag{2.15}$$

In both cases (the avalanche running to the left or the right of the system), the 4×4 block, which is the only difference between the toppling operator and the unit matrix, is placed on the diagonal. The nontrivial column is at position $i-1$, when the induced toppling is on the left of site i, and at the position i, when the avalanche is moving to the right. If an avalanche branches in both directions, the part of the toppling operator, which differs from the unit matrix is given by:

$$\underline{\underline{M}}_b^{i\pm1} = \begin{pmatrix} \ddots & & & & & & \\ & 1 & 0 & -\alpha & 0 & 0 & 0 \\ & 0 & 1 & 1+\alpha & 0 & 0 & 0 \\ & 0 & 0 & -\alpha & \alpha & 0 & 0 \\ & 0 & 0 & \alpha & -\alpha & 0 & 0 \\ & 0 & 0 & 0 & 1+\alpha & 1 & 0 \\ & 0 & 0 & 0 & -\alpha & 0 & 1 \\ & & & & & & \ddots \end{pmatrix} \quad . \tag{2.16}$$

The two nontrivial columns are at position $i-1$ and i. Matrix (2.16) is the only connection between the left and right part of the avalanche, since the toppling operators for the two branches commute pairwise with each other for different branches.

Of course, surplus columns and rows of the nontrivial blocks have to be removed in any case, when the toppling site is located at or near the boundary of the system.

As in the case of 3 or 4 sites, we are interested in the attractors of the system, and possibly in the recurrent configurations for periodic orbits.

In principle, there exists a closed expression for the latter, though it cannot be evaluated completely. Using the original representation of states, $\underline{z}$, each following configuration is calculated by alternating the two basic ingredients, an avalanche and the external growth. The transition from a given state to the following one is described by

$$\underline{z}(n+1) = \underline{\underline{A}}_n \underline{z}(n) + g_n \underline{d} \quad . \tag{2.17}$$

As before, $\underline{z}(n)$ is the state of the system in the n-th time step, just as $\underline{\underline{A}}_n$ denotes the avalanche operator in the n-th time step, (neglecting the arguments about the beginning and the endpoints of the toppling sequence). g_n is the amount of energy to be put into the system to obtain the next unstable configuration, and the vector $\underline{d} = (1, 1, \dots, 1)^T$ contains only unit entries to describe the uniform growth.

Because of the growth phases, a sequence of avalanches is not only a successive application of avalanche operators. Instead, starting with a first state $\underline{z}(1)$, the n-th configuration is determined by

$$\underline{z}(n) = \prod_{i=1}^{n} \underline{\underline{A}}_i \underline{z}(1) + \sum_{i=1}^{n} \left(\prod_{s=1}^{i} \underline{\underline{A}}_s \right) g_s \underline{d} \quad . \tag{2.18}$$

If $\underline{z}(1)$ is part of a periodic attractor, it turns up again after, say, N avalanches, where N is the length of the period (measured in avalanches, not topplings). Since $\underline{z}(N) = \underline{z}(1)$, we can recast equation (2.18):

$$\underline{z}(1) = \left(\underline{\underline{1}} - \prod_{i=1}^{N} \underline{\underline{A}}_i \right)^{-1} \left[\sum_{i=1}^{N} g_s \left(\prod_{s=1}^{i} \underline{\underline{A}}_s \right) \right] \underline{d} \quad . \tag{2.19}$$

The interesting configuration seems to be separated. But equation (2.19) is an implicit expression, since the right hand site contains N a priori unknown parameters, the energies g_s, which depend in each update step on the state itself and on subsequent configurations.

Exploiting the boundedness of the g_s (and the z_i) and general properties of the avalanche operators $\underline{\underline{A}}_n$, of their products, and of the OFC system [5] could be used to examine expression (2.19) further. Otherwise, for example, one could construct a configuration in the form $(\tilde{z}, \tilde{z}, \ldots, \tilde{z}, 0, \alpha + \alpha^2)^T$ or similar, analogous to the small systems in section 2.1.3 in order to gain some more insight into the dynamics of the chains. But these are tedious tasks and I did not follow that path. Moreover, we have already an approach at hand, which completely avoids the growth and its pitfalls. Although the properties of the states within a periodic cycle cannot be determined explicitly, the representation of chains as reduced state vectors and the notations (2.14) and (2.15) (and probably (2.16)) for subsequent topplings allow for a full classification of attractors. This classification is presented in the remaining parts of this section.

Suppose, a recurrent configuration, $\underline{z}_r$, as part of a periodic attractor was already found. A disturbed state, $\underline{z}_d$, is constructed by adding a small deviation, $\delta\underline{z}$. The reduction operator (2.10) acting on the disturbed state yields:

$$\underline{x}_d = \underline{x}_r + \delta\underline{x} \quad . \tag{2.20}$$

$\delta\underline{x}$ is assumed to be small enough that the disturbed configuration has the same toppling sequence as the unperturbed recurrent state, at least until one cycle of the period is complete.

In the following, it is discussed what happens to the small perturbation. Since a single toppling (an avalanche of size 1) consists only of adding a constant vector (2.13) to each state $\underline{x}_r$ and $\underline{x}_d$, the difference between the states will not be affected by isolated toppling events.

The evolution of $\delta\underline{x}$ (that is, the evolution of the difference of difference vectors) depends only on avalanches of size 2 or larger. Thus, in order for the perturbed state to approach the periodic cycle again, the largest eigenvalue of a series $\underline{\underline{S}}$ of matrices

[5] e.g. the $\underline{\underline{A}}_n$'s are projectors, products of $\underline{\underline{A}}_n$'s cumulate powers of α, and the shortest period is at least as long as the system size when each site topples once.

of the form (2.14) and (2.15) (and probably (2.16)) must be smaller than unity. Then the disturbance vector $\delta\underline{x}$ is decreased in every cycle. If the largest eigenvalue of

$$\underline{\underline{S}} = \underline{\underline{M}}^{i(N)}_{\nu(N)} \underline{\underline{M}}^{i(N-1)}_{\nu(N-1)} \cdots \underline{\underline{M}}^{i(2)}_{\nu(2)} \underline{\underline{M}}^{i(1)}_{\nu(1)} \tag{2.21}$$

is larger than one, the periodic orbit is unstable, and cannot be an attractor of the system. In equation (2.21), N denotes the number of matrices during the periodic cycle, $\nu(p)$ can be r, l or b, depending on the direction of the p-th induced toppling (to the left or to the right or in both directions) and $i(p)$ gives the nontrivial column in the p-th matrix (the first of the two, when the avalanche has two branches).

The matrix $\underline{\underline{S}}$ is obtained by starting with the unit matrix, and successively multiplying matrices $\underline{\underline{M}}^i_r$, $\underline{\underline{M}}^i_l$, and $\underline{\underline{M}}^i_b$ in the appropriate order.

The effect of $\underline{\underline{M}}^i_l$ or $\underline{\underline{M}}^i_r$ on any matrix is that row number i or $i-1$ is added to three neighboring rows (multiplied by a factor $(1+\alpha)$ or $\pm\alpha$, respectively). The said row itself is multiplied by $-\alpha$. In an expansion in powers of α and to order $\mathcal{O}(\alpha^0)$ the matrices $\underline{\underline{M}}^i_l$ and $\underline{\underline{M}}^i_r$ simply add one row to a neighboring row and replace the original row i (or $i-1$) with zero entries ($\underline{\underline{M}}^i_b$ adds two rows to their adjacent rows and leaves two neighboring rows with all entries being zero). If the induced toppling affects a site at the border of the system, all the unit entries that have been in the boundary row are flushed out of the system. We will see below (when discussing the marginally stable attractors in section 2.2.1.1) that the non vanishing unit entries in the original unit matrix on the very right of the product $\underline{\underline{S}}$ are all collected in the same row after a sufficient number of matrices $\underline{\underline{M}}^i_\nu$ has been applied, or that there is no such row left at all.

This argument is still valid, if we take higher order terms in α into account. Only polynomials with alternating signs for subsequent powers of α appear, due to the opposite signs for the terms of the next-to-leading order of $\mathcal{O}(\alpha)$ in adjacent rows, They do not result in sums larger than or equal to unity (as was the case for the maximal package transferred between neighboring sites, see equation (1.16) and its derivation). The only term, which is larger than unity, is $(1+\alpha)$, but since a just toppled site cannot topple again, before at least one of its neighbors has toppled in-between, this term is multiplied by several factors α before the next term $(1+\alpha)$ has to be taken into account. Thus, the leading term is of order of $\mathcal{O}(\alpha)$ at most. It is not necessary that the induced toppling of one of the neighbors takes place directly after the one under consideration, because the matrices describing topplings of sites at least two positions apart commute.

Of course, it is not given a priori that any site is subject to such an induced toppling. Indeed, there are instances, where not every site takes part in a (large) avalanche, but each occurring toppling of that certain site is either an isolated single toppling event or the starting point of a (larger) series of topplings. Nevertheless, if the latter case occurs, the largest eigenvalue of $\underline{\underline{S}}$ need not necessarily be as large as $1+\alpha$, since this is an off-diagonal element.

We now have all the necessary ingredients at hand to accomplish the classification of the different types of attractors for the OFC model in one dimension. All of the just to be described types already occur in systems of size $L = 4$, but they are also observed in larger systems. The discussion of the first class of attractors takes a little longer, but once the details have been explained, the remaining types are presented even faster.

2.2.1.1 Marginally stable attractors

These attractors occur, if the largest eigenvalue of $\underline{\underline{S}}$ is exactly 1. This is one example of the just above-mentioned scenario.

The product (2.21) contains no matrix $\underline{\underline{M}}_l^i$ or $\underline{\underline{M}}_r^{i+1}$. Sites $i+1$ and i never cause each other to topple. There is no avalanche that includes simultaneously site $i+1$ and site i. The two subsystems to the left and the right of site i are decoupled.

One can think of that as a *barrier* between sites $i+1$ and i. The total amount of the energy packages that site $i+1$ gives to site i during one period is identical to the total amount of energy that site i gives to site $i+1$.

Generally, marginally stable attractors are observed, when a column i of the matrix $\underline{\underline{S}}$ is identical to the unit vector, $\underline{e}_i$, which is just the case, if the matrices $\underline{\underline{M}}_l^i$ and $\underline{\underline{M}}_r^{i+1}$ are missing. Then, the original column i of the unit matrix is unaffected by the toppling series $\underline{\underline{S}}$. $\underline{e}_i$ is an eigenvector of $\underline{\underline{S}}$, and adding a small multiple $\epsilon\underline{e}_i$ to the periodic orbit gives again a periodic orbit with the same toppling sequence. In the original language and in terms of the energies z_j, this means that increasing or decreasing all energy values z_j with $j \leq i$ by a small amount results again in a periodic orbit.

For $L = 4$, this barrier is always in the middle of the system and one regime of the marginally stable attractors corresponds to the realization P_2 of the smallest possible period given in (2.7) with the corresponding state (2.8). There, the separation of the two decoupled subsystems was covered in the free value $\tilde{z} \in [\alpha + \alpha^2, 1]$ for the energy values in one of two subsystem.

For larger system sizes, the barrier need not be in the middle, but it is often found at the center of a system, (since the synchronization proceeds at constant speed from the boundaries, see below in section 2.3, where the synchronization process is thoroughly explained).

Sites i and $i+1$ to the right and left of the barrier must topple equally often during one period. If this was not the case, and if site i toppled more often, there would be an instance, where site i topples twice without site $i+1$ toppling in-between. After site i has toppled for the first time, its energy value is zero, and that of site $i+1$ is at least as large as α. In order for site i to reach the threshold before site $i+1$, it must receive a package from its left neighbor that is larger than α, while site $i+1$ receives no package. The largest possible package size is $p_{\max} = \alpha/(1-\alpha)$ (see equation (1.16)). For site i to reach the threshold, the missing energy $1 - p_{\max}$ has to be provided by the external growth, because site i cannot receive energy stemming from another toppling: neither from site $i+1$, by construction, nor from the left site, since its toppling already delivered a maximal package and reset site $i-1$ to zero. There is no way for the left neighbor to catch up with site i. Therefore site $i+1$ has at least the energy $1 - p_{\max} + \alpha = 1 - \alpha^2/(1-\alpha) > 1 - \alpha$ at the moment where site i reaches the threshold for the second time. This implies that site $i+1$ is lifted above the threshold by the toppling of site i, since the minimal package is just α, in contradiction to the assumption that there is a barrier between the two sites. Thus, the two sites must topple equally often.

We have seen there can be a barrier in the system. This barrier arose due to the fact that not all the 1's from the unit matrix are removed by subsequent topplings. Can there be a second barrier? And if not, what prevents the existence of several decoupled subsystems?

Actually, there exists no attractor with 2 or more barriers. This is shown in two steps.

First, let us assume that all energy packages passed over the barriers are of size α. Then, the region between the two barriers behaves like a system with periodic boundary conditions, and no package passed on within this region is larger than α. The two sites immediately outside the barriers must not be lifted above the threshold by their neighbors. Otherwise, they would pass packages larger than α over the barrier.

Furthermore, the two sites immediately outside the barriers must not topple more often than the sites between the barriers, which would break the periodicity of the inner region. To prevent this, the sites to the left and the right of the barriers are not allowed to receive packages larger than α from their outward neighbors. Otherwise, there would be a moment in time (after $1/\epsilon$ cycles, when the neighbors receive a package of size $\alpha + \epsilon$ per cycle), when they topple a second time in-between the topplings of the inward barrier.

This implies that the sites immediately outside the barriers in fact also belong to the domain of sites that are never lifted above the threshold, and which always receives packages of size α. By repeating this argument, we find that no site in the system at all can be lifted above the threshold. However, this situation cannot be realized within open boundaries. It occurs for periodic boundary conditions.

Now, since we have ruled out the possibility that the region between the two barriers receives only energy packages of size α from outside, let us assume next that they receive on average packages larger than α.

This setup is similar to a system with periodic boundary conditions, with one site being driven faster than any other site. The faster site is located just between the two boundary sites of the original chain, and it adds the extra packages larger than α. The examination of small systems has shown that the faster of two sites is always triggered by the slower one ([Mid95] and section 2.1.1). Adapted to the chain with extra energy input at the boundaries, this finding implies that the fictitious site outside the boundaries suffers induced topplings from within in order to stabilize the inner region. This resembles a contradiction, because the barrier site by assumption never triggers its outer neighbor.

Further numerical evidents for the impossibility of two barriers is given by simulating the region between the two barriers. Whenever a site at the boundary of that region has toppled, packages of size larger than α are inserted in the sites directly at the boundary. this leads to attractors where avalanches are triggered at the center of the system and are running outwards (which is just the mechanism to trigger the outer site). The attractors and therefore the number of topplings per unit time of the boundary site are determined by the size of the region and the size of the packages received from outside. On the other hand, this number of topplings must be identical to the number of topplings of the site on the other side of the barrier in the original system. However, there is no free continuous parameter left to match this condition, and it can therefore usually not be satisfied. This problem does not arise in the case of a single barrier, because the state of the system can be symmetric about the barrier, thus satisfying the matching conditions.

Finally, let us consider a periodic orbit at the boundary of the basin of attraction of the marginally stable attractors. In order to obtain this orbit, we increase or decrease all force values z_j with $j \leq i$ by an amount such that there is a moment in time where site i (or $i+1$) is lifted by site $i+1$ (or i) exactly to the threshold. The meta stable orbit has now become degenerate with an orbit where site i (or $i+1$) is lifted by site $i+1$ (or i) infinitesimally above the threshold. This orbit has no barrier, and the matrix

$\underline{\underline{S}}$ corresponding to this periodic orbit is different from the one corresponding to the meta stable orbit. Its largest eigenvalue will therefore be different from 1. Realizations of the interesting case, for which the largest eigenvalue becomes smaller than unity, are observed numerically.

This means that the periodic orbit that is at the boundary of the basin of attraction of the marginally stable attractors can itself be an attractor that is reached from a non vanishing set of initial conditions.

2.2.1.2 Strongly stable attractors

We have just seen that there exists at most a single row in the matrix $\underline{\underline{S}}$ containing unit entries, which correspond to the barrier in the system. Any given site of the system is reached by an avalanche that starts near the boundary, and therefore there cannot be 1's left in different rows. The marginally stable attractors have all 1's in a row i, where they stay forever. However, there is also the possibility that all the 1's are flushed out of the system by avalanches that extend from inside the system to the boundary. In this case, the largest eigenvalue of $\underline{\underline{S}}$ is of the order of α or even smaller, and the attractor is quickly approached. Many examples of such strongly stable attractors are observed.

2.2.1.3 Weakly stable attractors

If not all 1's are flushed out of the system, and if there is no barrier in the system, the largest eigenvalue of $\underline{\underline{S}}$ belonging to an attractor is $1 - \mathcal{O}(\alpha^n)$ with some large positive power n of α. This corresponds to the situation where the row containing the 1's remains in the system and is moved around by avalanches coming from both directions. If α is small or n is large, attractors are approached very slowly. For $\alpha = 0.2$, there are attractors with $n = 2$ for $L = 4$ and an estimated $n = 11$ for $L = 20$. However, I did not attempt a systematic survey of relaxation times towards the attractors as a function of the coupling α and the system size L.

2.2.1.4 Complex attractors

There exist attractors with strikingly long periods of the order of many thousands of topplings, even for small systems with $L = 4$, and still much larger for larger values of L. Typically, these attractors contain long quasi-periodic sections where the sequence of avalanches remains the same but the energy values change slowly, just as one would expect close to a weakly stable or weakly unstable periodic orbit. This quasi-periodic sequence is eventually interrupted by an intermittent phase containing other avalanches, until the quasi-periodic phase is entered again.

It was this behavior, which led to the beat-like-effect for a system of four sites, when the length of the attractors were determined numerically (see section 2.1.3 above).

One can understand the origin of such complex attractors in the following way. Imagine a weakly stable attractor for a certain value of α. Now change α slowly, and let the system follow adiabatically. The largest eigenvalue of $\underline{\underline{S}}$ on the resulting attractor will have the same coefficients, if expanded in powers of α, as long as the avalanches remain the same. Eventually, a value of α will be reached where two avalanches merge or an avalanche splits, changing the product of $\underline{\underline{M}}^{i(p)}_{\nu(p)}$ matrices, which now can have an eigenvalue larger than 1. Nevertheless, there may still be a region nearby in state space where the old sequence of avalanches can be maintained for a long time if the

largest eigenvalue of $\underline{\underline{S}}$ of the old attractor was only slightly smaller than 1, i.e. if the old attractor was weakly stable.

Now the possible occurring attractors are all understood, either in terms of the original chain, or using the language of the reduced states, and the classification is done. We now proceed with further analytical results concerning the overall toppling behavior of the sites.

2.2.2 The toppling profile

This section considers the toppling behavior of the sites in the one-dimensional OFC chain. The toppling mechanism couples neighboring sites, and hence all the sites in the system, especially as their energy balance is concerned. The current section's aim is to derive the average number of topplings per site as a function of the site's position, and to investigate the effect of the coupling on this toppling profile. The profile is derived for the stationary state.

For a system of L sites, there exists a total of L coupled local balance equations. These equations relate the total input of energy at any given site with the amount of energy lost due to the toppling mechanism. The topplings, in turn, add to the energy input of neighboring sites.

As in the previous section, we have to discern between induced topplings, and topplings that trigger an avalanche. For the latter, the amount of transferred energy is exactly of size α, and the local loss of energy is exactly 1, since the triggering site's value is reset from the threshold to zero. On the other hand, energy values can temporarily exceed unity for induced topplings, and therefor transferred packages can be larger than α, and the local loss is no longer determined to be exactly one.

At least for the stationary state, by far most of the avalanches are single toppling events, as will be discussed in section 2.3.2. Even in avalanches larger than one toppling, subsequent topplings lead to energy packages, which are only slightly larger than α, because relaxing sites lift their neighbor almost exactly at the threshold or marginally above the threshold. Bear in mind, this is definitely not true during the transient evolution of the system, which is essentially driven by the nonlinear toppling rule.

For totally uncorrelated sites, the average package size stemming from induced topplings would be given by $\alpha + (1/2)\alpha^2$, since a subsequent toppling requires former energy values in the interval $[1-\alpha, 1]$, and for uncorrelated sites, the energies are equally distributed in this interval. Although the real physical sites are not independent, a similar power law expansion of the average package size in α still holds. Moreover, the estimate above neglects single topplings, which further diminish the relative contribution of larger packages to the average value.

Figure 2.5 compares the average package size as a function of α to the smallest possible package of size α. The packages are given in absolute values, and the average is taken not only over distinct stationary systems, but also over all the sites in a chain. Later on we will see, there actually exists a certain dependency on the position with a pronounced structure near the boundaries (section 2.3.2). For the current discussion, we put on record that the packages are almost indistinguishable from α for small values of the coupling, and deviate considerably from the least possible package only for large couplings.

Figure 2.6 presents the average excess package for clearer visualization of the behavior for small α. Only that part of the packages that is larger than α is shown for

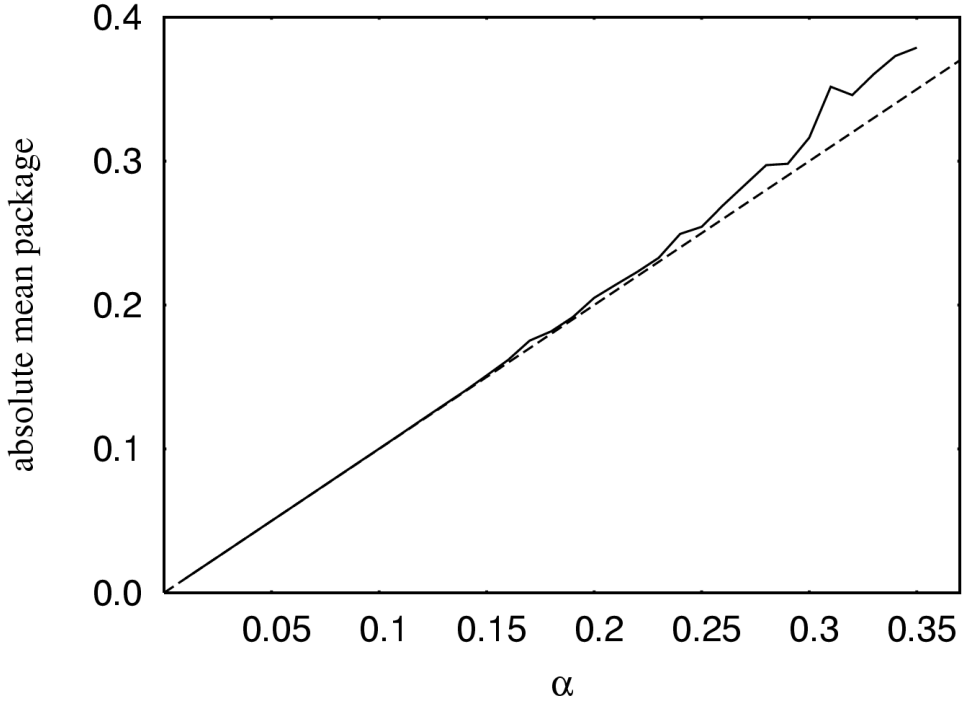

Figure 2.5: Average *absolute* size of packages $\bar{\alpha}$ as function of the coupling parameter α (solid line), averaged over hundred stationary systems of size $L = 128$ and 10^4 topplings per site; dashed line corresponds to the identity $f(\alpha) = \alpha$.

two different system sizes and on a log-log plot. To be concise, we consider $(\bar{\alpha} - \alpha)/\alpha$ as a function of the coupling, where $\bar{\alpha}$ denotes the average package size.

First, for decreasing α, the relative excess package decreases as well (the absolute excess value decreases even faster).

Second, we observe the overall less excess package size for the larger system. This result is due to the separation between small avalanches and system-wide avalanches. Their ratio increases for larger systems (as shown in section 2.3.3), i.e. the weight of single topplings increases with the system size, and hence the average package $\bar{\alpha}$ approaches the real α with increasing L.

As a third and minor point I remark on the rich structure in the range of large couplings. The large deviations between nearby values of α seem to come from the different possibilities how to distribute multiples of the smeared out quasi-particles within the unit interval $[0, 1]$ for stable systems (this will be discussed in detail in section 2.3).

Combining the observations, the following assumptions are used in the derivation of the toppling profile:

There exists a constant mean package size $\bar{\alpha}$, which is the same for all the sites and which is particularly independent of the site's position in the chain. In leading order, the behavior of $\bar{\alpha}$ as a function of the coupling is given by

$$\bar{\alpha} \sim \alpha + (1/L)\mathcal{O}(\alpha^{\omega}) \quad , \tag{2.22}$$

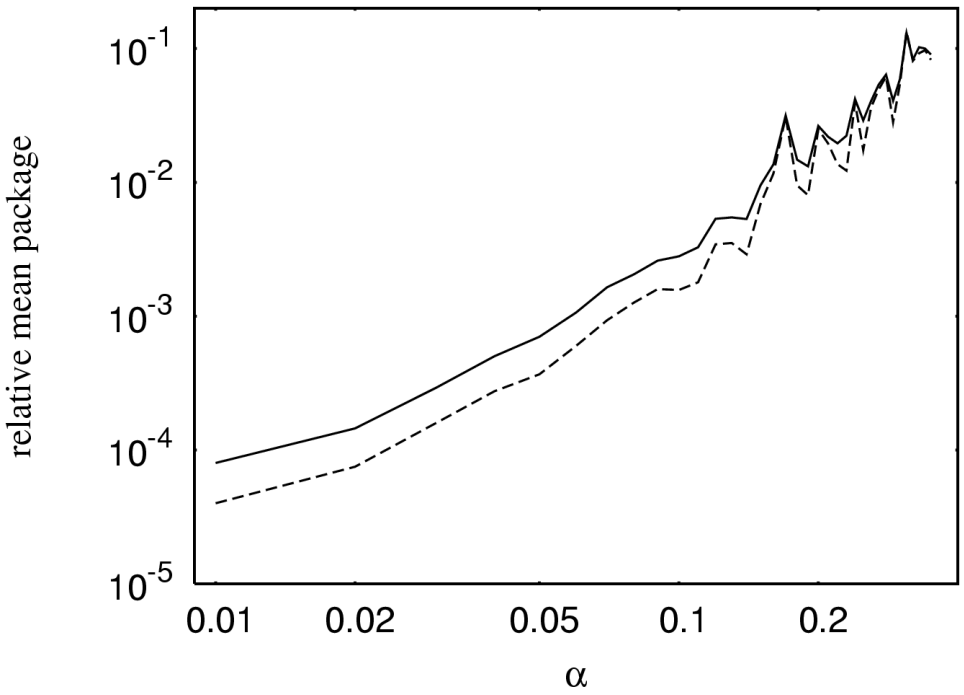

Figure 2.6: Average *relative* size of excess packages $(\bar{\alpha} - \alpha)/\alpha$ as a function of α for two different system sizes $L = 64$ (solid line) and $L = 128$ (dashed line). Statistics as in figure 2.5.

for some positive $\omega \approx 2$. The prefactor of the next-to-leading order decreases with increasing system size and vanishes for infinite system sizes. $\bar{\alpha}$ approaches α for $\alpha \to 0$ and $L \to \infty$.

The average loss of energy, $\bar{l}$, at a given site i corresponds to the total loss at that site divided by the number of topplings of site i. Just as $\bar{\alpha}$ asymptotically reaches α, this loss is unity for $\alpha \to 0$, and will be slightly larger than 1 for non vanishing α. Each toppling of a site increases the energy balance of neighboring sites by an amount of $\bar{\alpha}$, and diminishes the current site's balance by one such loss unit. Using the same argument as for the average package, we expand

$$\bar{l} \sim 1 + \mathcal{O}(\alpha^{\omega'}) \quad , \tag{2.23}$$

with another positive exponent ω', and in the following we set $\bar{l}$ exactly to unity, which allows for an identification of the total loss per site with the (integer) number of topplings per site.

At a certain moment in time, for which the current value of site i should be given by F_i, the overall energy input at that particular site consists of the initial value I_i, the total external growth (summed up over all time steps), and all the packages received from toppled neighbors. By increasing the time over which the average is taken, the constant difference $I_i - F_i$, which is of order $\mathcal{O}(1)$, can be neglected compared to the ever-increasing internal or external input of energy.

Intuitively, sites at or near the boundary should topple comparatively less often than sites in the center of the system. This toppling difference is due to the missing neighbor of sites at the boundary. On average, they receive less packages and topple less often, resulting in less packages for their neighbors in turn. On the other hand, nearby sites deep in the system should topple roughly the same number of times. Now, what is the average number $\langle t \rangle_i$ of topplings per site and unit time as function of the site index i?

Setting the total external energy input to be $\bar{g}$, taking the average loss per toppling to be unity, and assuming a position independent mean package $\bar{\alpha}$, the local balance equation is given by

$$\bar{g} + \bar{\alpha}\,(\,\langle t \rangle_{i-1} + \langle t \rangle_{i+1}) = \langle t \rangle_i \quad , \tag{2.24}$$

for each site i. The boundary conditions, $\langle t \rangle_0 = \langle t \rangle_{L+1} = 0$, correspond to the missing outer neighbors. Equation (2.24) can be written in matrix form:

$$\langle \underline{t} \rangle = \bar{g}\, \underline{\underline{\Gamma}}^{-1}\, \underline{d} \qquad , \tag{2.25}$$

where $\underline{\underline{\Gamma}}$ is tridiagonal and given by

$$\underline{\underline{\Gamma}} = \begin{pmatrix} 1 & -\bar{\alpha} & 0 & \dots & 0 \\ -\bar{\alpha} & 1 & -\bar{\alpha} & & \\ \vdots & & \ddots & & \vdots \\ & & -\bar{\alpha} & 1 & -\bar{\alpha} \\ 0 & \dots & & -\bar{\alpha} & 1 \end{pmatrix}_{L \times L} \qquad , \tag{2.26}$$

and $\underline{d}$ is a vector with constant unit entries as in (2.17).

For a given system size, L, a solution for equation (2.25) can be found by (numerically) inverting the matrix $\underline{\underline{\Gamma}}$. An example for this is given in figure 2.7 for $L = 30$. There, the result of such a matrix inversion is compared with the average topplings, as obtained by numerical simulation of the chain, and an analytical solution to be explained now. A detailed discussion of figure 2.7 is presented afterwards.

The analytical solution can be derived by making a continuum approximation of equation (2.24). The difference quotient $\langle t \rangle_{i-1} - 2\langle t \rangle_i + \langle t \rangle_{i+1}$ is replaced with the second derivative, and the mean number of topplings as a function of the integer site i becomes a continuous function, $t(x)$, of a continuous position x. We then obtain a boundary-valued problem with the following associated differential equation for the sought function $t(x)$:

$$\frac{d^2 t(x)}{dx^2} = \frac{1 - 2\bar{\alpha}}{\bar{\alpha}} t(x) - \frac{\bar{g}}{\bar{\alpha}} \quad . \tag{2.27}$$

The corresponding boundary conditions could be taken to be $t(0) = t(L) = 0$, analogous to the real boundaries of the chain. Choosing another set of boundary conditions yields a more suitable solution. Shifting the whole chain by half its length, $l = L/2$, along the x axis, gives a system symmetric to the origin. Of course, the differential equation (2.27) is still valid, and the boundary conditions now read $t(-l) = t(l) = 0$. The solution that satisfies the boundary conditions is

$$t(x) = g \left(1 - \frac{\cosh(\kappa x)}{\cosh(\kappa l)} \right) , \tag{2.28}$$

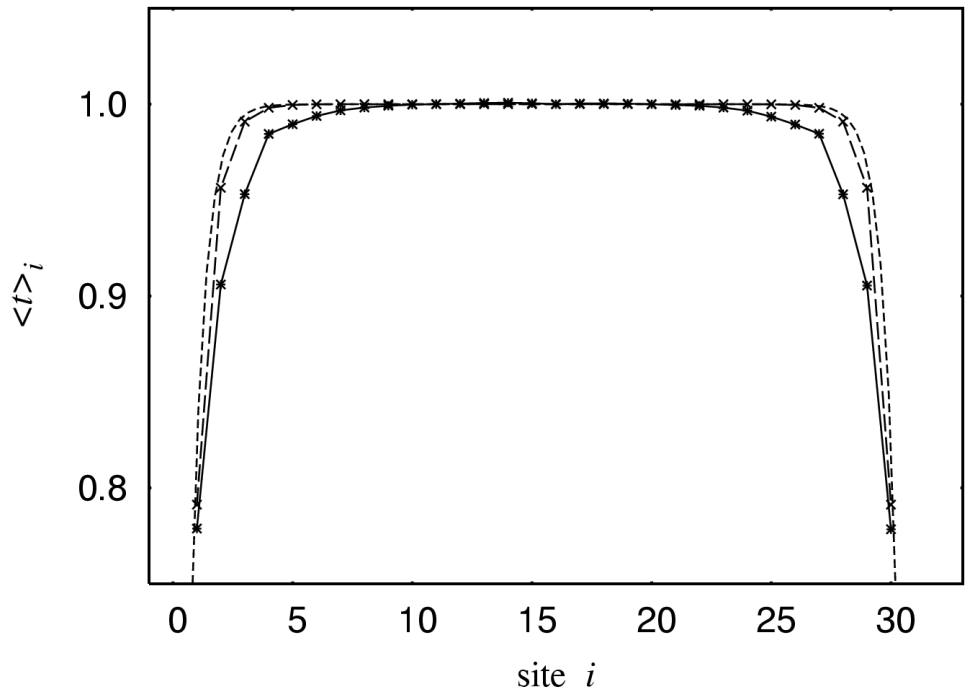

Figure 2.7: Toppling profile for a one-dimensional OFC system for $L = 30$ and $\alpha = 0.2$ as function of the site index i. Solid line with stars: numerical result obtained by averaging over 1000 different stationary systems for 10^4 topplings per site. Dashed line: Analytical solution (2.28) of the continuous approximation. Long dashed line with crosses: solution obtained by numerically inverting the matrix (2.26).

where two shortcuts are introduced:

$$g = \frac{\bar{g}}{1 - 2\bar{\alpha}} \tag{2.29}$$

measures the total external input, $\bar{g}$, in multiples of the unit growth increment of $1-2\bar{\alpha}$. This growth unit mirrors the fact that each toppling consumes on average one energy unit. At some time between two successive topplings of the same site, this site receives two packages $\bar{\alpha}$ from toppled neighbors and the missing amount of energy has to be provided by the external source.

The second shortcut,

$$\kappa = \sqrt{\frac{1 - 2\bar{\alpha}}{\bar{\alpha}}} \quad , \tag{2.30}$$

is a kind of inverse penetration depth or inverse decay length, i.e. it can be thought of as a measure for the thickness of the boundary layer, in the sense of how far into the system there is still a notable influence of the boundary. I want to emphasize that κ is independent of the system size and depends only on the coupling α. This finding is further confirmed in section 2.3.

As visible in figure 2.7, the thickness of this boundary layer is underestimated by both analytical methods, the inversion of the tridiagonal matrix $\underline{\underline{\Gamma}}$ for the integer case, and the continuous solution (2.28) of equation (2.27). This is a consequence of the approximation that $\bar{\alpha}$ is a constant throughout the system. Note that both analytically derived lines have the same characteristic shape.

The numerically obtained toppling profile in figure 2.7 (solid line with stars) was normalized such that the mean number of topplings in the center of the system equals unity. Accordingly, g in equation (2.28) was chosen to be 1 as well, and the continuous function $t(x)$, a valid solution in the interval $[-L/2, L/2]$, was re-shifted by $L/2$ for comparison. $\bar{\alpha}$ was assumed to equal $\alpha = 0.2$ for the matrix inversion. The calculated data points had to be multiplied by a factor 0.6 to match the plateau in the center. This factor is just the inverse of the standard growth unit $1 - 2\bar{\alpha}$ for $\bar{\alpha} = 0.2$.

We will come back to the stationary properties of the one-dimensional OFC system in section 2.3.2. This section closes with a remark on the limiting cases of the analytical solution. The differential equation (2.27) is not valid for $\alpha = 0$. In fact, it even cannot be derived properly. The balance equation (2.24) takes on a form $\bar{g} = \langle t \rangle_i$ for vanishing coupling. Each site topples as often as it is fed an energy unit from the outside, independent of its position in the chain. Nevertheless, for $\alpha \to 0$ but $\alpha \neq 0$, equation (2.27) holds, and κ diverges as $\kappa \sim \sqrt{1/\alpha}$. Then, the *cosh* terms can be approximated with simple exponential expressions:

$$\begin{aligned} t(x) =& g\left(1 - \frac{\cosh(\kappa x)}{\cosh(\kappa l)}\right) = g\left(1 - \frac{\exp(\kappa x) + \exp(-\kappa x)}{\exp(\kappa l) + \exp(-\kappa l)}\right) \\ \sim& g\left(1 - \frac{\exp(\kappa x)}{\exp(\kappa l)}\right) = g\left(1 - \exp[\kappa(x - l)]\right) \end{aligned} \tag{2.31}$$

This approximation is valid, as long as x is positive. Note that l is always larger than zero, and the exponentials with $-\kappa$ tend to zero for diverging κ. For negative x, the other exponential term in the numerator survives, but the same expression (2.31) is obtained, and the following argument applies for both cases, since the extra minus sign in x is then cancelled by the minus sign stemming from the negative exponent. In the above form, x takes on values in $[0, l]$, where l stands for the outermost missing neighbor on the right, and one obtains correctly $t(l) = 0$. For any other value of x, the resulting exponent is negative and large. In fact, the whole exponential expression is non-analytical for $\alpha \to 0$ as

$$\sim \exp(-\frac{1}{\sqrt{\alpha}}) \quad . \tag{2.32}$$

However, the remaining term approaches zero faster than any power in α, and in leading order the mean number of topplings is determined by the external input only, just as for the discrete balance equation, since g itself is given by $\bar{g}$ for vanishing $\bar{\alpha}$ (see equation (2.29)).

2.3 Numerical results

This section presents simulation results for larger systems. The findings that were obtained by using the analytical approaches as discussed in the previous sections, are confirmed, and evidence missing until now for claimed properties is given. A complete understanding of the OFC systems in one dimension will be achieved by combining the gained insights of both ways to investigate the model.

On several occasions the importance of the stationarity of the systems was already mentioned. It should be the aim of every theory to establish an understanding of the final behavior of its subject. However, for valid statements concerning these asymptotic features, one has to know about the transient times and its dependence on the relevant parameter of the theory.

Thus, the transition from a random initial configuration towards the stationary state is studied first, and the characteristics of this evolution are reviewed. Afterwards, the properties of the steady state are discussed in detail in section 2.3.2.

2.3.1 The transient stage

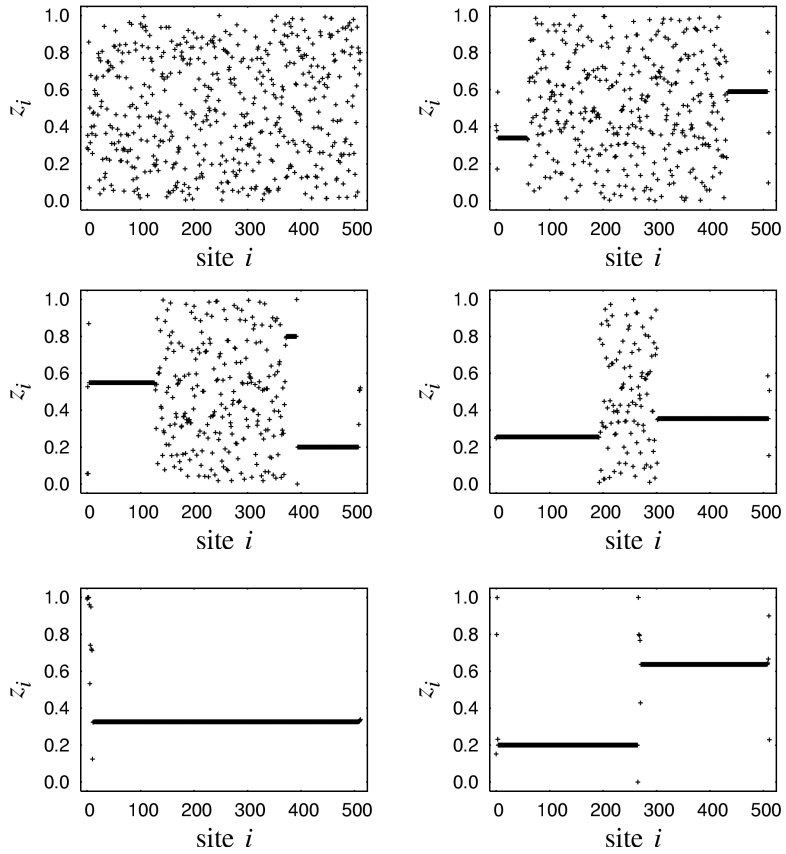

Figure 2.8: Random initial configuration and after 1400, 2800, 4200, and 5600 topplings per site in configuration space for a system with $L = 512$ and $\alpha = 0.2$ (from top left to bottom right). The two figures at the bottom represent stationary systems with different initial states, both after 5600 topplings per site. The synchronization proceeds into the system starting at the boundaries. Synchronized sites within the left (right) block need not take on the same energy value, as indicated by the bottom right figure.

Figure 2.8 shows the energy values throughout a system of size $L = 512$ at different times during the evolution towards the steady state. The most remarkable feature

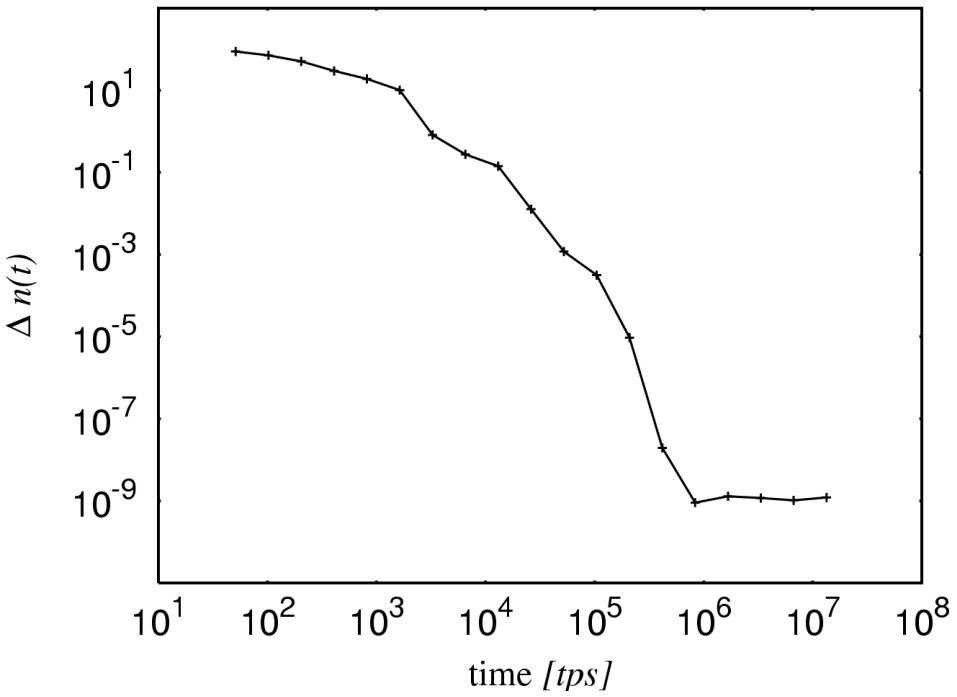

Figure 2.9: $\Delta n(t)$ as defined in equation (2.33), the difference between the stationary size distribution of avalanches and the current size distribution as a function of time, measured in topplings per site (denoted as *tps*), averaged over 100 systems for $\alpha = 0.12$ and $L = 64$. Theoretically, the final value reached after about 10^6 topplings per site should vanish. The different lengths of the time intervals over which the distributions were obtained might be the reason for the non vanishing result around 10^{-9}.

is the *synchronization* of sites, in the sense that their energies lock to the neighbors' values. One can see that starting from the boundary more and more sites become synchronized, until in the stationary state all sites within the left and/or right half of the system have almost the same energy z_i, apart from a few sites at the boundary. Note that the right block belonging to the second figure in the left column is split into two sub blocks. This feature is explained in section 2.3.2.

The two snapshots at the bottom of figure 2.8 are two different steady states, obtained by running the simulation with different initial configurations. Whether the system approaches a fully synchronized state, such that the two half systems are phase-locked to each other, or whether two independent subsystems are generated by the time evolution, depends on these random initial values. As for small systems, i.e. systems with 4 sites, the relative weight of realizations with two uncoupled subsystems is larger than that of systems with a single block of synchronized sites (see section 2.1.3). Evidence for this finding is seen in the size distribution of avalanches below.

The transient time is the number of topplings necessary to synchronize all the sites in the system. It was determined as a function of the system size L and the coupling α, and measured in the number of topplings per site. To do so, it was necessary to

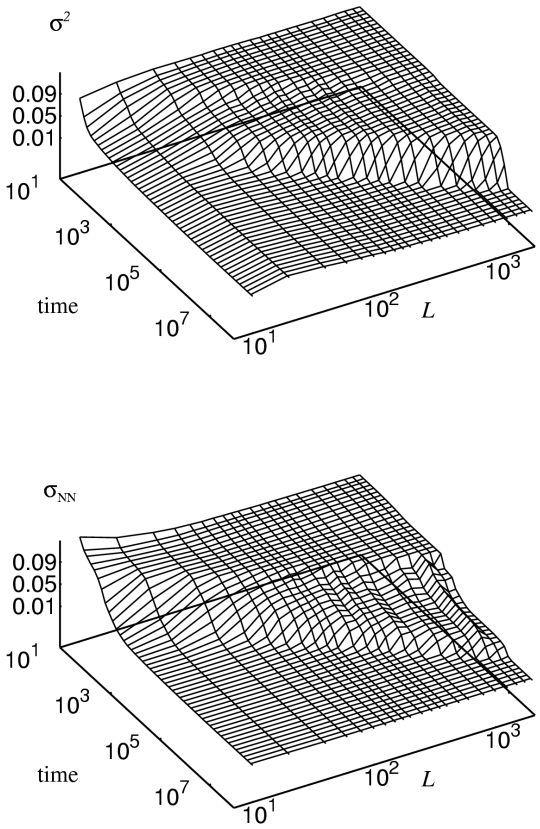

Figure 2.10: Standard deviation σ^2 (top) and nearest-neighbor deviation σ_{nn} (bottom) as defined in equations (2.34) and (2.35) as a function of the system size L for a fixed coupling $\alpha = 0.35$. Data obtained by averaging over 1000 random initial configurations. Time measured in total number of topplings.

have a convenient and reliable definition for the degree of synchronization to allow for a classification of stationarity.

In the literature it is common to examine some dynamic quantity, such as, for example, the distribution of avalanches, and to compare their characteristic shapes taken at different times. Stationarity is then observed for identical distributions or some other statistical value reaching its steady state value.

Figure 2.9 presents as an example the time evolution of the difference $\Delta n(t)$ between size distributions $c(s,t)$ and the stationary distribution $n(s)$ for $L = 64$ and $\alpha = 0.12$ averaged over 100 different initial configurations. The $c(s,t)$ are normed distributions for the current time interval t, taken for exponentially increasing time intervals. The difference $\Delta n(t)$ was calculated as the cumulative sum of the quadratic

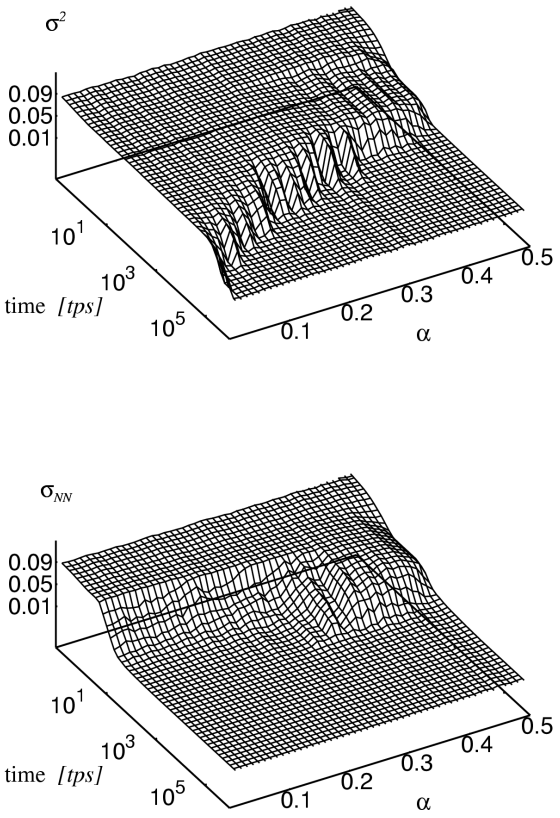

Figure 2.11: Standard deviation σ^2 (top) and nearest-neighbor deviation σ_{nn} (bottom) as defined in equations (2.34) and (2.35) as a function of the coupling α for a fixed system size $L = 200$. Data obtained by averaging over 1000 random initial configurations. Time measured in topplings per site.

deviation between $n(s)$ and the current $c(s,t)$ for each data point s,

$$\Delta n(t) = \sum_s \left(n(s) - c(s,t)\right)^2 \quad . \tag{2.33}$$

It is necessary to compare the distributions against the same final distribution each. Successive distributions could apparently be similar, but hide a slow deviation, This shortcoming is also found in the literature, where presumably stationary systems have been investigated, yielding unreliable statements (see the discussion at the end of section 3.1 for the two-dimensional model).

Of course, the just-described proceeding resembles a somewhat circular statement. Moreover, distributions have to be obtained over a certain time interval and one can never be sure, whether there will be another transition after an even longer time interval. Since it is rather easy for the human eye to rank systems by simple observation as

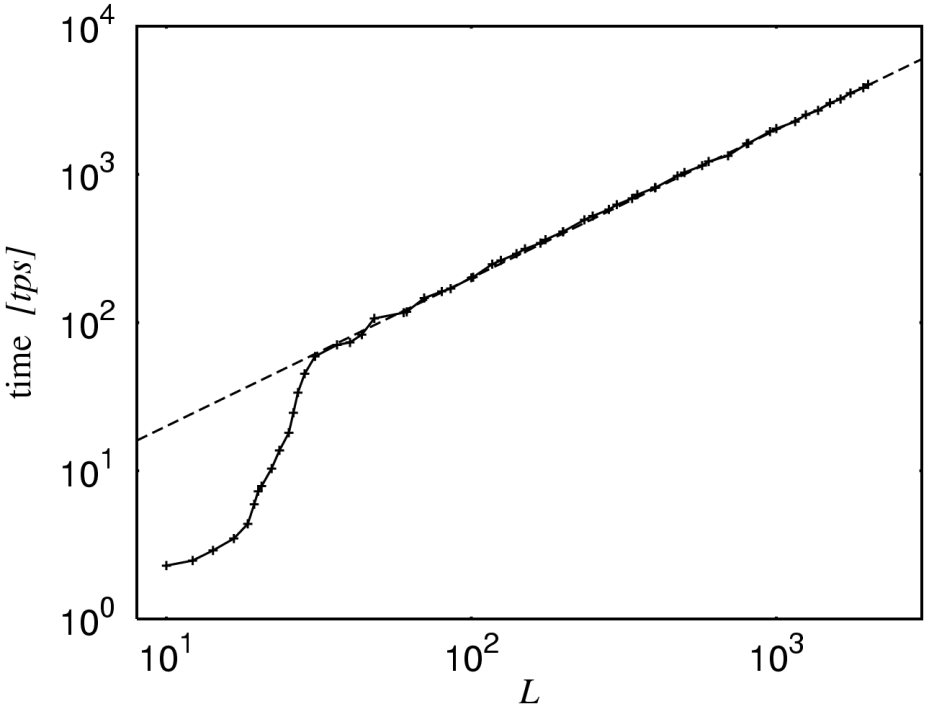

Figure 2.12: Contour along the (arbitrary) value $\sigma^2 = 0.03$ to depict the dependence of the total number of topplings in the upper figure 2.10 on the system size L for fixed coupling $\alpha = 0.35$. Dashed line corresponds to $f(L) = 2\,L$.

was done in figure 2.8, a suitable measure, which depended on the current configuration only, was required. There are two appropriate quantities:

The standard deviation

$$\sigma^2(t) = \min_{0<\tau\leq t} \left(\bar{z}^2(\tau) - \overline{z^2}(\tau) \right) \quad , \tag{2.34}$$

and the nearest-neighbor deviation

$$\sigma_{NN}(t) = \min_{0<\tau\leq t} \left(\overline{z_{NN}}(\tau) - \overline{z^2}(\tau) \right) \quad , \tag{2.35}$$

as function of α and L, where the bar denotes the average taken over all sites i, and

$$\overline{z_{NN}} = \frac{1}{N-1} \sum_{i=1}^{N-1} z_i\, z_{i+1} \tag{2.36}$$

is the average product between neighboring sites. In a sense, the nearest-neighbor deviation as defined in equation (2.35) is the correlation function for a fixed distance. The figures 2.10 and 2.11 show the results for these two synchronization measures, averaged over 1000 random initial configurations and as a function of the coupling α or the system size L, respectively. Time was either measured as the number of topplings per site, denoted as *tps*, or as the total number of topplings as in figure 2.10.

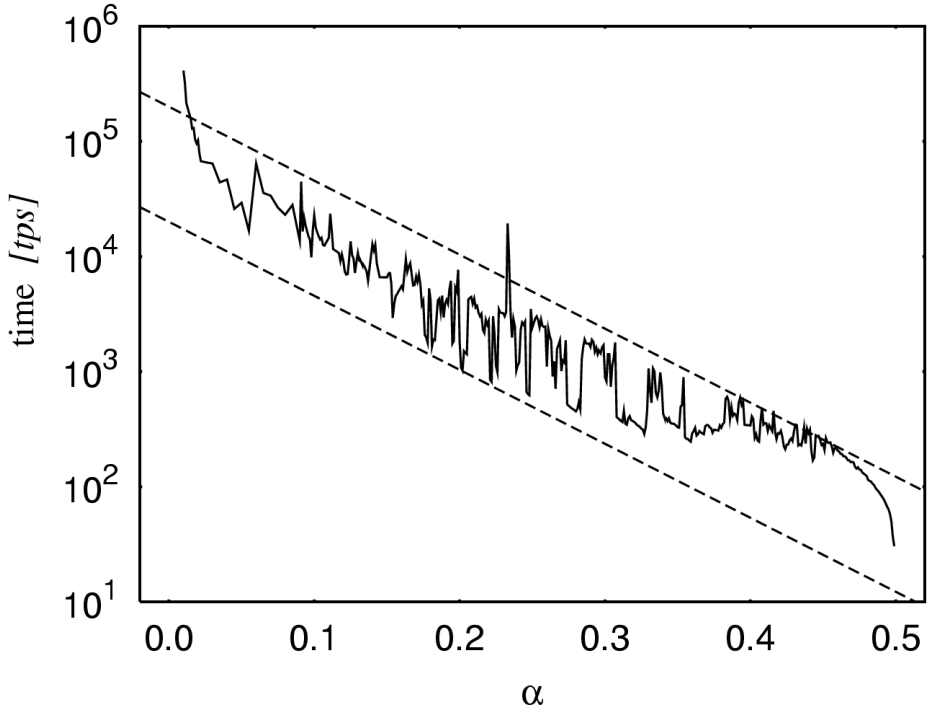

Figure 2.13: Time (measured in topplings per site) needed to reach $\sigma^2 = 0.01$ for a system of $L = 200$ sites as a function of α, averaged over 1000 different random initial systems. The peaks are real and are not statistical fluctuations. The dashed lines are proportional to $f(\alpha) = A\exp(-14.8\alpha)$ with amplitudes $A = 2 \times 10^4$ and $A' = 2 \times 10^5$ respectively.

It is necessary to take the minimum value of both measures over the time $\tau \in [0, t]$ rather than the mean value, because σ^2 and σ_{NN} are very fast oscillating functions of time, and restricting the investigation on the minimum value gives smoother data. Since the numerical simulations always begin with random and uncorrelated initial conditions, the minima decrease with time as long as the system is not yet in the stationary state. For other, more correlated initial configurations, one might have to measure the closeness to the stationary state in a different way.

In the first figure (2.10), the behavior of σ^2 (top) and σ_{NN} (bottom) is presented as a function of time and of the system size L.

The lower plateau indicates clearly the stationary state. One finds that the transient time is proportional to the system size, corresponding to a linear increase with L in a contour plot with log-log axes in figure 2.12. This result is due to the inward proceeding synchronization, which takes place at a constant rate, if L is sufficiently large. The idea suggests itself that the slope's value of 2 stems from the two sides from where the synchronization begins its journey towards the center, but this is only a mere coincidence and is not likely to occur for other values of α, besides the fact that the contour plot was taken at an arbitrary value of $\sigma^2 = 0.03$.

For small L, the boundary layer takes a large part of the system, and there is

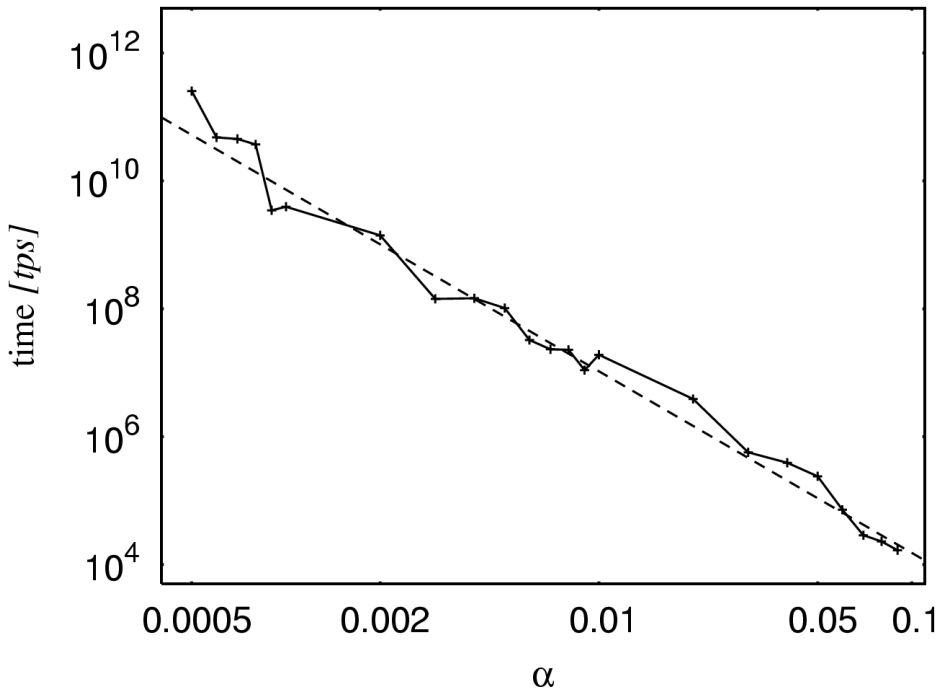

Figure 2.14: Time (measured in topplings per site) needed to generate the first avalanche of size ≥ 21 as function of α, averaged over 1000 different random initial states for systems of size $L = 50$. The straight dashed line corresponds to $f(\alpha) \propto \alpha^{-2.84}$.

therefore little synchronization visible or the transition is not as sharp as for larger systems, for which there is a clear separation between the boundary sites and the sites in the center of the system. Apart from the transition to the stationary state with a small value of σ^2 and σ_{NN}, one can also distinguish an earlier transition, where the two measures leave the value 1/12 corresponding to a random initial configuration. The interpretation of this transition is the onset of the formation of synchronized blocks, after the boundary layer has been set up. The characteristic shape of the curves between these two transitions is strikingly different. While the nearest-neighbor deviation decreases rather fast once the synchronization starts, the standard deviation remains on a second plateau until its final decrease. This feature comes from the two synchronized blocks, which usually have a different energy value, as one can see for instance in the pictures in the middle of figure 2.8.

A similar behavior is found for the dependency on α as shown in the figures 2.11 for a fixed system size $L = 200$. For values of α smaller than the critical value, below which no secondary topplings occur, $\alpha_c \sim 0.365$, the nearest-neighbor deviation depends only weakly on α. Indeed, the sharp transition at the end of the high plateau of σ_{NN} is linear in α and it denotes the number of topplings until the sites in the boundary layer organize such that the synchronization of the adjacent sites is about to begin. This time is of the order of $\mathcal{O}(10)$ topplings per site. The bulky part above α_c must be

due to the fact that a site can now topple twice during the same avalanche. While the onset of synchronization is better visible in the data for σ_{NN}, which decay very rapidly, the transition to the stationary state is much better visible in the data for σ^2, which remain close to the initial value for a longer time. A more detailed investigation of the transition time to the stationary state reveals the following:

Over a wide range of α values this transition time depends exponentially on α, as shown in figure 2.13, where the time is plotted that is needed to reach $\sigma^2 = 0.01$. Except for very small and rather large α, the graph is not very smooth, although the data were obtained by averaging over 1000 different systems for a system size $L = 200$. This signifies that the richness in the structure is not due to statistical fluctuations. Nevertheless, the general trend of the data follows an exponential decay proportional to $\sim \exp(-c\alpha)$. Two lines with $c \approx 14.8$ are added to the data in figure 2.13. The many peaks and the alternating absolute amplitudes of the data points must be an effect of the possible partitions of unity with multiples of the coupling α (see below).

For very small values of α, the data show a power law in α with an exponent around -2.84 (see figure 2.14). Since for such small couplings the synchronization proceeds extremely slowly, the exponent was not determined by evaluating systems until they reach the stationary state. Instead, the topplings necessary for an avalanche to be larger than 21 topplings for the first time was surveyed, after a sufficient number of avalanches had been discarded in the first place right after random initialization of the systems. This choice guarantees that boundary effects are overcome, because such an avalanche is larger than the boundary layer and requires a certain number of synchronized sites. Still, the systems need not be in the stationary state. There might be some not yet synchronized sites left at the center of the systems, which were never reached by large avalanches. However, the remaining synchronization should not change the result drastically and yields only an overall shift for the transient time.

The following analytical arguments suggest that the transient time should indeed diverge at least as fast as α^{-2} with α. As before, we use the definition of a time unit as the time during which an energy $1 - 2\alpha$ is added to the system. A site at the center receives two packages of size α from its neighbors per unit time and topples on average once per unit time. A boundary site receives only one package and has on average approximately $1 - \alpha$ topplings per unit time. A site in the synchronized block topples on average y times per unit time, with y being intermediate between these two limit cases, $1 - \alpha < y < 1$. Initially, the energy difference between the synchronized block and the site that will be synchronized next, is of the order of $\mathcal{O}(1)$. In order to decrease this energy difference to a value of the order of $\mathcal{O}(\alpha)$, the difference in the total number of topplings between the block and its neighbor must be of the order of $\mathcal{O}(1/\alpha)$, which is achieved after a time of the order of $\mathcal{O}(1/\alpha(1 - y))$. This increases with decreasing α at least as fast as $1/\alpha^2$.

Before the focus turns on the properties of the stationary state and the size distribution of avalanches in the coming section, the remarks in the context of figures 2.6 and 2.13 should be complemented. There, the strong α dependence of either the average package size or the transient time was associated with the possible partitioning of unity.

Besides the formally continuous external energy inflow, each site receives two discrete packages during a cycle of length $1 - 2\alpha$. Since the threshold is set at unity, or when considered as a continuous dynamic process, at any integer modulo 1, the missing energy between subsequent topplings of the same site can also be regarded as multiples of that cycle.

Generally, these multiples will be detuned to values smaller than an amount of $1-2\alpha$ away from each other, for packages are at least of size α and typically involve also higher order terms in α. This nonlinearity was already mentioned in section 2.1.3, where the same mechanism was discussed from another point of view. There the question arose, why small periodic orbits are preferred over others for certain values of α.

Sites can change their energy values relative to each other in steps of higher order terms in α only (see section 2.2.1 and a further detailed discussion in 2.3.2). Thus, it makes a large difference, whether sites are increased just below, exactly at or slightly above that threshold by toppling neighbors. Some values of α allow for a relatively faster fragmentation of the remaining energy difference between subsequent topplings of the same site. Put another way, for certain values of the coupling, it takes less cycles between induced topplings of the same site, in the sense of least common multiples of the basic units $1-2\alpha$ and $\bar{\alpha}$. As a rule, the larger the average package, the smaller the number of single topplings (with packages of α) in-between, and therefore the less cycles are necessary, and accordingly the faster is the synchronization.

Theoretically, one should still obtain smooth curves in functions of α and not the observed peak-like structures. This smoothness is hindered by the computing precision, even if one is not working with an integer representation of the sites. The just-described mechanism is always superposed by the finite definition of the used floating numbers.

2.3.2 The stationary state

This section now turns to systems already in the stationary state and gives an overview of their statistical behavior.

The most striking feature of the stationary state are the large synchronized blocks already introduced and presented in figure 2.8. The system splits into the two boundary layers at the left and the right, and a single synchronized block, or in two blocks of synchronized sites possibly separated by a few sites centered around the middle of the system at $L/2$.

The dynamics within such a block can be described as follows. Sites within a block topple the same number of times, while sites closer to the boundaries topple less often. From time to time, a large avalanche that begins outside the block runs through the entire block. Between the large avalanches, the sites within a block topple mostly one by one, lifting each other almost exactly to the threshold.

This behavior of the OFC systems in one dimension was already hinted at by examining the different types of attractors in sections 2.2.1.1 to 2.2.1.4 and is now supported by analytical considerations and further numerical investigations. Taking all the evidence into account, a coherent picture of the one-dimensional OFC model is obtained.

Let us first consider a small region within such a synchronized block. Sites in this region must have approximately the same energy value, given the dynamics just described: when the sites topple one by one, the differences in their energies are exactly the same as before, after each site has toppled once. A change in the differences can only be imposed by avalanches of size larger than 1. Single topplings move packages of size α to and fro, but do not alter the overall energy profile after one cycle (an energy input of $1-2\alpha$ or L topplings). When an avalanche enters the region from the outside and extends several sites beyond it, the change in the energy differences is calculated by multiplying the reduced state vector $\underline{x}$ from the left with an appropriate product $\underline{\underline{S}}^{av}$

of $\underline{\underline{M}}^i_\nu$ matrices as in equation (2.21). If this avalanche passes the region for instance from the right to the left, the elements of the corresponding avalanche operator $\underline{\underline{S}}^{av}$ in a row k belonging to this region are

$$\underline{\underline{S}}^{av}_{kj} = \begin{cases} \alpha^{2+j-k} & \text{for} \quad k-1 \leq j \leq j_{ini} \\ 0 & \text{else} \end{cases} \tag{2.37}$$

with $j_{ini}+1$ being the site that triggered the avalanche. If x_i and x'_i denote the values of the energy differences within the region before and after the avalanche, we have

$$x'_i = \alpha(x'_{i+1} + x_{i-1}) < 2\alpha \max(x'_{i+1}, x_{i-1}) \tag{2.38}$$

for an avalanche passing through the region from the right to the left. The asymptotic values of the x_i after many avalanches satisfy

$$x_i = \alpha(x_{i+1} + x_{i-1}) \tag{2.39}$$

within the synchronized region. This condition can only be satisfied with all x_i being zero, or with x_i decreasing by a factor of the order of $\mathcal{O}(\alpha)$ from one value of i to the next. Deep inside the synchronized region, the x_i become therefore very small. Since the reduced state $\underline{x}$ actually represents the energy differences, the proper energy values of the sites, z_i, are at least approximately, if not exactly, at the same level within the synchronized blocks.

Still, at some given moment in time, even sites, which are exactly synchronized and phase locked to each other, can have a relative energy distance of order $\mathcal{O}(\alpha)$ or of order $\mathcal{O}(1)$. This arises due to the dynamics of the avalanche mechanism, when neighboring sites are not lifted above the threshold, but a series of single topplings proceeds through the block. Assume this progression moves from the right side to the left, as above. The just toppled site is then reset to zero, $z_i = 0$, while its left neighbor has a z_{i-1} of about unity, which would be the next site to topple, and z_{i+1}, the right neighbor, is slightly larger than α. The reason for the latter is that this particular neighbor had toppled itself a moment before, and received the single toppling package α from the toppling of site i. Since we are considering single topplings only right now, there must have been a small amount of external energy input in-between the topplings. Only if site i is lifted *exactly* at the threshold, this energy input vanishes.

A hint for this can be seen in the second figure of the left column in the snap shots of the systems (figure 2.8). Because the pictured system is not yet in the steady state, the already synchronized sites within the right block are distributed along two different energy values. After a necessary number of intermediate toppling events all over the system and in particular in the center of the chain, eventually these two sub blocks merge again into a single one. I want to accentuate that the outer of the two separated blocks on the right takes on a value around 0.2, which is just the coupling's value. The series of single topplings is just about to proceed to the left. Since the system is not yet finally synchronized, this series does not happen in a row, but is interrupted by topplings elsewhere in the system.

Directly related to these synchronized blocks is the behavior of $\langle t \rangle_i$, the mean number of topplings at a site i, which was already observed as a function of the site index i and compared to the mean-field like solution (2.28) in figure 2.7.

The mean size of all the avalanches triggered at a given site, $\langle s \rangle_i$, and the relative number of avalanches triggered at site i, $\langle \#_a \rangle_i$ was also observed. The results for a

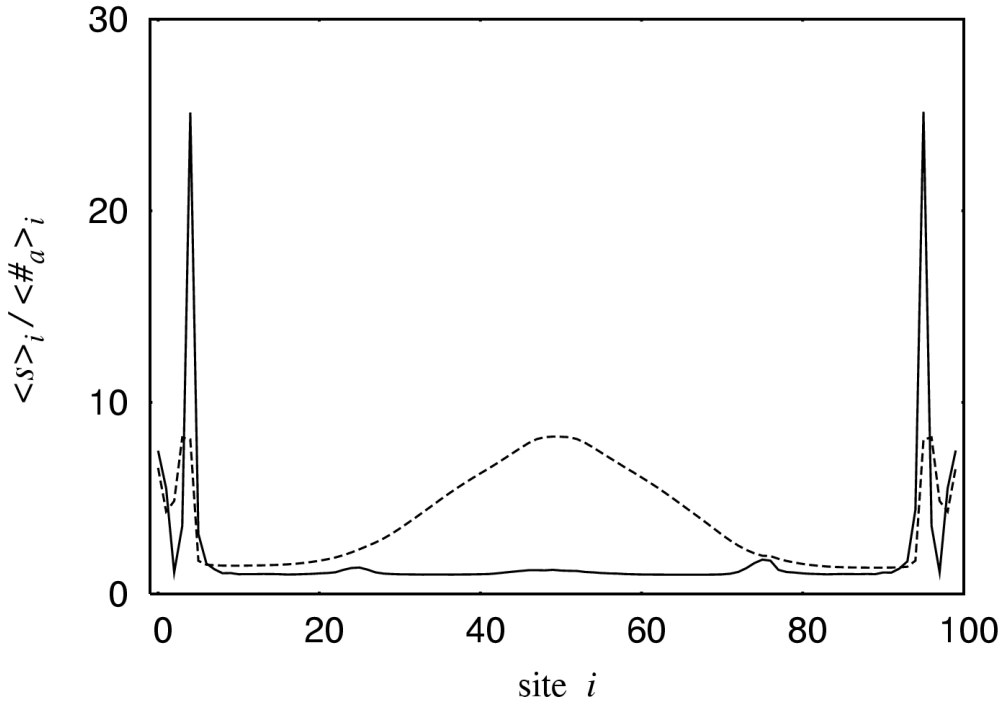

Figure 2.15: Solid line: average size of avalanches triggered at site i; dashed line: average number of avalanches triggered at site i. Both data sets are plotted as function of the site index i, averaged over 10^4 different synchronized systems for $\alpha = 0.2$, $L = 100$.

coupling of $\alpha = 0.2$ and a system size $L = 100$, averaged over 10 000 synchronized systems, are shown in figure 2.15.

Almost all of the large avalanches are triggered near the boundaries, where the average number of triggered avalanches also shows narrow peaks. But the latter has also a broad bump in the middle of the system with its maximum centered at half the system size. The structure of the peaks at the boundary of both the curves in figure 2.15 depends on α, and results from averaging over many different stationary states.

Combining the two data sets, we arrive at the following scenario: in the stationary state, most of the avalanches are single topplings. All large avalanches are triggered near the boundaries and extend far into the synchronized block. If they do not reach the end of the synchronized block, the rest of the block topples in a series of smaller avalanches, mostly of size 1. These small avalanches cause the broad peak at the center in the distribution of $\langle \#_a \rangle_i$. For the chosen coupling, $\alpha = 0.2$, the maximal mean size of the avalanches triggered at the boundaries is about one fourth of the system size in figure 2.15. If we assume only avalanche sizes of unity (single topplings) and half the system size, we conclude that it takes roughly two cycles in-between subsequent avalanches of size $L/2$. This assumption is approximately confirmed in the following section, focusing on the size distribution of avalanches. The cycles of single topplings within the synchronized blocks between the larger events are needed for the boundary layer to reorganize, and for the preparation of the synchronized sites, i.e. to lift them to an energy value at most an amount of the order of $\mathcal{O}(\alpha)$ below the threshold to

allow for the next large avalanche. Note that the level of the blocks can take on a value even slightly below $1 - \alpha$, if only the first toppling of a boundary site (or the last site within the boundary layer, but next to the synchronized ones) yields a package large enough to compensate for the missing energy.

2.3.3 The avalanche distribution

This section unfolds the properties of the avalanche size distributions. Especially, it concentrates on the distributions' dependence on the system size and the coupling The influence of the computing precision on the obtained distributions is also discussed. For two-dimensional systems the distribution of avalanches is believed to obey a power law (see section 1.3.1, the discussion therein, and the coming chapter 3 for an ultimate conclusion). However, for the one-dimensional systems this feature is only present for short time intervals during the transient evolution or for small system sizes, if at all.

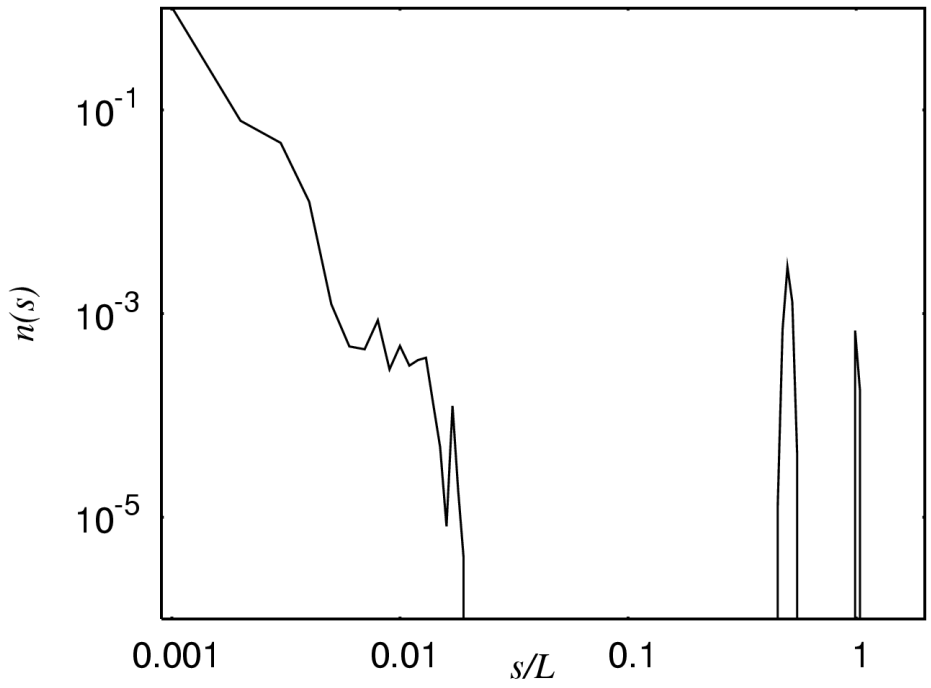

Figure 2.16: Typical size distribution $n(s)$ of avalanches of size s, divided by the total number of topplings and the system size, averaged over 2140 systems. $L = 1000, \alpha = 0.2$. Note the larger weight for avalanches of about half the system size compared to avalanches with a size of around the system size.

In the stationary state, the avalanche size distribution typically looks like the one presented in figure 2.16. It was obtained by averaging over 2140 different systems and 10^9 topplings, where the first 10^9 transient topplings of each system were discarded. The size of the avalanches is measured with respect to the system size L, hence the s axis ranges from a small fraction up to unity. This plotting style is rather convenient

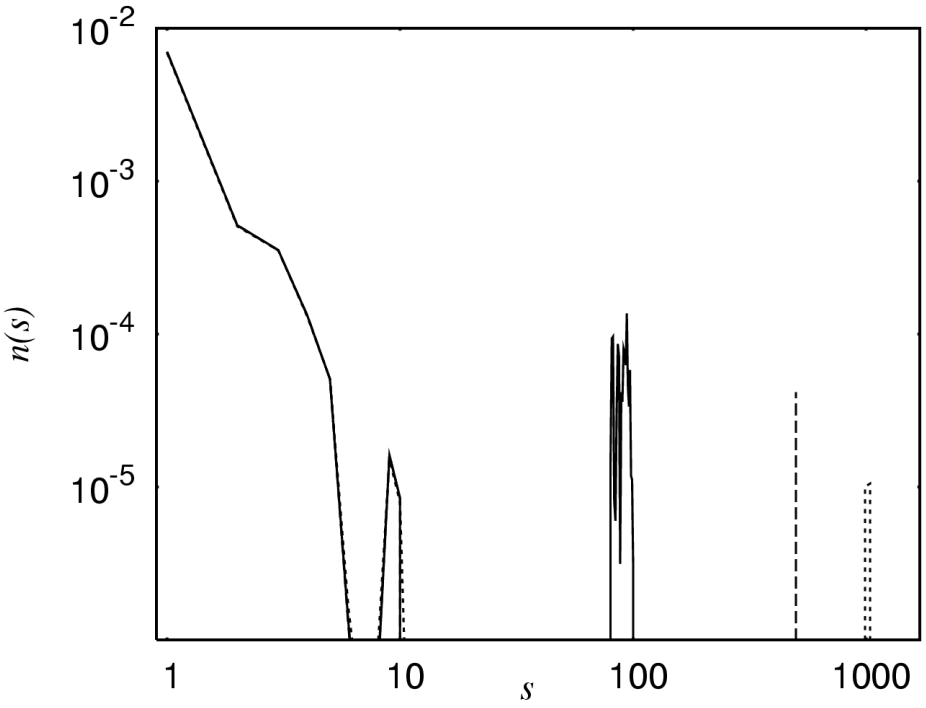

Figure 2.17: Size distribution $n(s)$ of avalanches of size s divided by the total number of topplings for different values of L and a coupling of $\alpha = 0.15$, averaged over at least 3300 systems. Solid line: $L = 100$; dashed line: $L = 500$; dotted line: $L = 1000$. The low-size regime is independent of the system size, depends only on α, and is determined by the dynamics within the boundary layer. The relative weight for the avalanches of order $\mathcal{O}(L)$ decreases with increasing system size.

and used for all the distributions presented in this section. Only figure 2.17 is an exception, where distributions taken for different L are directly compared.

Coming back to figure 2.16, a power law is arguable for small avalanche sizes, but only for a single decade and up to the sharp cutoff. We see a large gap, followed by peaks centered at the system size and half the system size (actually at 0.5 and 1 along the s/L axis). Note that the peak around $L/2$ (0.5) is both, broader and larger than its counterpart at L (1). While the first finding might stem from the numerical technique of *binning* the distributions, the second one indicates the larger weight of systems, which are decoupled into two subsystems of about half the system size. Binning allows for smoother curves when there are only a few events distributed over a wide range of possible outcomes. If one bins data points over increasing intervals, rare events are averaged over the corresponding ranges. Of course, one has to take care to use the right normalization. Usually a linear mesh as a basic grid for all avalanches smaller than 128 was used for the data presented here. For larger avalanche sizes the mesh still had integer bins, but their size was increasing by a factor 1.05 or 1.1 for adjacent intervals.

The shape of $n(s)$ for small s depends only on the value of α and on the precision used in the simulations, but not on the system size L. This was checked by inserting

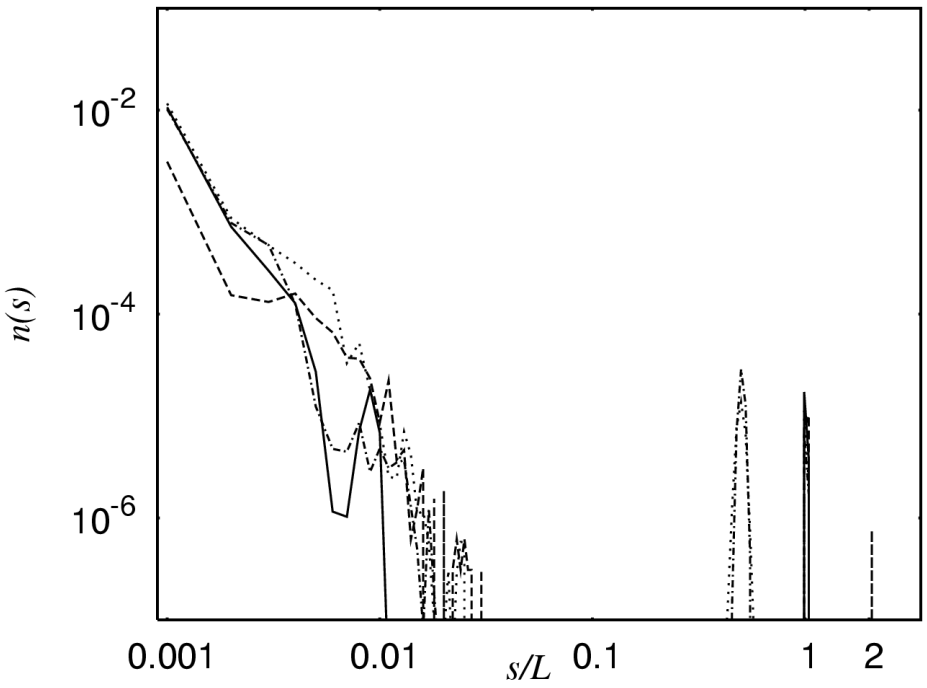

Figure 2.18: Size distribution $n(s)$ of avalanches of size s divided by the total number of topplings and the system size for different values of α and a system size $L = 1000$, averaged over at least 2000 systems. Solid line: $\alpha = 0.1$; dash-dotted line: $\alpha = 0.2$; dotted line: $\alpha = 0.3$; dashed line: $\alpha = 0.4$. Note the non vanishing weight for avalanches larger than the system size for $\alpha = 0.4$.

more sites into the synchronized blocks and by subsequently comparing the resulting avalanche size distributions, which only differed for the number and size of the large avalanches. More evidence is seen in figure 2.17, where the distributions for different L are shown, obtained by averaging over independent systems (and not increasing the synchronized blocks by adding sites). I want to stress that the weight of the peaks, which are of the order of the system size, decreases with increasing L. That is, the absolute number of large avalanches is the same for systems with different L, but the single toppling events and generally the small avalanches do depend on the number of sites, and we can conclude that the peaks' weight decreases as $1/L$. In the thermodynamic limit of infinite system sizes, the systems would end up with purely localized avalanches only. However, this can only be reached asymptotically, since an infinite transient time would be necessary as well.

Distributions for different values of α and fixed system size are compared in figure 2.18. Smaller values of the coupling result on average in smaller avalanches also. The reason for this effect lies in the energy differences between adjacent site, which typically scale with powers of α, as remarked in sections 2.1.3 and 2.3.2. In order to obtain larger avalanches, a higher precision is needed to resolve these energy differences. For given precision, a smaller coupling results in energy packages that are more likely to be truncated, and neighboring sites are lifted *at* the threshold, not above. This finding

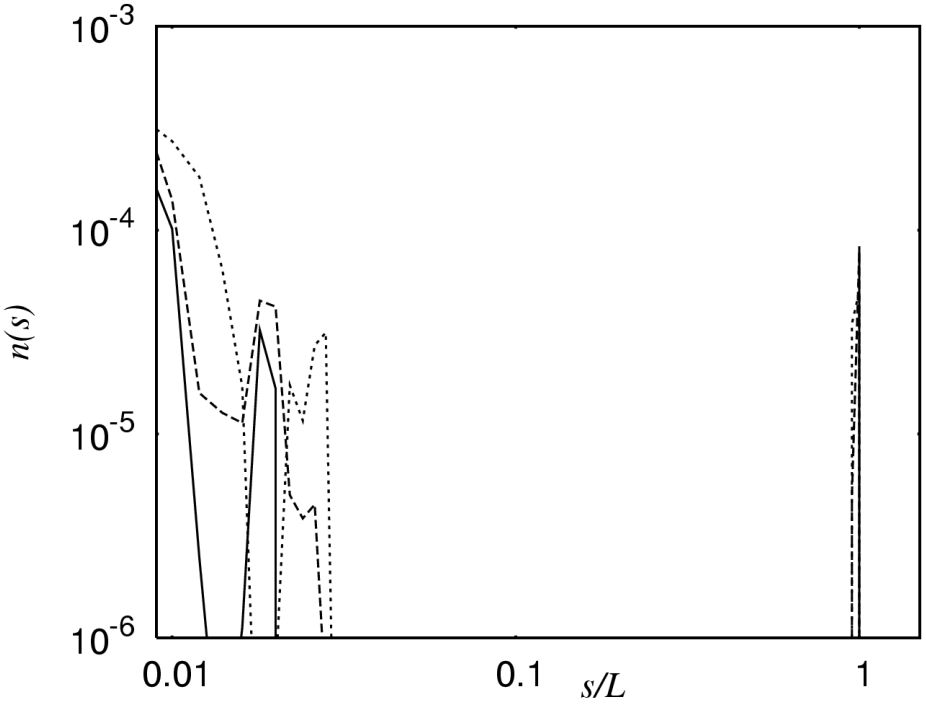

Figure 2.19: Size distribution $n(s)$ of avalanches of size s divided by the total number of topplings and the system size for different precisions. $L = 500$ and $\alpha = 0.15$, averaged over at least 6300 systems. Solid line: precision 2^{-12}; dashed line: precision 2^{-20}; dotted line: precision 2^{-28}.

is analogous to the effect of increased precision, explained below. Note also the non vanishing weight for avalanches of size $2L$ for $\alpha > \alpha_c$ in figure 2.18.

An investigation of different precisions yields the following: for larger precision, more diverse avalanche sizes are found, especially in the low-size regime (see figure 2.19). The number of avalanches of the order of the system size $\mathcal{O}(L)$ (or of order $\mathcal{O}(1)$, respectively) seems rather unaffected. The reason for this is that the period of the stationary state is longer, as stated before in section 2.1.3. Since sites in the center of the system take part in very large or very small avalanches only, the length of the period is determined by the dynamics in the boundary layer of the model. And it is the boundary layer, where one finds the medium-sized avalanches, which in turn regulate the shape of the size distributions in the lower decades.

The results for $n(s)$ confirm the picture that the one-dimensional OFC system is composed of a boundary layer that controls the dynamics and determines the stationary state, and a synchronized block of sites that topple the same number of times and that can be made larger without modifying the boundaries.

A complete description of the relevant dynamics and the main properties of the OFC model in one dimension for the transient stage and the steady state can now be given.

2.4 Summary $d = 1$

The investigation of the one-dimensional version of the OFC earthquake model has revealed many intriguing features.

Randomly initialized systems soon develop boundary layers due to the open boundary conditions. The lack of outer neighbors destroys the otherwise regular ordering of the system. Within periodic boundaries, this ordered state consists of sites that are decoupled from their neighbors; the decoupling is found in an energy gap of at least α between neighboring sites, and only single toppling events are observed in a periodic cycle of length L or $1 - 2\alpha$, respectively.

For open boundary conditions, the boundary layers enslave the center part of the system: a synchronization is imposed on the inner sites. These become phase-locked to each other, i.e. already phase-locked or synchronized sites have approximately the same energy value and show the same toppling behavior. The synchronization proceeds one site at a time and simultaneously from the left and the right border. Thus, the transient time is linear in the system size L (i.e. a power law with an exponent 1). The not yet synchronized sites in the middle of the system behave as if they were part of a periodic system with no boundaries and topple one by one. The transition from a totally uncorrelated initial configuration towards this pseudo-closed state happens within a short time interval of a few topplings per site, and while the boundary layers itself are formed. The time to build up the layers is not significant compared to the time necessary to fully synchronize the system. The underlying mechanism for the synchronization is generated by avalanches, which are triggered within the boundary layers, and the synchronization itself is driven by nonlinear terms in α.

Sites that are not part of the boundary layer topple for themselves in-between the increasingly larger avalanches, which span the synchronized blocks, during the transient evolution. Avalanches of size 2 or larger (but not as large as the synchronized blocks) are only found in the boundary layer, and at the frontier between the synchronized blocks and the still free inner sites. The large avalanches transport extra energy packages of the order of $\mathcal{O}(\alpha^2)$ into the center of the system and thus disturb the pseudo-periodic part. As shown in [Mid95] by using Poincaré maps, this extra amount of energy causes the synchronization. Between the large avalanches, which are running through the synchronized parts, a number of cycles $1 - 2\alpha$ is necessary to reorganize the boundary layer in order to prepare the next large avalanche. This number of cycles depends only on the coupling α, as well as the number of avalanches to incorporate the next site into the synchronized part.

The expression (2.28) for the continuous toppling profile within a mean-field-like derivation suggests a penetration depth for the boundary effect of the order of (see equation (2.30)

$$\frac{1}{\kappa} = \sqrt{\frac{\alpha}{1 - 2\alpha}} \quad . \tag{2.40}$$

The numerical results confirm a slightly larger boundary layer. Still, the dynamics within the layer and the possible types of orbits are independent of the system size. As a function of the coupling, the transient time is of exponential type for almost all α. Very large α near the conservative case were not explored, but for $\alpha \to 0$ the transient time follows a power law with an exponent around -2.84,

$$\begin{aligned} T(\alpha, L) &\sim L \, \exp(-14.8\alpha) \qquad \text{for} \quad \alpha > 0 \\ &\sim L \, \alpha^{-2.84} \qquad\quad \text{for} \quad \alpha \to 0 \quad . \end{aligned} \tag{2.41}$$

Thus, in view of the questions raised at the end of the first chapter, at least in one dimension, the transient time does depend on the coupling α and the dependence is rather non trivial.

When viewed as a dynamic system, the model shows 4 different types of attractors, all of them being periodic. Despite the results for a 2-site version of the model, where the variables can only change continuously in time [dV99], and for a many-site version, where the reset rule is $z_i \to z_i - z_c$ [Cri92] (see also section 1.2.1.2 in the introductory chapter), no chaotic attractors are found. In contrast to the one-dimensional Zhang model, which is conservative and has a stochastic force input [Bla00], the phase space volume does not necessarily shrink for systems that have the same sequence of topplings and avalanches. This is mirrored in a non vanishing weight for astonishing long complex attractors, even for small systems.

In the stationary state, the model consists of the two boundary layers, the thickness of which is larger for longer attractors, and an inner part consisting of two synchronized blocks. They can be made larger without changing the dynamics of the boundary layer or the period of the attractor. Depending on the initial configuration, these two blocks possibly match each other, resulting in a completely synchronized system and allowing avalanches, which are almost of the size of the system. More likely, the system consists of two almost decoupled subsystems, and a few sites in the center are potentially trapped in the middle between the two blocks. Large avalanches are always triggered near the boundary. They either cover almost all the sites (except those in the boundary layer responsible for the triggering of the large avalanche), or span half the system, until the trapped sites in the middle are reached. In the latter case, the center sites catch up with their affected neighbors in a sequence of smaller avalanches.

These features are clearly reflected in the avalanche size distribution, where the small avalanches are independent of the system size for sufficiently large systems, while the large avalanches are proportional to it. In the thermodynamic limit, the weight of large system-wide avalanches decreases as $\sim 1/L$. That the inner part can be made larger without changing the dynamics of the boundary region, must be a special property of the one-dimensional system due to the fact that the boundary of a synchronized block is merely a point and that avalanches can propagate only along lines. For better numerical precision, the periods become larger, and the L-independent part in the size distributions for small avalanches increases towards larger avalanches as well. The number of different small avalanches also increases with precision, and it depends on the coupling, the smaller α, the smaller the avalanches on average. However, no clear trend can be spotted for different α as far as the shape of the low-size regime of avalanches is concerned, and the dependency on α and the dynamics in the boundary layer are rather complex.

A shortcut version of the results for the OFC model in one dimension can be found in [Wis05].

Chapter 3

The OFC-model in two dimensions

Everything has been said before, but since nobody listens
we have to keep going back and beginning all over again.
Andre Gide

After having dealt thoroughly with the OFC systems in one dimension, this chapter focuses on the model in two dimension. While the second chapter of the thesis can be thought of as a preparing and rather purely academic work, comprehensive results are given below for the original version of the OFC model. Although there is no real connection to earthquakes for the system in $d = 1$, it turns out that the tools developed and the findings obtained for that case are very useful for the two-dimensional model.

As stated in the introduction (1.2.2), and especially in the sections (1.3.1) and (1.3.2), concerning the state of the art in the investigation of the OFC model and the open questions, there are many features and properties of the systems not yet understood completely. How does the transient time depend on the model parameters? Is the steady state different for different couplings? What are the system's properties for various limiting cases, such as, for example, infinite system size or vanishing coupling? The answers to those questions are of great importance for understanding the OFC systems, and they also might play a role for modified versions of the OFC model.

For the reader's convenience the rules for the OFC model are repeated once again. Afterwards, the mean-field ansatz for the toppling profile as derived in section 2.2.2 is used to obtain a time-dependent profile during the transient evolution. With some minor changes, which match the fact that we now have to struggle with two-dimensional systems, the transient regime and the behavior in the stationary state is explored, and a phenomenological theory is finally derived for the OFC model in two dimensions.

Naturally, the OFC system in two dimensions consists of sites placed on a two-dimensional grid. This grid is assumed to be a square lattice, not at last for historical reasons, because this setup simplifies the numerics. It might be interesting to examine the OFC model in other geometries. Especially suited seems a closed topology as a sphere, which might then be taken as a model of the earth's crust, probably along with some modifications to the update rules (the OFC model generically describes the dynamics within a single fault). Note that the topology of the periodic OFC system

is a torus, which contains a hole [1]. However, these considerations are not part of this thesis.

The sites z_{ij} on the square lattice of linear size L are randomly initialized within the interval $[0, 1]$, fed from external sources at a constant rate, and coupled to the nearest neighbors by α, which in $d = 2$ can be chosen from $[0, 0.25]$. The upper bound of the interval constitutes the conservative case. Due to the growth, the biggest site reaches the threshold $z_c = 1$ and topples. A toppling adds the fraction α times the current energy value to each neighbor and resets the given site to $z_{ij} = 0$. Now possibly unstable neighbors are treated according to the same rule and many toppling sites resemble an avalanche. As shown in [Chr93] and mentioned in 1.3.1, no secondary topplings are possible for α below 0.2, i.e. even the site that triggered an avalanche, and received the maximal possible package of its neighbors, cannot be lifted above the threshold for a second time. $\alpha \leq 0.2$ is used in the following.

Throughout the chapter, I also concentrate on open boundary conditions. Periodic systems are known to settle in a periodic cycle of length L^2, measured in single topplings, or of size $1 - 4\alpha$, measured in units of external energy input. No avalanches of size 2 or larger are found within periodic boundaries (see the introductory section 1.3). For open systems, the mechanism to drive the systems towards the steady state is the loss at the boundaries, just as in one dimension.

In two dimensions, it is not very promising to follow the previous chapter, which began examining small systems. The smallest possible system consists of 2×2 sites. Due to the open boundary conditions, this geometry is equivalent to a periodic system of 4 sites along a chain in one dimension. For those, the final state is already known, which is a periodic cycle of length 4, and each site is at least an energy amount of α away from its neighbors. The second to smallest system is of size 3×3. I do not see any reasonable way to track this in a manner comparable to the return maps in section 2.1.

The aim is the investigations of generally large systems. While in one dimension for all practical purpose there were no constraints for the system size, in two dimensions one has to cope with the restrictions imposed by the technical possibilities. Currently available (and affordable) storage and computer power limited the numerics on system sizes of about 10^6 sites, which corresponds to a linear size of L up to 1024 (as explained in appendix A.2, the newly engineered search algorithm to determine the largest site in the system requires system sizes given in powers of 2).

Although the simulations could be sped up drastically (from order $\mathcal{O}(L)$ to order $\mathcal{O}(\ln L)$), I could not average over at least several systems, and obtain statistics for all sets of parameters, since the transient time for the OFC model is awfully long. I could have collected average data for smaller system sizes, though, but for too small L, the boundary effects predominate the dynamics disproportionately. We see below that, just like in one dimension, the system splits into a boundary layer, which is rather a frame, and the interior of the lattice. Unlike in $d = 1$, that interior has its own structure and dynamics, and does not consist of one or two synchronized blocks only.

While it is rather easy to visualize the systems in one dimension along a line, where all the sites are shown with its current energy value z_i at the corresponding position i, this representation is not possible for two-dimensional systems. Thus, snap shots of the lattices are presented, seen from a bird's eye perspective. Each site's energy value

[1] Actually, from a topologist's point of view, the torus, T, belongs to the manifolds with two holes, i.e., the first homotopy group (the fundamental group) $\pi_1(T) \simeq Z \bigoplus Z$

z_{ij} in the square lattice is represented by a brighter or darker gray shade, where the convention is used, the larger the z_{ij}, the brighter the color. Due to intrinsic details of the graphical tools (I used a postscript format and interpreter), the unit interval $[0, 1]$ could only be divided into 16 different gray tones, ranging from pure black (standing for an energy between zero and 0.0625) to pure white (representing a z_{ij} somewhere between 0.9375 and unity).

3.1 The transient time

This section investigates the properties and dynamics of the transient evolution, and determines the time that is necessary for the two-dimensional OFC systems to reach the stationary state.

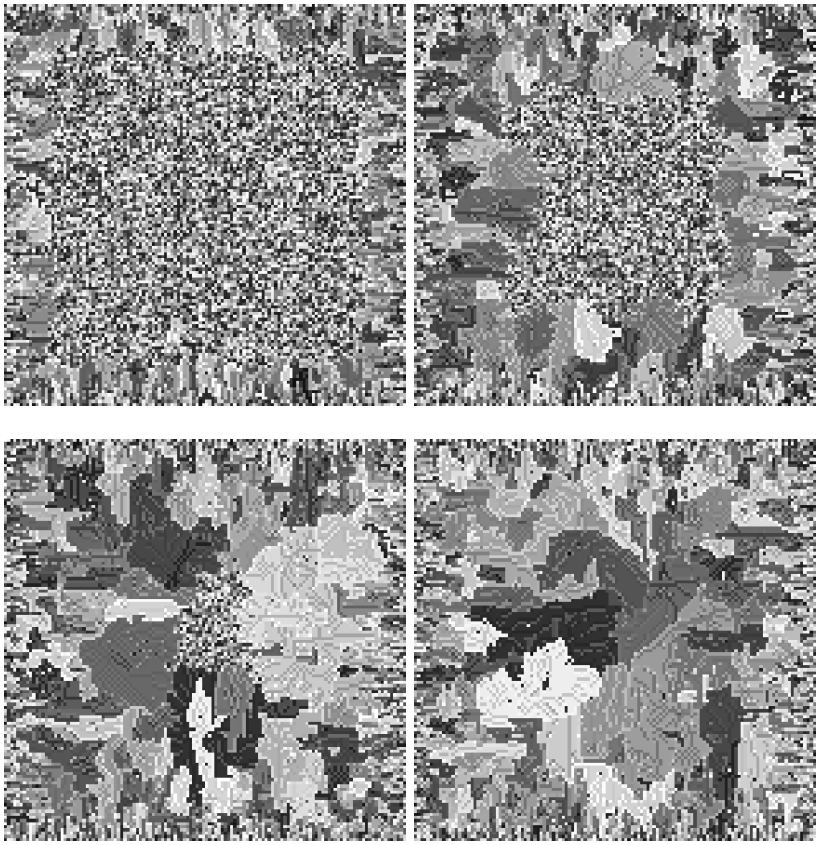

Figure 3.1: Configuration after 10^3, 10^4, 5×10^4, and 8.5×10^4 topplings per site in top view for a system with $L = 128$ and $\alpha = 0.09$ (from top left to bottom right). The darker a site, the lower the energy value z_{ij}. As in $d = 1$, the synchronization proceeds into the system starting at the boundaries. Instead of the synchronized blocks in one dimension, patches are formed, the size of which increases with distance to the boundaries. The disordered center of the system behaves similarly to one within periodic boundary conditions, until the patches invade more and more area of the system.

Snap shots of a particular system taken at different times for a system size $L = 128$ and for a coupling $\alpha = 0.09$ are presented in figure 3.1 to exemplify the behavior of the model. The top left figure depicts the system after 10^3 topplings per site. Compared to the total transient time, this is only a fraction of the topplings necessary to reach the steady state. Nevertheless, this time was already enough for the system to form a boundary layer around an inner block. This center seems to be rather disordered, with energy values randomly distributed, but it behaves as if it was part of a system with periodic boundary conditions and the corresponding properties. In detail, all the center sites have at least an energy gap of α to its nearest neighbors and no triggered topplings are observed deep in the system. Except for sites in the two or three outermost layers (measured in units of single sites), sites in the vicinity of the boundary started to form patches. Neighboring sites within a patch tend to have an energy value distributed within a narrow interval. Thus, correlations already emerged for the boundary frame as well as for the center of the lattice, the characteristics of the correlations are different, though. The evolution from a purely random initial configuration towards such a state is very fast and takes only of the order of $\mathcal{O}(10)$ topplings per site.

In the following two figures an invasion of the patch-like structure into the system is observed (top right and bottom left, after 10^4 and 5×10^4 topplings per site, respectively). The pseudo-periodic center becomes more and more diminished, while the ordered region increases. The size of the patches itself also grows with increasing distance to the boundaries.

In the last snap shot (bottom right in figure 3.1, after 8.5×10^4 topplings per site) no more inner part is left, all the sites are now part of one or the other patch. Still, patches are larger, the deeper they are located within the system, and sites in the outer frame along the boundaries show an alternating behavior, in the sense of that they are decoupled from their neighbors and their gray shades change from dark to bright along the edges of the lattice in each step of one site.

I now *define* the transient time of the two-dimensional OFC model to be the number of topplings (or normalized, the topplings per site) necessary for the system to have no inner block left.

Of course, this definition is inspired by the observation of the invading patches, which usually happens by watching the evolution of the system on the computer screen. It is quite complicated to find a suitable definition of a numerical quantity, which would reflect the progression of the patches and the vanishing of the disordered block, and which would also be numerically precise and reliable (e.g. the inner block need not always be in the geometrical center of the lattice). For a limited range of applications, appropriately defined correlation functions are used, similar to the quantities defined in equations (2.34) and (2.35) for the OFC model in one dimension. See the discussion of the stability of the boundary regions below (section 3.2).

However, the definition just given seems to be the natural choice, at least for a first transition of the dynamics. As long as some sites in the center are decoupled from each other in the above-described way, the weight of avalanches of size 1 is enhanced compared to any other avalanche size. This enhancement vanishes together with the centered block and constitutes the transition (the size one avalanches will still have a larger weight in the steady state, but this stems from a different mechanism, which is discussed in section 3.3).

On the other hand, by purely visual control one can never tell what actually happens, once the patches hit the center, and whether there might be a second transition due to the interplay between patches that have already met. For example, one could

think of a bouncing wave in the dynamics, which spreads from the center outwards just when the block of decoupled sites has vanished.

At least for times as long as the original transient times after reaching the steady state (obtained by using the above definition), a second transition can be excluded. This finding is confirmed in the examination of the size distribution of avalanches. Those were evaluated immediately after the patches had reached the center, and at much later times. These distributions agreed with each other. Further evidence for the stationarity of the systems once the patch formation has reached the center comes from the examination of statistical quantities, such as the correlation function, and from the observation that patches, which have been formed initially, do not change their characteristic size at later times. We will come back to these topics in the discussion of the stationary state and of the correlation functions and lengths in sections 3.2 and 3.3.

Now, a series of snap shots for different sets of parameter and taken at different times during the time evolution is presented. Doing so allows for a first statement on the parameter dependencies on a purely phenomenological level.

Figure 3.2: Snap shots of systems during the transient stage for a system size $L = 256$ and different values of the coupling. From left to right: $\alpha = 0.10$ after 2500 topplings per site; $\alpha = 0.15$ after 250 topplings per site; $\alpha = 0.20$ also after 250 topplings per site.

All the system in figure 3.2 have the same system size, $L = 256$, but differ in the coupling's value. The left system and the system in the middle, both show a patchy boundary region of approximately the same thickness. However, the elapsed time after random initialization differs by a factor of 10. The reason for this distinction is found in the different values for α. For the left system $\alpha = 0.10$, and the figure is taken after 2500 topplings per site, while the coupling is $\alpha = 15$ for the system in the middle, which was simulated for only 250 topplings per site. On the other hand, the very right system's coupling was chosen to be $\alpha = 0.20$ and this system is also depicted after 250 topplings per site. The invasion of the patches advanced more than twice as far into the center compared to the case $\alpha = 0.15$. There is also a difference in the structure of the patches, but this is better visible in figure 3.3. There, the system size is $L = 128$, and α takes on values $0.04, 0.12$, and 0.20 (from left to right). Although these systems already reached the steady state pattern, and have no disordered inner block left, the just to be named findings are also valid for the transient evolution:

First, the extension of the patches increases with increasing α. Secondly, the smaller α, the less variety is visible within a patch, and the more pronounced is the contrast

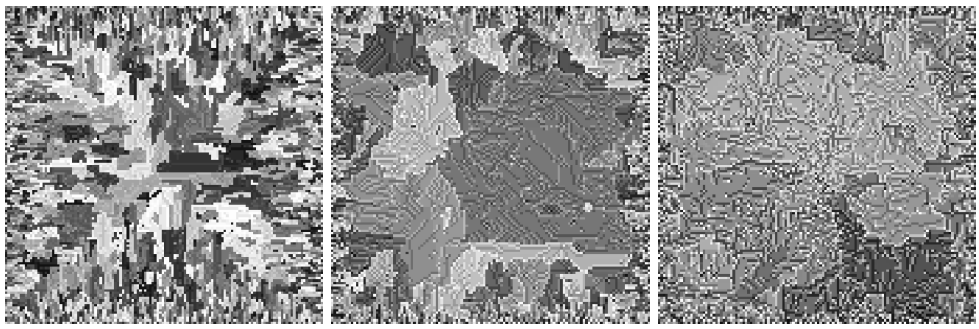

Figure 3.3: Snap shots of systems in the stationary state for a system size $L = 128$ and different values of the coupling. From left to right: $\alpha = 0.04$ after 1.34×10^9 topplings per site; $\alpha = 0.12$ after 8×10^3 topplings per site; $\alpha = 0.20$ after 200 topplings per site.

between adjacent patches. While the patches for a large coupling (the very right system in figure 3.3), show a rich internal structure with very dark or very bright sites within a surrounding bath of gray shades, the patches in the left figure have a rather uniform filling with less islands in-between. The figure in the middle, for $\alpha = 0.12$, shows an intermediate behavior. There are still some sites in a patch, the energies of which differ from their environmental average, but the patches itself are not as blurred as in the case of large α, and are clearer separated from another.

The reasons for the above phenomena lie in the distribution of the energy values within a patch, and the tendency of the sites within the same patch to act collectively as one effective site. This concept of effective sites is very important for understanding the OFC model in two dimensions and is to be explained in detail below. A precise definition of the patches, which by now are only a visual effect, and a quantitative description of their intrinsic dynamics is also given below. For now, I only recall the energy gap of at least α between sites within a periodic system. A similar effect is also observed for sites within a patch, and this difference cannot be resolved appropriately in figure 3.3 for small α. Therefore, the patches seem to be less disturbed.

Combining what was just said and illustrated, we are safe to conclude the transient time to be indeed depending on α, and to be longer for smaller couplings. Although the case $\alpha = 0$ is not to be mistaken for a vanishing coupling like $\lim_{\alpha \to 0}$, we can already expect a divergent behavior for small α, since for no coupling at all, the transient time will be infinite.

Of course, the transient time is also expected to be longer for larger systems. But it is not yet sorted out how the transient time depends on α and the system size in detail. In the following, the transient time is to be determined, including, as far as possible, the functional dependence on the said parameter.

Figure 3.4 shows the simulation results for the transient time for different system sizes L as a function of α. I stress again that each data point is based on the simulation of one system only. As stated above, averaging over several initial conditions is not possible because of the long computational times. The topplings per site were determined by visual inspection: snapshots of the systems were looked at at regular time intervals in order to see whether the stationary state was reached.

Usually, these intervals were taken at about the order of $\mathcal{O}(100)$ topplings per site

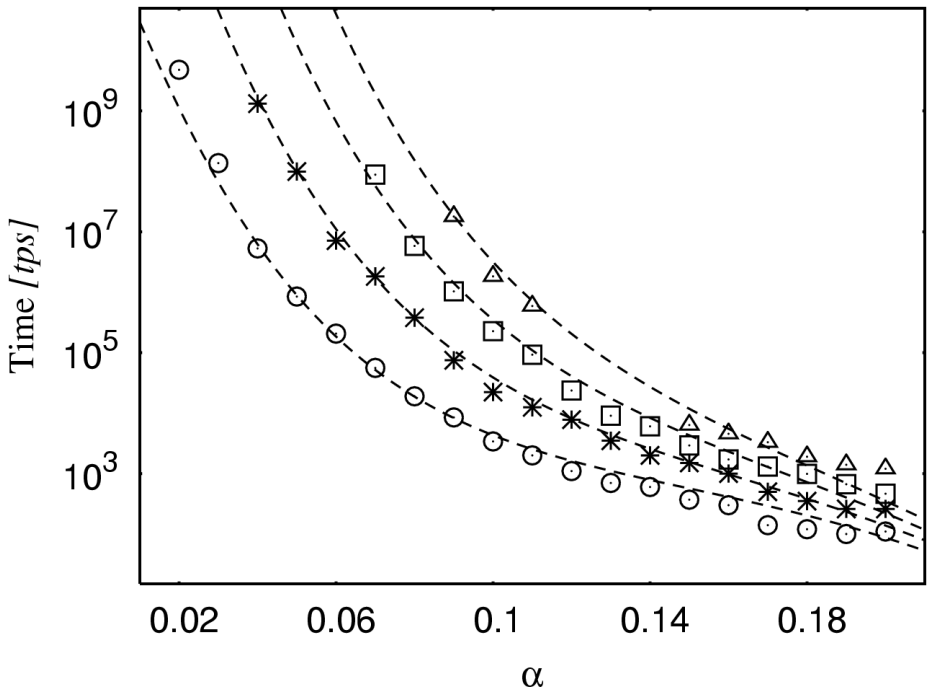

Figure 3.4: Time measured in topplings per site until the inner block vanishes for system sizes $L = 64$ (circles), $L = 128$ (stars), $L = 256$ (squares) and $L = 512$ (triangles) as function of α; the dashed lines correspond to the set of functions $T(\alpha, L) = \tilde{f}(\alpha)L^{\tilde{\mu}(\alpha)}$ as given below in equation (3.23)

and are large enough to recognize the vanishing of the disordered center within that precision. For larger α, the transition is even sharper (within ten topplings per site), but for very small couplings there is a certain ambiguity in the visual perception. For these cases the time, for which some remaining sites in the center still had a discernible disordered structure, was determined, and the time, when there were safely no sites left, which could possibly not have been part of some patch. The corresponding data point in figure 3.4 is the mean of these two times. Still, the error bars are too small to be visible in the above figure. For instance, for a coupling of $\alpha = 0.03$ and a system size $L = 64$, the two times are 1.2679×10^8 and 1.3869×10^8 topplings per site, respectively.

Coming back to figure 3.4, we observe that the transient time increases with decreasing α and increasing L, and it becomes very large for $\alpha \to 0$. For small α, one might therefore obtain the impression that the dynamics get completely stuck before the disordered block vanishes (as was suggested by Grassberger [Gra94]). However, I found no solid evidence and no good reason why this process should stop before the patches fill the entire system, although I could not yet determine the transient times for certain combinations of the parameter, e.g. very small α and/or large systems.

The dash-dotted lines in figure 3.4 are fits of the form (3.23), which is a generalized version of the result obtained in the following by using mean-field-like arguments, and which will be discussed in more detail further below.

Starting point are again the local balance equations, which will lead us to an expression for the toppling profile. This approach is similar to the one applied in section 2.2.2 for the one-dimensional case and reuses many of the insights. In contrast to section 2.2.2, where the toppling profile is derived in the stationary state, for two-dimensional systems this profile is now considered a dynamic quantity, i.e. it is considered as a function of time during the transient stage. The stationary profile is also given below, since this is a straightforward extension to the results in $d = 1$.

Let now $\langle t \rangle_{ij}$ be the mean number of topplings of site ij per unit time. Additionally, let $\bar{g}$ denote the rate of uniform energy input per unit time, and $\bar{\alpha}$ the average amount of energy passed to a neighbor during a toppling event.

When discussing the size distribution of avalanches further below (section 3.3), we will see that with increasing system size the proportion of avalanches larger than 1 decreases towards zero. This finding implies that the average amount of energy passed to a neighbor approaches α even for large values of the coupling. In the steady state, most sites are exactly at the threshold when they topple, but this might not be true for the transient regime. While for the stationary profile we can thus use again the vanishing weight of large avalanches, and while we are allowed to replace $\bar{\alpha}$ with α, this approximation needs a sure footing also during the transient time.

At least the disordered inner block is known to exhibit only single topplings, and avalanches of size one are also dominant within the patches, as is shown below. However, we are interested in the toppling profile of the boundary region, for which topplings may result in rather large packages and the above relation is not given a priori. Nevertheless, a power law expansion as

$$\bar{\alpha} \sim \alpha + \mathcal{O}(\alpha^{\omega}) \tag{3.1}$$

is valid in any case (see equation (2.22)), even for systems not yet stationary, and for small α, the value of $\bar{\alpha}$ deviates very little from the true coupling. Therefore, $\bar{\alpha}$ is generally replaced with α. The same argument can be used to count the average topplings per site in terms of the integer loss of unit energy per toppling, since the power law

$$\bar{l} \sim 1 + \mathcal{O}(\alpha^{\omega'}) \tag{3.2}$$

also still holds and the approximation of the mean loss per toppling, $\bar{l}$, with unity is of the same order as replacing $\bar{\alpha}$. For a detailed presentation of the approximations and assumptions, see the discussion in the vicinity of equations (2.22) and (2.23) in section 2.2.2.

In other words, the following derivation is a valid approximation for small α. Note that the exponents ω and ω' are not necessarily the same as for the one-dimensional case, and might differ from their $d = 1$ counterparts.

The assumption that the value of $\bar{\alpha}$ is constant throughout time and throughout the system is a mean-field assumption. While this ansatz neglects spatial and temporal variations of $\bar{\alpha}$, it does take into account other aspects of the spatial structure, in particular the fact that the toppling rate depends on the distance to the boundary. Due to the approximations involved, we can expect that the theory makes predictions that are qualitatively correct, but that the quantitative features could be different.

With the mentioned assumptions, the two-dimensional balance equation reads (see equation 2.24):

$$\langle t \rangle_{ij} = \bar{g} + \bar{\alpha} \left(\langle t \rangle_{i-1,j} + \langle t \rangle_{i+1,j} + \langle t \rangle_{i,j-1} + \langle t \rangle_{i,j+1} \right) \quad . \tag{3.3}$$

Let the site index i be the one that counts the distance to one of the boundaries, and let j accordingly be the site index parallel to this boundary. For large enough system sizes and for j being around half the system size, the average topplings of the two sites $i, j \pm 1$ are assumed to be equal to the average number of topplings of the particular site ij. The possible influence of the system's corners is thereby neglected, which should not fundamentally change the argument. In any case, one could consider a system that is periodic in one dimension and open in the other, in order to avoid corners altogether. Thus, we now consider a one-dimensional stripe perpendicular to the one boundary and far enough away from the other (parallel) boundaries to be disturbed. Equation (3.3) then becomes effectively one-dimensional and reads

$$\langle t \rangle_{i(j)} = \bar{g} + \bar{\alpha} \left(\langle t \rangle_{i-1,(j)} + \langle t \rangle_{i+1,(j)} + 2\langle t \rangle_{i,(j)} \right) \quad , \tag{3.4}$$

and the site index j can be ignored from now on.

The structure of the system during the transient time has now to be taken into account. The outer part consists of patches of different sizes, and sites in the disordered block topple like in a system with periodic boundary conditions, i.e. they receive the same input from all four neighbors. For these sites we have therefore $\langle t \rangle = \bar{g} + 4\alpha \langle t \rangle$, or

$$\langle t \rangle = t_0 \equiv \frac{\bar{g}}{1 - 4\alpha} \quad . \tag{3.5}$$

The concept of patches as effective sites is now thoroughly explained: sites within the same patch have energy values distributed in a narrow energy interval, which was already shown in figure 3.3. The size of this interval is of the order of $\mathcal{O}(\alpha)$. Since we are already working in the regime of small couplings only, the assumption of almost constant values z_{ij} in a patch is a good approximation [2]. In the chapter concerning the one-dimensional case, the dynamics of the constant inner block, which was not part of the boundary layer, was already understood (see section 2.3.2). Remember, sites within this block have the same toppling behavior. Each site topples either isolated or in large avalanches that affect all the sites in the block. This mechanism has to be modified slightly for two-dimensional patches. Still, sites sitting in the same patch have to topple equally often for the patch to persist for a long time, which is observed by watching the system on the computer screen over many hundreds of cycles $1 - 4\alpha$, and therefore a patch is treated as one effective site. Sites within a patch topple within a short time interval, and from time to time all sites belonging to the same patch participate in the same patch-wide avalanche and in a series of aftershocks, the distribution of which is to be discussed in section 3.3. The patch size itself cannot be predicted by this mean-field theory, since patches are the product of a local synchronization process, and their extension will be determined further below by numerical methods (section 3.2).

Since toppling differences occur between effective sites only, the value of $\langle t \rangle_{i(j)}$ depends on the distance to the boundary, measured in terms of the number of patches, x, between (effective) site $i(j)$ and the boundary. The balance equation (3.4) is now assumed to be applied to these effective sites, and not to real sites, since the effective sites are the units that experience toppling differences.

In terms of the parameter x, the above balance equation (3.4) for the patchy part of the system becomes

$$t(x) = \bar{g} + \alpha(t(x-1) + t(x+1) + 2t(x)) \, , \tag{3.6}$$

[2] This assumption is not really used in the following argument, but it simplifies the perception of patches as rather uniform entities, for which the global behavior is more important than the internal structure.

or, in a continuum notation,

$$\frac{1-4\alpha}{\alpha}t(x) - \frac{d^2}{dx^2}t(x) - \frac{\bar{g}}{\alpha} = 0 \quad , \tag{3.7}$$

where the replacement of the differential quotient with the second derivative was used once more, and the mean number of topplings $\langle t \rangle_{i(j)}$ are written as a continuous function $t(x)$. The boundary conditions are $t(0) = 0$ ($x = 0$ signifying the non-existent neighbor of a boundary site) and $t(r) = t_0$, with $r - 1$ denoting the index of the patch next to the disordered block. The solution of the balance equation is (compare with the solution (2.28) in one dimension)

$$t(x) = t_0 \left(1 - \frac{\sinh\left(\kappa(r-x)\right)}{\sinh\left(\kappa r\right)}\right) , \tag{3.8}$$

where κ in two dimensions is given by

$$\kappa = \sqrt{(1-4\alpha)/\alpha} \quad . \tag{3.9}$$

For the sake of simplicity and better readability, I did not bother to discriminate between the κ's for different dimensions, just as for the exponents ω and ω' above. A general expression would be $\kappa = \sqrt{(1-2d\alpha)/\alpha}$. Note that the patch index r is a dynamic quantity, monotonously increasing in time. Once the index reaches a maximum $r_{\max}$, to be determined by equation (3.15) below, the system enters the steady state, since then there is no inner center left.

Next, we have to consider the advancement of the patchy structure into the inner part of the system. A site that is part of the inner block can become part of a patch only, if the difference of its energy value z to that of its outer neighbor is less than α. This difference changes with time due to the different toppling rates. The patch next to the inner block topples less often than a neighbor of that patch, which is part of the inner block. The difference Δ in the number of topplings per unit time is given by

$$\Delta = t_0 \left[\sinh(\kappa)\right] / \left[\sinh\left(\kappa r\right)\right] \quad , \tag{3.10}$$

which is obtained from (3.8) by inserting $x = r - 1$. The difference in the number of topplings per unit time is identical to the rate of change of the difference in the energy value z between the two neighbors. When this difference has increased by 1, it has taken any intermediate value (in steps of size α) and has therefore certainly assumed a value smaller than α. At that moment, the site of the inner block becomes part of the patch. The time (or number of topplings per site) needed to add an additional site to a patch is therefore proportional to

$$n_c(\alpha, r) \propto \frac{\sinh \kappa r}{\sinh \kappa} . \tag{3.11}$$

In the limit of small α , $n_c(\alpha, r)$ is given by

$$n_c(\alpha, r) \sim \exp\left(\frac{r-1}{\sqrt{\alpha}}\right) \quad . \tag{3.12}$$

This expression was obtained by first approximating κ as

$$\kappa = \sqrt{\frac{1-4\alpha}{\alpha}} \sim \sqrt{1/\alpha} \quad , \tag{3.13}$$

and then neglecting one of the two exponentials in the definition of the hyperbolic functions, because the smaller exponential approaches zero in the limit of vanishing coupling, as presented in detail in equation (2.31) [3].

Expression (3.12) has to be summed over all patches, weighted with the mean size of each generation of patches. The total transient time is therefore given by

$$T(\alpha, L) \sim \sum_{r=1}^{r_{\max}(\alpha,L)} l(r) n_c(\alpha, r) \tag{3.14}$$

with $l(r)$ being the extension perpendicular to the boundary of a patch of type r. Below in section 3.2, it is shown that $l(r) \sim Q(\alpha)^{r-1}$, where Q is an increasing function of α only and approaches 1 (from above) for $\alpha \to 0$. The latter stems from the fact that single sites remain isolated, and no patches at all are formed for vanishing α. From the geometrical condition that the summed lengths of all the patches have to span the system size,

$$\frac{L}{2} = \sum_{r=1}^{r_{\max}} l(r) \quad , \tag{3.15}$$

we can determine the number of generations of patches necessary to fill the entire system (half the system, that is, since the patches invade the system simultaneously from both directions). The result is

$$r_{\max}(\alpha, L) = \frac{\ln\left[\frac{L(Q-1)}{2q_0} + 1\right]}{\ln Q} \simeq \frac{\ln \frac{L(Q-1)}{2q_0}}{\ln Q} \quad , \tag{3.16}$$

where the geometric series

$$\sum_{r=1}^{r_{\max}} Q^{r-1} = \sum_{r=0}^{r_{\max}-1} Q^r = \frac{Q^{r_{\max}} - 1}{Q - 1} \quad , \tag{3.17}$$

was used, and the approximation in equation (3.16) is valid for large enough system sizes L. q_0 is some constant, the extension of the patches of the first generation, and can be taken to be unity (the smallest possible extension is a single site). Combining equations (3.14) and (3.16), using again a geometric series for the sum

$$\sum_{r=1}^{r_{\max}} Q^{r-1} \exp\left(\frac{r-1}{\sqrt{\alpha}}\right) \quad , \tag{3.18}$$

the result for small α is given by

$$T(\alpha, L) \simeq \left(\frac{L(Q-1)}{2q_0}\right)^{\mu(\alpha)} \exp\left(\frac{-2}{\sqrt{\alpha}}\right) \quad , \tag{3.19}$$

with an exponent

$$\mu(\alpha) = 1 + \frac{1}{\sqrt{\alpha} \ln Q(\alpha)} \quad . \tag{3.20}$$

[3] There, it was demonstrated for the hyperbolic *cosine*, but of course, this is also valid for the hyperbolic *sine*.

As motivated in section 3.2, we can use the ansatz $Q(\alpha) = \exp(f(\alpha))$, with a leading term $f(\alpha) \simeq A\alpha^a$, and A and a being positive. Thus, we are allowed to rewrite

$$\mu(\alpha) = 1 + \frac{1}{A\alpha^{a+0.5}} \tag{3.21}$$

and

$$T(\alpha, L) \simeq \left(\frac{L}{2q_0} f(\alpha)\right)^{\mu(\alpha)} \exp\left(\frac{-2}{\sqrt{\alpha}}\right) \quad . \tag{3.22}$$

In the above equation (3.22), the expansion $\exp(f(\alpha)) \sim 1 + f(\alpha)$ was used, which is justified within the approximation of small couplings, due to the monomial structure of the function $f(\alpha)$.

Inspired by this result of the mean-field theory, we can expect that the transient time for small α is given by an expression of the form

$$T(\alpha, L) \sim \tilde{f}(\alpha) L^{\tilde{\mu}(\alpha)} \quad . \tag{3.23}$$

The data shown in figure 3.4 agree with this expression, but the details differ from the mean-field predictions in equation (3.19) or (3.22), as can be shown by numerical investigation.

Equation (3.19) (or equation (3.22)) implies that the transient time indeed scales as a power law with the system size L, and that the exponent μ (or $\tilde{\mu}$) does indeed depend on α. Of course, the general trend was already contained in the data, and one could have assumed a combination as equation (3.23) a priori, but the derivation above confirms qualitatively the underlying mechanism, and allows a precise understanding of the dynamics in the OFC model.

The functional form of $\tilde{\mu}(\alpha)$ and $\tilde{f}(\alpha)$, which appear in the expression (3.23), is now also determined quantitatively, as far as possible.

In order to find a good fit for the two functions, the logarithms of the transient time for different values of the coupling were first plotted as a function of $y = \log(L)$,

$$\log T(\alpha, L) \sim \log \tilde{f}(\alpha) + \tilde{\mu}(\alpha) \log L \quad , \tag{3.24}$$

corresponding to

$$\log T(\alpha, y) \sim \tilde{t}(\alpha) + \tilde{\mu}(\alpha) y \quad . \tag{3.25}$$

The obtained curves were then fitted with linear functions $\tilde{\mu}\, y + \tilde{t}$. For this fit, $\tilde{\mu}$ and $\tilde{t}$ were used as mere fit parameter, which in the next step were interpreted as functions of α and fitted in turn, accordingly. The result for $\tilde{\mu}$ is shown in figure 3.5, and the functional dependence on α seems to be

$$\tilde{\mu}(\alpha) \sim E \exp(-e\,\alpha) \quad , \tag{3.26}$$

with parameter E, e. Once the slope was determined, the values $\tilde{t}(\alpha)$ were then fitted to obtain $\tilde{f}(\alpha) = \exp(\tilde{t}(\alpha))$ also explicitly as a function of α. For the function $\tilde{f}(\alpha)$, I found as best fit (see figure 3.6)

$$\tilde{f}(\alpha) \sim \exp(m\,\alpha + l + C\,\alpha^c) \quad . \tag{3.27}$$

The numerical values of the parameters m, l, C, c are given in table 3.1.

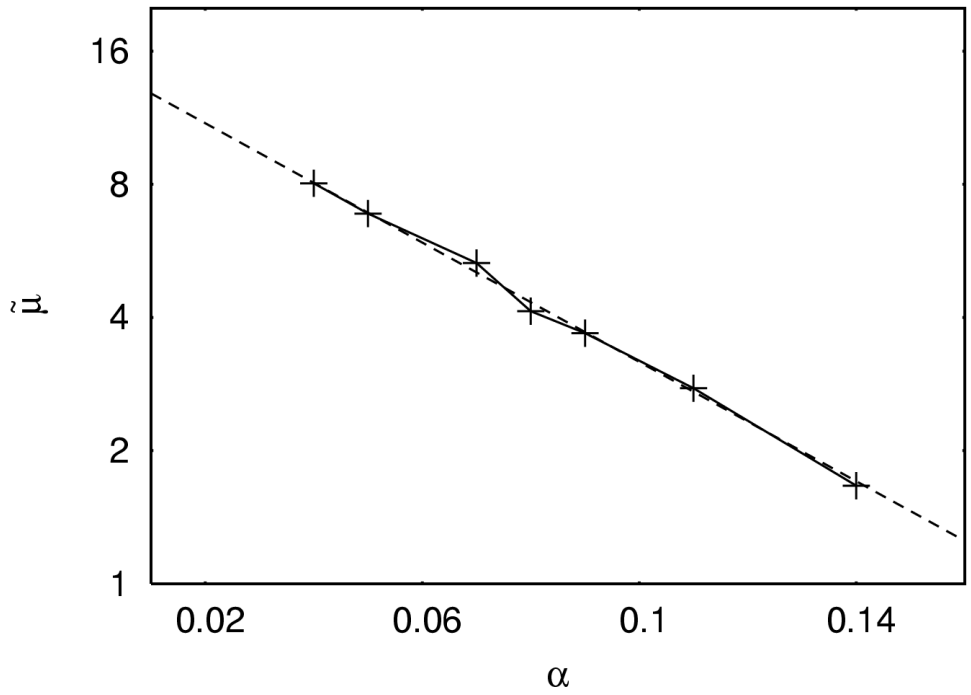

Figure 3.5: The exponent $\tilde{\mu}(\alpha)$ as obtained from the data shown in figure 3.4. The dashed line corresponds to the function $E\exp(-e\alpha)$. Numerical values for the fit parameter E and e are given in table 3.1.

While the data for $\tilde{\mu}$ appear too good to allow for other fits, the function $\tilde{f}(\alpha)$ might well have a somewhat different analytical form. Thus, the simulation results do not show the non-analytical divergence of the mean-field theory, which was due to the factor $\exp(r/\sqrt{\alpha})$ in the number of topplings n_c needed to integrate the next site into patch number r in equation (3.12). The dependence of this factor on α in the two-dimensional system appears from the fit to be instead the exponential of a negative exponential of α. However, since very small values of α were not accessible to the simulations, it cannot be ruled out that $\tilde{\mu}$ diverges after all for $\alpha \to 0$. If this was the case, the limit $\alpha \to 0$ would agree with the case $\alpha = 0$, where the transient time is infinite.

In view of the results in this section, I am now in the position to check how trustworthy the results reported in the literature are. As already pointed out by Grassberger [Gra94], transient times are extremely long, and the first publications [Ola92b, Chr92d, Ola92a, Chr92b] can have considered stationary systems only for the largest values of α.

It appears that many avalanche size distributions presented in the last decade were actually obtained during the transient stage. This claim can only be checked when the authors state how many initial avalanches they discarded for given L and α. Unfortunately, not all authors state, how they decided if the system is in the stationary state.

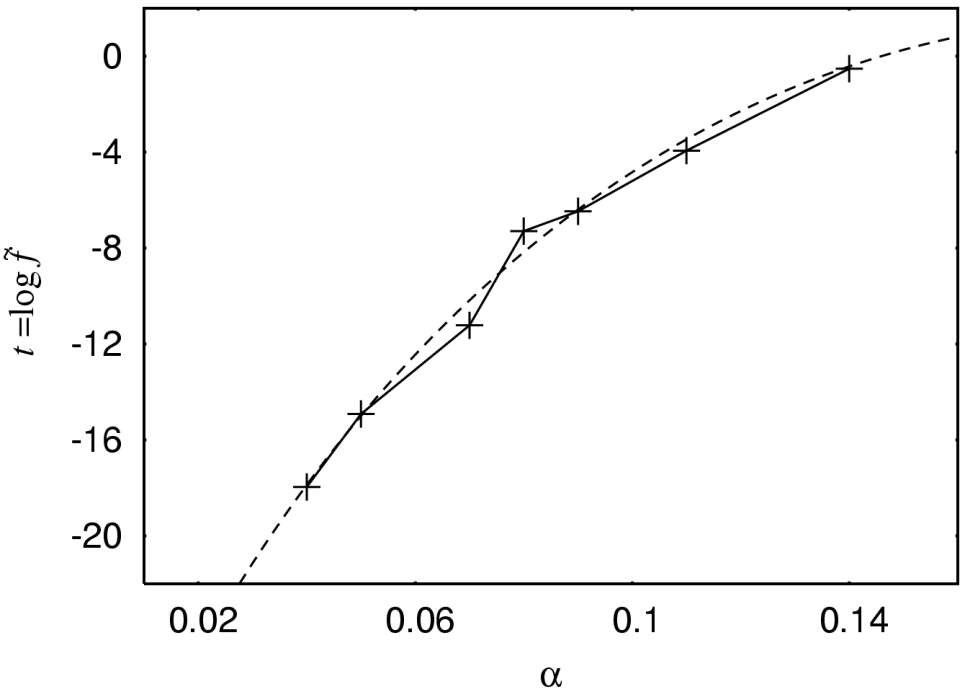

Figure 3.6: The function $t(\alpha) = \log \tilde{f}(\alpha)$ as obtained from the data shown in figure 3.4. The dashed line corresponds to the function $m\,\alpha + l + C\,\alpha^c$. Numerical values for the fit parameter m, l, C, c are given in table 3.1.

By observing statistical properties and comparing them at different times, one can be mislead to believe that the system has become stationary, although the advancement of the patches has only become very slow. This phenomenon was already mentioned at the beginning of this section.

Generally, the larger α and the smaller the system size, the more likely is it that the published avalanche size distributions were obtained in the stationary state. For example, the results published in [Cev95, Cev98] with $L = 25, 45$ were probably not taken in the stationary state for α below 0.2. Even Grassberger was evaluating avalanche size distributions during the transient stage in some parameter regimes.

Prado et al. considered a three-dimensional OFC model [Pei04b]. However, they did not aim at the size distribution of avalanches, but considered a network built up from sites that triggered an avalanche. In view of the trend that the transient time increases when going from one to two dimensions, an even longer transient time is to be expected for systems in three dimensions. Thus, it might be doubted that their evaluation was performed with stationary systems.

Now, that the transient time is understood (if not fully analytically, at least by reasonable dynamics derived within the mean-field picture), the interplay and stability of the patchy structure build up during the transient evolution can be explained. Before we go on with a deeper investigation of the patches, the solution for the toppling profile

$m \sim 887$	
$l \sim -35$	$E \sim 15.00$
$C \sim -1079$	$e \sim 15.53$
$c \sim 1.126$	

Table 3.1: Numerical values of the fit parameter for the the L-independent function $\tilde{f}(\alpha) \sim \exp(m\,\alpha + l + C\,\alpha^c)$ (left column) and for the exponent of L in figure 3.4, $\tilde{\mu}(\alpha) \sim E \exp(-e\,\alpha)$ (right column).

in the stationary state is presented.

Going back to the expression (3.3) and its continuous form, the replacement of the differential quotients with second derivatives is applied twice, once for each direction,

$$\begin{aligned} \langle t\rangle_{ij} &= \bar{g} + \bar{\alpha}\,(\langle t\rangle_{i-1,j} + \langle t\rangle_{i+1,j} + \langle t\rangle_{i,j-1} + \langle t\rangle_{i,j+1}) \\ t(x,y) &= \bar{g} + \bar{\alpha}\left(\frac{\partial^2}{\partial x^2}t(x,y) + \frac{\partial^2}{\partial y^2}t(x,y) + 4t(x,y)\right) \quad . \end{aligned} \tag{3.28}$$

Shifting the system by half its linear extension $l = L/2$, which yields the same simplification as in one dimension (see the remark to equation (2.27)), the boundary conditions read

$$\begin{aligned} t(x,-l) =& t(x,l) \stackrel{!}{=} 0 \quad , \\ t(-l,y) =& t(l,y) \stackrel{!}{=} 0 \quad . \end{aligned} \tag{3.29}$$

The solution for the stationary toppling profile is given by

$$t(x,y) = g\left(1 - \frac{\cosh(\kappa x)\cosh(\kappa y)}{\cosh^2(\kappa l)}\right) \quad , \tag{3.30}$$

with the same abbreviations as above.

3.2 Correlation functions and correlation length

The current section is a link between the determination of the transient time (3.1) and the discussion of the stationary properties (3.3). As has become clear from the previous section, the notion of patches and their size distribution (as function of the system size and of the coupling, as well as of their distance from the boundary) is an important feature of the system. It affects not only the transient time, as we have just seen, but also the size distribution of avalanches itself, which will be presented in the next section. This section puts results used in the last section on a firm ground, and ties together the internal behavior and the global distribution of the patches. Both, the first and the latter, are important for the transient dynamics and for the avalanche size distribution in the steady state.

This section therefore investigates how the extension of the patches in the directions parallel and perpendicular to the boundary increases with the distance from the boundary. The stability of the patchy structure, which has already emerged, while there might still be a disordered center left inside the system, is also discussed.

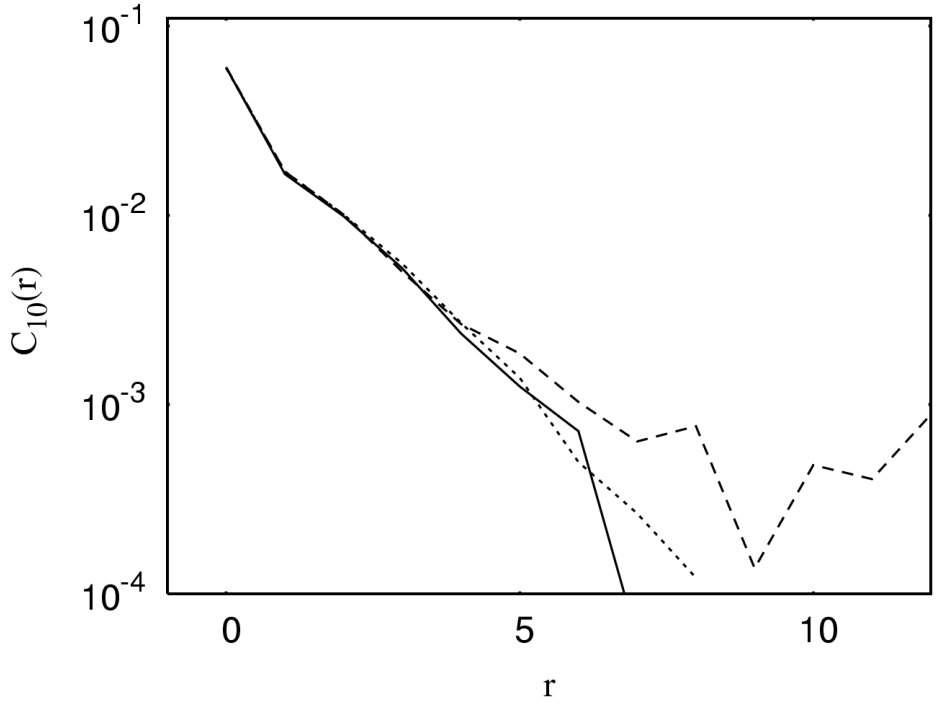

Figure 3.7: Correlation function $C_{i=10}(r)$ for $\alpha = 0.08$ for a distance $i = 10$ sites from the boundary at three different times (after 2570 (solid line), 5130 (dashed line), and 12490 (dotted line) topplings per site).

For this purpose, the effectively one-dimensional correlation function

$$C_i(r) = \langle (z_{ij} - z_{i,j+r})^2 \rangle - \langle z_{ij} \rangle^2 \tag{3.31}$$

is evaluated for a fixed distance i from the boundary, measured in number of sites, for different times, starting again at a random initial configuration.

The simulations are performed with systems that are periodic in the direction of the second coordinate, i.e. site $j+L$ is identical to site j. The extension L was chosen to be 2^{15} in order to obtain good statistics. The length of the system in the other direction was taken just as large as needed, between 48 (for small α, where the invasion front proceeds very slowly) and 512 (for large α, where L had to be reduced to $L = 2^{12}$ for technical reasons).

Figure 3.7 and figure 3.8 both present the correlation function $C_i(r)$ for $\alpha = 0.08$ and for three different times, at a distance $i = 10$ and at a distance $i = 20$ from the boundary, respectively. One can see that at distance $i = 10$ the correlation function does not change any more with time, which means that the patchy structure has been established at least up to this depth before the first measurement. We can furthermore conclude that the typical scale of the patches at a given distance from the boundary does not change any more when new patches are formed further inside. At distance $i = 20$, we see that the correlation function builds up with time from zero to an exponentially decaying function of the form $C_i(r) \sim e^{-r/\xi}$.

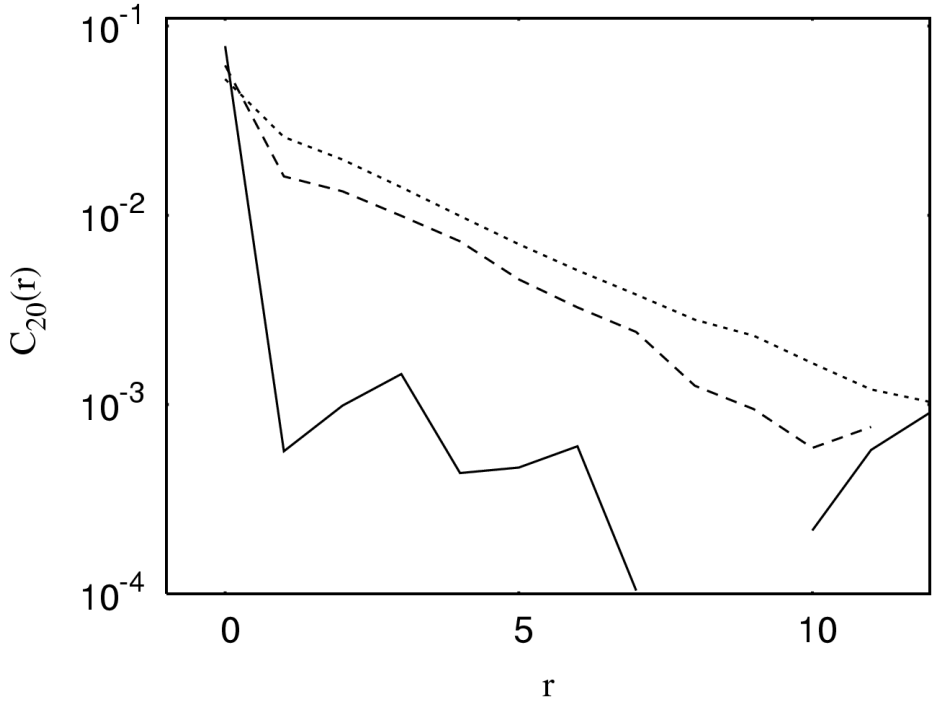

Figure 3.8: Correlation function $C(r)$ for $\alpha = 0.08$ for a distance $i = 20$ sites from the boundary at three different times (after 2570 (solid line), 5130 (dashed line), and 12490 (dotted line) topplings per site).

Using this ansatz, the correlation length $\xi(i, \alpha)$ was determined numerically as a function of the depth and for various couplings. For example for $\alpha = 0.12$, this ξ is shown in figure 3.9 as function of the distance i from the boundary for three different times. In the region where the patches are already present, ξ appears to increase as a power law in the distance i and then falls down to zero. We observe again that ξ remains constant, once the patches have emerged. The large oscillations seen before the decrease to zero occur in the region where the patches are just being formed. Due to large fluctuations in space, the averaging over the length of the system does not lead to a smooth curve for the system sizes used. Note that the smooth part of the curves breaks down at distances of about 30, 40, and 50 sites, and that the number of topplings is about twice as long between the first and the second, and the second and the third line. This indicates the slow invasion according to a power law in L as derived in the previous section.

Figure 3.10 shows the correlation length ξ as function of depth i for different values of α. The data are compatible with a linear increase of ξ with the distance i from the boundary, but with a coefficient that decreases with decreasing α. However, a power law $\xi \sim i^{\eta}$ with an exponent $\eta < 1$ that increases with α, cannot be ruled out.

Since the correlation length ξ measures the average range, over which sites are coupled, and coupled sites in turn resemble the patches, we are allowed to treat the correlation length as a measure for the average extension of patches for a given distance

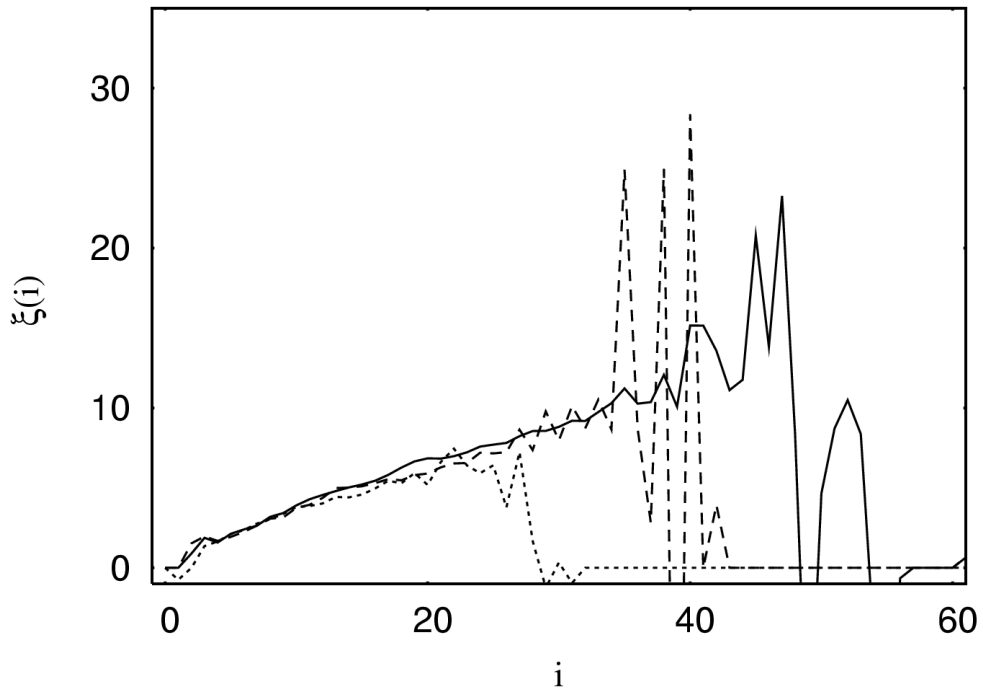

Figure 3.9: Correlation length ξ as function of the distance i to the boundary (measured in number of sites) for $\alpha = 0.12$ after 650 (dotted line), 1290 (dashed line) and 2570 (solid line) topplings per site.

i from the boundary. The linear (or power law) increase of the correlation length together with the patchy structure and the phenomenological observation leads to the following schematic picture (see figure 3.11):

The characteristic size of the patches increases with distance from the boundary. From one generation of patches to the next, the width and height of the patches increase with factors $P(\alpha)$ and $Q(\alpha)$, respectively. In the case $\eta = 1$, we have $P = Q$. Of course, the patches at a given distance from the boundary do not all have exactly the same size, but a size of the indicated order of magnitude. From snap shots of the systems, it is clear that $P(\alpha)$ and $Q(\alpha)$ increase with α. Furthermore, there must be a lower bound of 1 to both factors in the limit $\alpha \to 0$. Thus, we can write

$$Q(\alpha) = \exp[f(\alpha)] \tag{3.32}$$

with a monotonically increasing function $f(\alpha)$ and $f(0) = 0$. The leading dependence on α can therefore be expected to be $f(\alpha) = A\alpha^a$ with both, A and a, being positive. This assumption was used in the previous section for the derivation of equations (3.21) and (3.22). The same argumentation holds for the factor $P(\alpha)$.

The self-similarity implied by these considerations is quite convincingly confirmed by the snap shots in figure 3.12. These systems, all in the steady state for the same coupling $\alpha = 0.11$, seem to have a boundary frame of approximately the same thickness. The patchy inner structure is obviously build up from patches of about the same

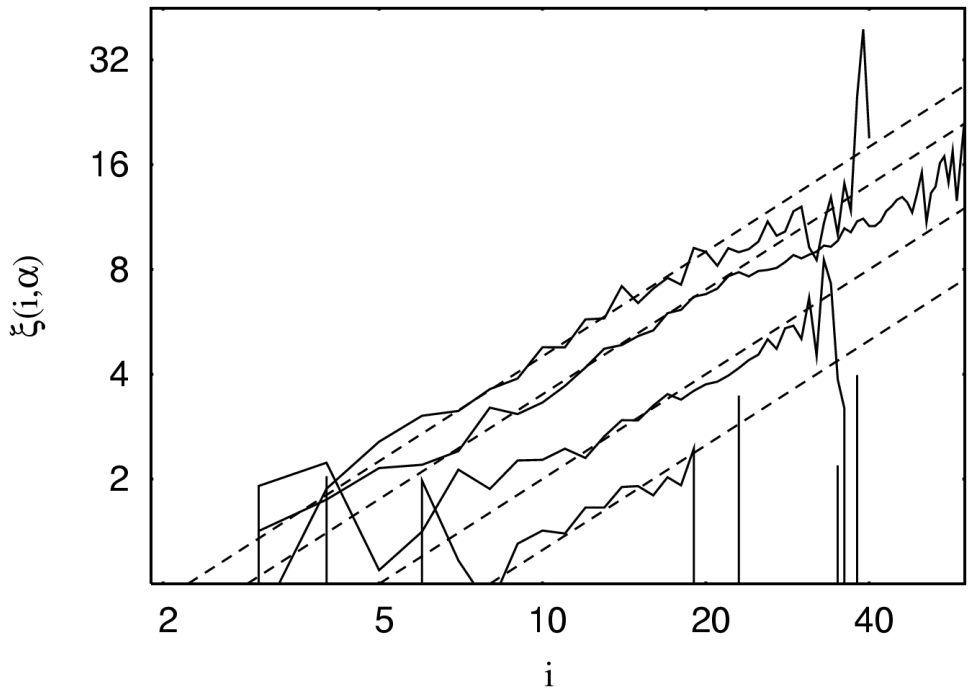

Figure 3.10: Correlation length ξ as function of the distance i to the boundary (measured in number of sites) for $\alpha = 0.06, 0.09, 0.12$, and 0.15 (from bottom to top) at the largest times simulated for a given value of α (solid lines); the dashed lines correspond to lines of slope 1.

type, though the detailed arrangements differ. Even the patches seem to have a similar internal structure, naturally within the same system, but as well when compared between different systems. The striking point is that the system sizes in the series 3.12 increase by a factor of 2 between the figures from left to right.

Using that ξ can be taken as the mean patch size parallel to the boundary, the correlation length in the m-th generation of patches (counting from the boundary) is connected with the m-th power of the factor P

$$\xi \sim P^m \sim i^\eta \quad , \tag{3.33}$$

while the distance from the boundary itself is determined by

$$i \sim \sum_{j=1}^{m} Q^j \quad . \tag{3.34}$$

On the other hand, the average height, h, of a patch of the m-th generation is proportional to $h \sim Q^m$, since the extension of the patches increase by the factor Q from one generation to the next. For patches deep in the system (or large Q), we can approximate the sum in equation (3.34) with the last summand and use equation (3.33) to derive a relation

$$h \sim \xi^{1/\eta} \quad . \tag{3.35}$$

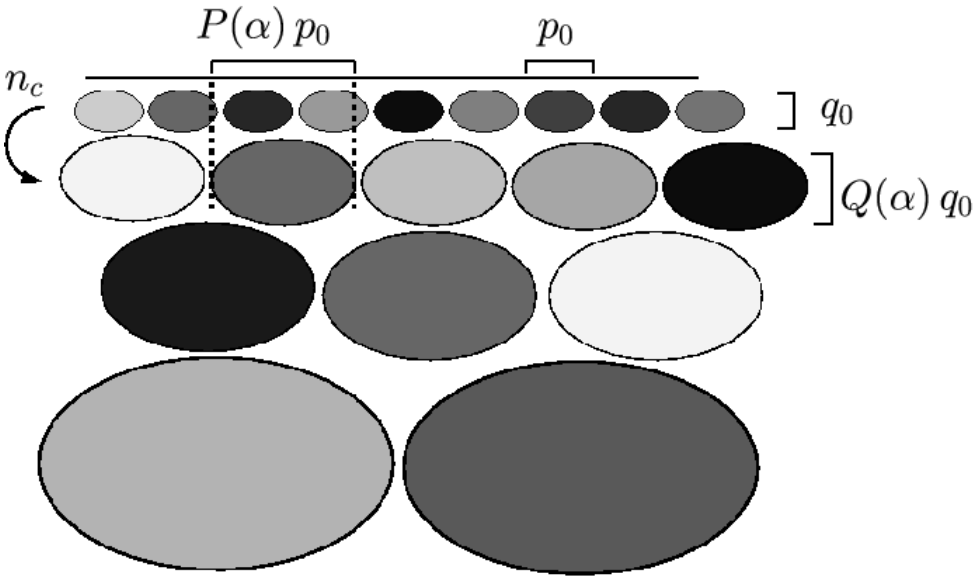

Figure 3.11: Schematic view of the system's structure: the width and height of patches increase with a power law in the distance to the boundary. Different generations of patches are coupled via n_c (as derived in equation (3.11)), the increase in the size of the patches is $P(\alpha)$ parallel to the boundary and $Q(\alpha)$ perpendicular to it, starting with a size $s_0 = p_0 q_0$.

Based on this picture, we can write down an expression for the size distribution of patches, which will be an important tool when discussing the size distribution of avalanches below.

If the patches were all perfect rectangles with no overlap between the generations, the number of patches in each generation would decrease by just the factor P in each step (counted in numbers of generations). But the generations of patches do overlap, and we have to take into account a blurring effect. The maximum overlap for a given patch is just the extension of this patch perpendicular to the boundary. Thus, a line at the distance i from the boundary cuts only through approximately $\sim L/(\xi h)$ new patches of width ξ and height $h \sim \xi^{1/\eta}$, through which a line at the distance $i-1$ from the boundary does not cut, since there are L sites along this line. The width distribution of patches is therefore given by

$$n_P(\xi) d\xi = \frac{L}{\xi h} d\,(i) \quad . \tag{3.36}$$

Using again expression (3.33) leads to

$$n_P(\xi) \sim \frac{L}{\xi^2} \quad , \tag{3.37}$$

where the proportionality is given by $1/\eta$ and thus has a value around unity, but increases with decreasing α. Transforming this into the size distribution $n_P(s)$ with $s \sim \xi h$, we obtain

$$n_P(s) \sim L s^{-\tau_p} \quad , \tag{3.38}$$

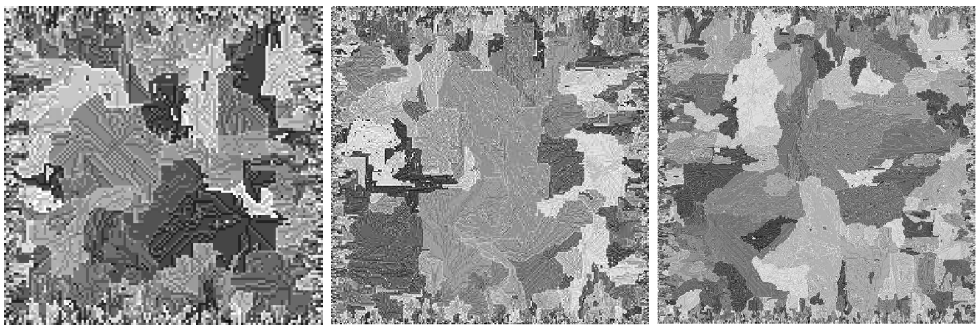

Figure 3.12: Snap shots of systems in the stationary state for a coupling $\alpha = 0.11$ and different values of the system size: from left to right: $L = 128$ after 10^4 topplings per site; $L = 256$ after 102700 topplings per site; $L = 512$ after 592000 topplings per site.

for which the exponent τ_p is given by

$$\tau_p = \frac{1+2\eta}{1+\eta} \quad . \tag{3.39}$$

In the likely case that $\eta = 1$, we have an exponent $-3/2$ in the size distribution of patches. Expressed in terms of P and Q instead of η, the last equation becomes

$$\tau_p = \frac{\ln P}{\ln PQ} + 1 \quad , \tag{3.40}$$

where P and Q still depend on α and the relation $P = Q^\eta$ was used. The expression (3.38) for the size distribution of patches can also be obtained directly from the recursion relation

$$\int n_P \left(sP(\alpha)Q(\alpha)\right) ds = \int n_P(s) \frac{1}{P(\alpha)} ds \quad , \tag{3.41}$$

where the integral is taken over one generation of patch sizes.

3.3 The stationary state

The focus now turns on the stationary state of the OFC model in two dimensions. While some features of the steady state were already discussed in the previous section, especially the size distribution $n(s)$ of avalanches is investigated and explained now.

Of course, I made sure that the process of patch formation has reached the center of the system, before avalanche size distributions were evaluated [4]. Taking small system sizes has the advantage of reaching the stationary state fast, but small systems have the disadvantage of being strongly affected by finite-size effects. It is therefore very difficult to predict the avalanche size distributions in the thermodynamic limit.

Figure 3.13 shows avalanche size distributions for varying α with fixed L. Distributions for varying system sizes with a fixed coupling are presented in figures 3.14 and 3.15. The value of L in the first figure (3.13) has been chosen small enough that the

[4] Following the definition in section 3.1, a system is treated as stationary, once the patches have reached the center of the system and there is no disordered inner block left.

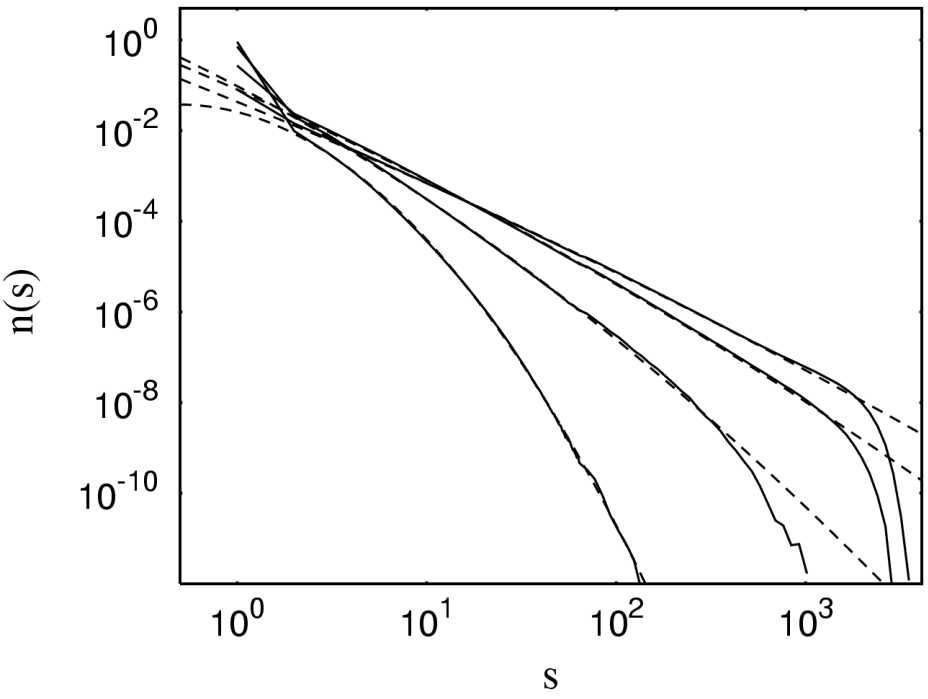

Figure 3.13: Size distribution of avalanches for a system size $L = 64$ and $\alpha = 0.03, 0.08, 0.13, 0.18$, steeper curves correspond to smaller α (solid lines); the s axis extends up to the total number of sites within the system, 4096; the distributions are normalized on the total number of topplings; dashed lines correspond to $f(s) \sim s^{-\tau-\sigma \ln s}$.

system could reach the stationary state even for the smallest value of α, which was 0.03. We can discern the following features:

1. At least for values of α smaller than 0.17, the avalanche size distribution is no power law. A fit of the form
$$n(s) \sim s^{-\tau(\alpha)-\sigma(\alpha) \ln s} \tag{3.42}$$
approximates the data much better than a pure power law.

2. $n(s)$ changes its shape with increasing system size, implying that the system size affects the relative weight even of small avalanches, at least for the system sizes considered. This effect is stronger for smaller α. Only for the largest value of α, the main effect of the finite system size is a rather sharp cutoff at L^2.

3. The weight of avalanches of size 1 increases with increasing system size, while the weight of all larger avalanches decreases as $1/L$ (see below). Note that the distributions in figures 3.14 and 3.15 for various system sizes are normalized such that the frequency of avalanches of size 2 is unity. This presentation pictures the increasing weight of single topplings.

In the following, these features are explained based on the results obtained in the previous sections, and on what is known from literature (see section 1.3.1). Described in

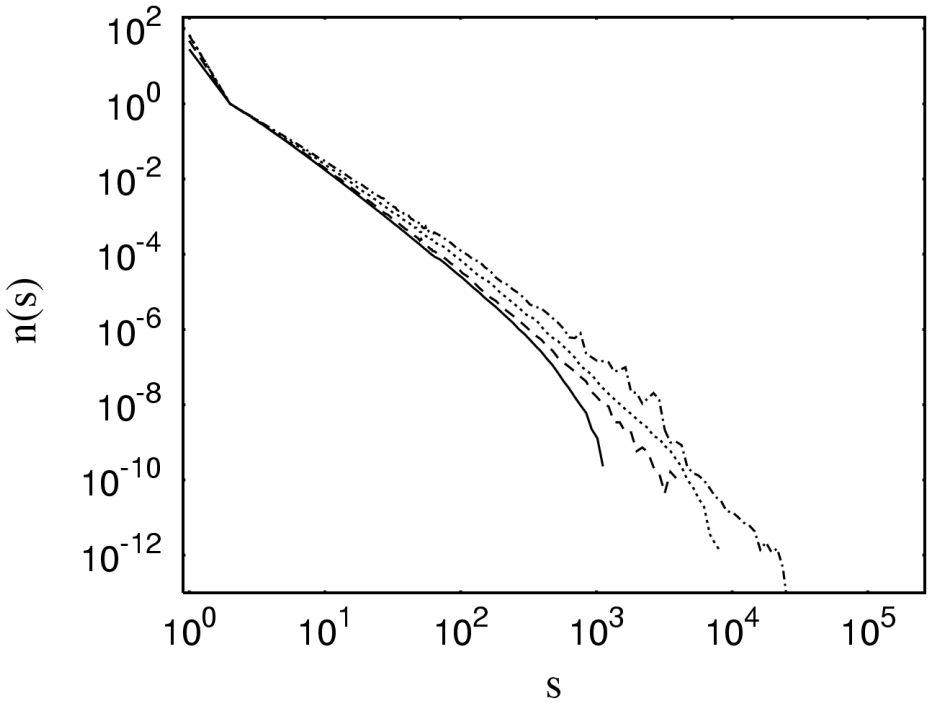

Figure 3.14: Size distribution for system sizes $L = 64$ (solid line), $L = 128$ (dashed line), $L = 256$ (dotted line), and $L = 512$ (dash-dotted line) and coupling $\alpha = 0.09$; the distributions are divided by $n(2)$.

words, the scenario is the following: patches persist for a long time before they change their shape [Bot97] due to an avalanche that enters the patch from outside [Gra94], and patches further inside the system are rearranged less often. Large, patch-wide avalanches are mainly triggered at the boundaries of the system [Lis01b]. Whenever a patch-wide avalanche took place, there is a sequence of 'aftershocks' with decreasing size according to Omori's law [Her02], and after a short time there occur mostly single topplings within a patch until the next large avalanche comes from a patch of the previous generation.

These statements now must be quantified. Analogous to the process of synchronizing neighboring sites discussed in section 3.1, neighboring patches also need a certain number $n_c(\alpha, r)$ of patch-wide avalanches in the patch closer to the boundary, before the inner patch experiences a patch-wide avalanche. As for the incorporation of a new site into a patch during the transient evolution, the energy difference between patches must be smaller than α in order to trigger an avalanche from outside the patch. This difference can only be changed by large events in the patch closer to the boundaries, because single topplings do not affect the difference (compare with the findings in section 2.2.1). This mechanism can be evaluated using the implicitly time-dependent solution for the toppling profile from equation (3.8) for the situation that $r = r_{\max}$. The patches are treated again as single effective sites as far as the toppling behavior of sites within the same patch is concerned. Hence it is allowed to use the same expres-

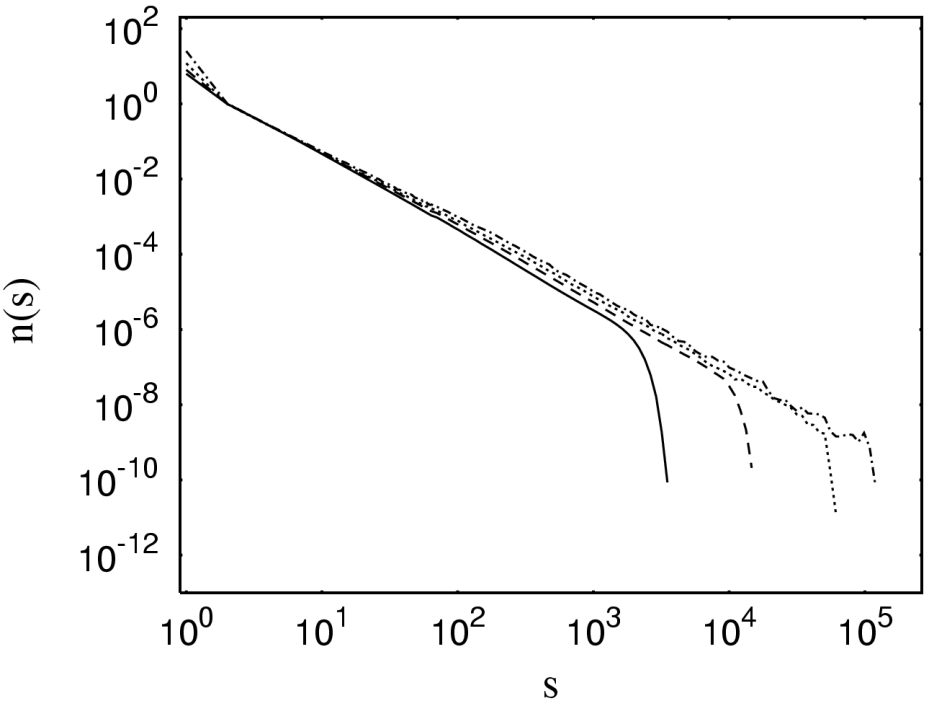

Figure 3.15: Size distribution for system sizes $L = 64$ (solid line), $L = 128$ (dashed line), $L = 256$ (dotted line), and $L = 512$ (dash-dotted line) and coupling $\alpha = 0.17$; the distributions are divided by $n(2)$.

sion for the coupling, $n_c(\alpha, r)$, which has been derived as an estimate for the necessary number of topplings to add a site to a patch (see equation (3.11) and the discussion before). We therefore obtain the recursion relation

$$\int n_{pw}\left(P(\alpha)Q(\alpha)s\right) ds = \int n_{pw}(s) \frac{1}{P(\alpha)n_c(\alpha, r)} ds \quad , \tag{3.43}$$

for the size distribution of patch-wide avalanches, similar to the one found for the distribution of patch sizes (compare with equation (3.41)).

If n_c was independent of the generation number r, this relation would result in a power law

$$n_{pw}(s) \propto L s^{-\tau(\alpha)-1} \tag{3.44}$$

with an exponent

$$\tau(\alpha) = \frac{\ln\left[P(\alpha)n_c(\alpha)\right]}{\ln\left[P(\alpha)Q(\alpha)\right]} \quad . \tag{3.45}$$

For systems not too big, and for large enough α, as they have been used in the first publications on the OFC model, there are only a few generations, and the approximation of a constant n_c is not too bad. Evaluating equation (3.8) for small α, we obtain

the following result for n_c that depends on the generation index r,

$$n_c(\alpha, r) \sim \exp\left(\frac{r-1}{\sqrt{\alpha}}\right) , \tag{3.46}$$

(see also equation (3.12)). The average number of sites in a patch of the r-th generation is given by

$$s = (PQ)^r \, s_0 \quad , \tag{3.47}$$

where $s_0 = p_0 q_0$ is the number of sites in a patch of the first generation, as remarked in figure 3.11. Since the smallest possible patch is a single site, we can take $s_0 = 1$ and use the relation (3.47) to express the generation index r in terms of the size s and the incremental factors P and Q:

$$r \sim \frac{\ln s}{\ln PQ} \quad . \tag{3.48}$$

For the iteration of equation (3.43), we need to evaluate the product

$$\prod_{j=1}^{r} \left(\frac{1}{P(\alpha) n_c(\alpha, j)}\right) = \left(\frac{1}{P(\alpha)}\right)^r \exp\left(-\frac{r(r-1)}{2\sqrt{\alpha}}\right) \quad , \tag{3.49}$$

where

$$\prod_{j=1}^{r} \exp(-j) = \exp\left(-\sum_{j=1}^{r} j\right) = \exp\left(-\frac{r(r-1)}{2}\right) \tag{3.50}$$

was used. Using $r \sim \ln s / \ln(PQ)$ from equation (3.48), the expression (3.49) leads to a size distribution of patch-wide avalanches of the form

$$n_{pw}(s) \sim L s^{-\tau(\alpha)-1-\sigma(\alpha)\ln s} \quad . \tag{3.51}$$

The factors $\tau(\alpha)$ and $\sigma(\alpha)$ are given by

$$\begin{aligned} \tau(\alpha) &= \frac{1}{\ln(P(\alpha)Q(\alpha))}\left(\ln P(\alpha) - \frac{1}{2\sqrt{\alpha}}\right) \\ \sigma(\alpha) &= \frac{1}{2\sqrt{\alpha}(\ln(P(\alpha)Q(\alpha)))^2} \quad . \end{aligned} \tag{3.52}$$

Just as in the case of the transient time, the precise analytical form of σ and τ is expected to be different from this result, which is based on mean-field arguments. In particular the factors $1/\sqrt{\alpha}$ will most likely have to be modified. However, the qualitative features of the result are captured in the simulation data, as shown below.

Equation (3.51) gives the distribution of avalanches, which affect all the sites in a patch. In order to estimate the global size distribution of avalanches, the effect of 'aftershocks' has additionally to be taken into account. These aftershocks will lead to an avalanche size distribution that differs from that of the patch-wide avalanches. Aftershocks are avalanches that occur within a patch after a patch-wide avalanche. Their size distribution is assumed to be a power law with a cutoff at the size of the patch. This assumption is motivated by the finding that systems, which are dominated by one large patch, display a power law size distribution of avalanches. This observation

is found for couplings near the conservative case, $\alpha = 0.25$, as reported in the literature [Ola92b, Lis01a] (see also [Her02, Hel04] for a detailed discussion of the aftershocks).

Therefore, the number of aftershock avalanches, $n_{as}(s|s')$, of size s in a patch of size s' can be approximated by

$$n_{as}(s|s') = s'^{\tau_0} s^{-\tau_0} \theta(s' - s) \quad . \tag{3.53}$$

The exponent τ_0 has a value around 1.8, which is the value found in [Lis01a] for systems that have essentially one large patch. The size distribution of avalanches is then given by

$$\begin{aligned} n(s) &\propto L \int_s^\infty n_{pw}(s') n_{as}(s|s') ds' \\ &= L s^{-\tau_0} \int_s^\infty s'^{-\tau(\alpha)-1-\sigma(\alpha)\ln s'} s'^{\tau_0} ds' \\ &\sim L s^{-\tau(\alpha)-\sigma(\alpha)\ln s} \quad , \end{aligned} \tag{3.54}$$

apart from a factor containing terms that depend on $\ln s$. Thus, the avalanche size distribution is not a power law, but has an exponent that depends logarithmically on s. As shown above in figure 3.13, the data agree well with such a law.

Figure 3.16 shows the results obtained for the coefficients σ and τ by fitting the numerical size distributions of avalanches with the just-derived expression (3.54). Although the data is likely to be affected by finite-size effects particularly for small α, the fit parameter σ and τ appear to coincide for different system sizes, and at least for larger α.

$\sigma(\alpha)$ and $\tau(\alpha)$ as a function of the coupling show a behavior that is in qualitative agreement with the mean-field expressions (3.52): for small α, the incremental factors $P(\alpha)$ and $Q(\alpha)$ reach unity from above (see equation (3.32) and the logarithms $\ln P$ and $\ln Q$ are small and positive. The behavior of τ is dominated by a factor

$$\left(\mathcal{O}(\alpha) - \mathcal{O}(1/\sqrt{\alpha})\right) \quad . \tag{3.55}$$

Thus, τ decreases rapidly and will eventually become negative for small couplings, while σ tends to large positive values. Note that the s-independent part of the exponent, τ, has a value around $\tau_0 = 1.8$ for larger couplings, while σ is rather small. The latter might eventually vanish for even larger α. It must vanish for the conservative case, $\alpha = 0.25$, which is known to result in a real SOC state [deC00, Mil02, Mil03b]. Whether this transition occurs already for smaller and thus dissipative couplings cannot be determined by the data. At least for $\alpha \leq 0.2$, the coefficient σ is finite.

The cutoff in the (global) avalanche size distribution is determined by the size of the largest patch. As this size becomes smaller with smaller α, the cutoff decreases also. Furthermore, since larger patches make a contribution to smaller avalanches via aftershocks, the effect of the finite system size will be felt down to avalanche sizes much smaller than the largest patch. This feature is observed in the data.

Finally, the weight of avalanches of size 1 should be addressed. After a patch-wide avalanche and the resulting aftershocks, only single topplings occur within the patch, i.e. avalanches of size 1. The dynamics within a patch are just as within a system with periodic boundary conditions, until a new patch-wide avalanche is induced from

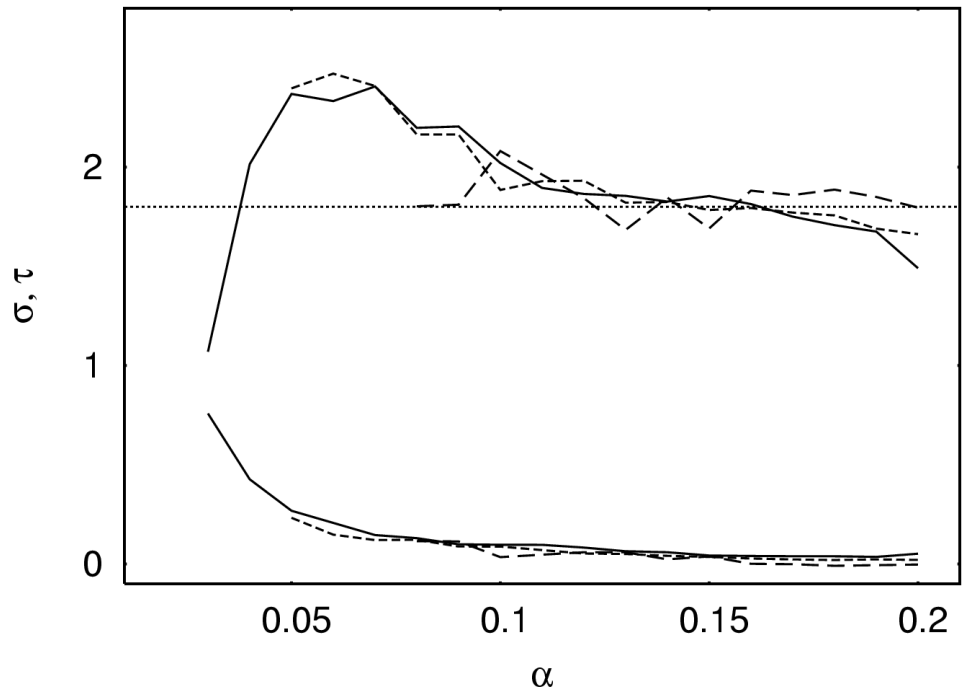

Figure 3.16: The coefficients $\sigma(\alpha)$ (lower set of curves) and $\tau(\alpha)$ (upper set) as function of α as found by fitting the distributions $n(s)$ for $L = 64$ (solid line), $L = 128$ (dashed line), and $L = 256$ (long dashed line) for those values of α, for which the stationary state of the systems was reached. Dotted line indicates the value $\tau_0 = 1.8$.

outside the patch. The total number $N(s > 2)$ of avalanches of size larger than 1 per unit time is given by

$$N(s > 2) = \int_2^\infty n(s)ds \propto L \quad . \tag{3.56}$$

However, the total number of topplings per unit time is proportional to the number of sites in the system, L^2, and therefore only a proportion of the order of $\mathcal{O}(1/L)$ of avalanches has a size larger than 1. Thus, the relative weight $w(s > 2)$ of the tail decreases as $1/L$. For large L, where finite-size effects are less dominant, $n(1)$ should therefore approach unity as

$$\lim_{L\to\infty} n(1) = 1 - \frac{1}{L} \quad . \tag{3.57}$$

This result is confirmed in the data. Since the distributions $n(s)$ are very fast decreasing functions of the avalanche size s, the frequency of $n(2)$ can be taken as an approximation for the weight $w(s > 2)$. The ratio between avalanches of size 1 and avalanches of size 2 should accordingly be proportional to the system size, $(1 - 1/L)/(1/L) \sim L$. In figure 3.17 this ratio, $n(1)/n(2)$, is shown as a function of the system size L for a coupling $\alpha = 0.17$. For larger system sizes, the data agree with a linear increase in L.

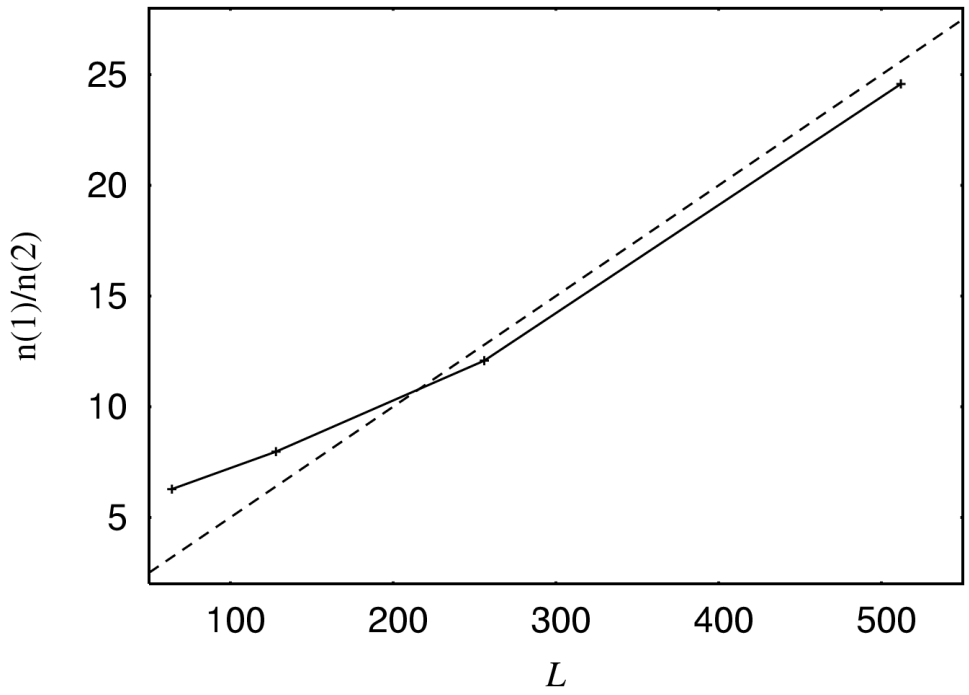

Figure 3.17: The ratio $n(1)/n(2)$ obtained from the size distribution in figure 3.15 for $\alpha = 0.17$ as function of the system size L. The dashed line corresponds to $f(L) \sim L$.

3.4 Summary $d = 2$

Numerous important results have been derived for the OFC model in two dimensions. The main feature of the system is the emergence of patches, which are a result of the open boundary conditions. They determine the dynamics of the model during the transient stage, when they are formed, as well as the statistics in the stationary state.

After random initialization, the center of the system soon settles in a pseudo-periodic state, which behaves as if it was part of a system with periodic boundaries, i.e. only single topplings are observed deep in the system, as long as the patches did not reach the center. This disordered inner block is disturbed by the formation of patches, which starts at the borders and is driven by the lack of neighbors for boundary sites.

The extension of the patches increases with distance to the boundaries and with increasing coupling α. A patch comprises several sites, all of them showing a synchronized behavior: their energy values z_{ij} are close to each other and differ only by an amount of the order of $\mathcal{O}(\alpha)$. For small couplings, the patches are clearly separated and have less inner structure, while larger α result in a more blurred appearance of the patches as seen by visual inspection. Within a patch, sites topple one by one, or in patch-wide avalanches and a series of aftershocks. The patches are stable over many cycles $1 - 4\alpha$. Thus, sites in a patch have to topple the same number of times and a patch can be treated as a single effective site.

The transient time of the two-dimensional OFC model is defined to be the number of topplings necessary for the patch formation to reach the center of the system. The transient time can be estimated within a mean-field-like theory using a time-dependent toppling profile. This approach is inspired by the evaluating of local balance equations in one dimension. In contrast to the one-dimensional case, the expression for the toppling profile has to be applied for patches, i.e. for effective sites and not for single sites. Sites, which are not yet part of a patch, or patches of subsequent generations, are coupled by a certain number of topplings $n_c(\alpha, r)$. These topplings are necessary to diminish the energy differences between a patch and its counterpart (a single site or another patch). Thus, either a new site is added to a patch, or a patch-wide avalanche is triggered within an adjacent patch. The mean-field calculation yields an expression for the transient time of the form

$$T(\alpha, L) \sim \tilde{f}(\alpha) L^{\tilde{\mu}(\alpha)} \quad , \tag{3.58}$$

with an diverging $\tilde{f}(\alpha) \sim \exp(-1/\sqrt{\alpha})$ for small α. Numerically, the transient time is found to obey equation (3.58), but lacks the non-analytical divergence. This deviation might stem from the fact that the regime of very small α could not be accessed by computer simulations. However, the important result is the power law dependence on the system size L. Furthermore, the exponent $\tilde{\mu}$ is a rapidly increasing function of decreasing α, whether estimated using mean-field assumption or found by numerical investigations. This finding is in contrast to earlier predictions that the transient time increases as a (α-independent) power law with system size [Lis02a], or that the transient time becomes infinite when α is smaller than some threshold value [Gra94].

By evaluating the correlation length of the energy values, the size of the patches is found to increase as a power law with distance from the boundary, leading to power law size distribution of the patches. The dynamics in the steady state are also governed by the mechanisms in the patches. Even if the size distribution of avalanches within a patch is assumed to be also a power law, the overall size distribution of avalanches, $n(s)$, is no power law. Instead, it has a logarithmic dependence on the avalanche size, s, in the exponent,

$$n(s) \sim L s^{-\tau(\alpha) - \sigma(\alpha) \ln s} \quad , \tag{3.59}$$

i.e., $n(s)$ is a log-normal distribution. This finding is supported by the simulation data and is valid at least for not too large α, where the system is not dominated by one large patch.

Although the simulation results were obtained by using an efficient algorithm, the sharp increase of the transient time with the system size, especially for small α, made it impossible to study system sizes as large as necessary to see the true asymptotic behavior of the avalanche size distributions. However, a key feature could be observed: The weight of avalanches of size 1 increases with the system size, while the tail's weight of the distribution $w(s > 2)$ decreases as $1/L$. Thus, in the thermodynamic limit of infinite systems, only single topplings would be observed. This result is explained in the enormous number of topplings necessary to reorganize a patch in order to prepare the sites for the next patch-wide avalanche. Additionally, the statistics are dominantly determined by the largest patch, which itself becomes of the order of the system size for larger and larger L.

A shortcut version of the results for the OFC model in two dimensions can be found in [Wis06].

Chapter 4

Conclusion

If there are any more ways I can make this
more confusing, please let me know.
Robert Dorsett

This section summarizes the main results for the OFC model in $d = 1$ and $d = 2$ and recapitulates the answers to the question raised in the introduction 1.3.2. The properties of the OFC model in one and two dimensions are compared, using results collected from the literature and obtained in the previous chapters 2 and 3. The chapter closes with a remark on the relevance of the OFC model.

4.1 The transient stage in one and two dimensions

Within periodic boundaries and for the simple cubic lattice, the system settles in a periodic cycle, where only single toppling events take place, and only packages of exactly α are redistributed among neighboring sites. The period length is $1 - 2d\alpha$ in units of the external energy input, which corresponds to a number of topplings equal to the number of sites in the system, L^d. All sites have an energy gap of at least α to its nearest neighbors, thus no triggered toppling can be induced [Soc93, Gra94]. These findings are valid for one and two dimensions, and such a periodic state is also expected in higher dimension, but this expectation is not yet confirmed.

The situation changes for open boundary conditions. Now, the time evolution of the OFC model towards the stationary state is driven by nonlinear terms in the coupling α, stemming from the open boundaries. The lack of neighbors for boundary sites results in an effectively less growth rate compared to sites in the bulk. Accordingly, sites at the border of the system topple less often than bulk sites, resulting in turn in less energy input for their neighbors. Thus, the effect of the boundaries continues into the center of the systems. A mean-field-like theory exploits local balance equations and hints at a penetration depth of about

$$\frac{1}{\kappa} = \sqrt{\frac{\alpha}{1 - 2d\alpha}} \quad . \tag{4.1}$$

While in one dimension the system splits into two boundary layers and one or two synchronized blocks in the center, a patch formation is observed in two dimen-

sions. During the transient stage, the systems have a disordered inner part, which is characterized by a pseudo-periodic behavior in both dimensions, $d = 1$ and $d = 2$.

The thickness of the boundary layers in *one* dimension is numerically found to be larger than the estimation (4.1). However, the boundary layers are explicitly independent of the system size L, and the detailed dynamics within the layer are determined by the coupling α only. Once these layers have formed (within several topplings per site), they enslave the center of the system, and are responsible for a synchronization process. Within the disordered center only single topplings occur. Sites in the already synchronized blocks also topple one by one or in large avalanches, which are triggered near the boundaries and reach through the entire block of synchronized sites. The synchronization proceeds inwards one site at a time, incorporating more and more sites from the pseudo-periodic inner part. As a function of the coupling, the transient time is proportional to a negative exponential for a large range of couplings:

$$T_{d=1}(\alpha) \sim \exp(-14.8\alpha) \quad , \tag{4.2}$$

but for $\alpha \to 0$ it obeys a power law:

$$T_{d=1}(\alpha) \sim \alpha^{-2.84} \quad . \tag{4.3}$$

The numerical values -14.8 and -2.84 are both obtained by fitting the simulation data.

In *two* dimensions, the system also separates into a pseudo-periodic center and a boundary frame during the transient regime. This boundary region increases with time and finally covers the whole system in the stationary state. In contrast to the synchronized blocks in one dimension, a rich structure is observed for the two-dimensional case. Patches are formed, starting at the boundaries and a result of the open boundary conditions. The size of these patches increases with distance from the boundary and for increasing α. Sites within a patch act collectively as a single *effective* site. They topple one by one or in a series of patch-wide avalanches and aftershocks. The total number of topplings is the same for all sites in the patch and the energies z_{ij} are distributed in a narrow interval of the order of $\mathcal{O}(\alpha)$. The patches are stable over many cycles $1 - 4\alpha$. The mean-field approach using the local balance equations has to be applied for patches and not for single sites. The process of building up more patches, or to incorporate another site into a patch, is again driven by the nonlinearity in α. Two adjacent patches are coupled by a number $n_c(\alpha, r)$ of large avalanches occurring in the smaller patch, where r is the generation index of that patch. The number of topplings per site to increase a patch by one site is also determined by n_c. Using this expression and summing over the extension of each generation of patches yields the transient time as a function of the system size L and the coupling α:

$$T_{d=2}(\alpha, L) \sim \tilde{f}(\alpha) L^{\tilde{\mu}(\alpha)} \quad . \tag{4.4}$$

The expression (4.4) is a mean-field result and is in parts confirmed by computational simulations. While the theory predicts a diverging transient time in the limit of vanishing α, a numerical fit suggests a finite transient time. However, for $\alpha = 0$, the transient time is infinite, and the result obtained by extrapolating the data to a coupling of zero might be adjusted, when simulations can be performed for smaller α. In any case, the transient time is awfully long, even for non vanishing α, and it increases as a power law with the system size, as suggested in [Mid95]. The exponent $\tilde{\mu}$ is found to increase very fast for smaller α.

4.2 The stationary state in one and two dimensions

Several features of the one-dimensional model are very similar to the two-dimensional model, while others differ. The computing precision affects the avalanche size distribution in both cases. However, while there are less large avalanches for smaller computing precision in one dimension, there are more large avalanches in two dimensions [Dro02].

In both versions, large avalanches are only triggered at or near the boundaries [Lis01b], and the interior of the system is to some extent slaved to the dynamics in the vicinity of the boundaries. The inner part of the system is dominated by avalanches of size 1 [Gra94, Bot97, Dro02], irrespective of the dimension.

In one dimension, the size distribution of avalanches splits into two clearly separated regimes. Peaks at about the system size or half the system size have a weight, which decreases as $\sim 1/L$ with increasing L. Smaller avalanches dominate the distributions. The precise shape of that low-size regime depends only on the coupling α.

In two dimensions, avalanches of all sizes are observed up to an upper bound, which decreases with decreasing α and resembles a sharp cutoff only for α above 0.17. For those larger couplings, a pure power law in the avalanche size, $n(s) \sim s^{-\tau}$, is arguable, but a much better general expression for the distribution is given by

$$n_{d=2}(s) = s^{-\tau-\sigma \ln s} \quad . \tag{4.5}$$

The coefficients σ and τ are functions of α. The distribution (4.5) is justified within a mean-field theory and confirmed by fitting the numerical data. The large range of possible avalanche sizes is due to the patchy structure of the systems. Within a patch, avalanche distributions obey a pure power law, up to the size of the patches [Ola92b, Lis01a]. The patch size itself is also distributed according to a power law, which is recognized in the self-similar structure, seen in snap shots of the systems. The superposition of patch-wide avalanches and aftershocks from all the patches in the system results in the logarithmically corrected exponent, which depends on the avalanche size s. Thus, the OFC model is clearly not self-organized critical in the usual sense and certainly not for values of α below 0.2. Nevertheless, for a conservative coupling, $\alpha = 0.25$, the SOC state is reached [deC00, Mil02, Mil03b]. The coefficient σ for the logarithmic term $\ln s$ in the size distribution (4.5), which prevents a proper power law, decreases with increasing α and eventually vanishes, possibly already for nonconservative α, but the transition point cannot be spotted.

4.3 The relevance of the OFC model

The above-listed results are interesting for several reasons:

First, the OFC model appears to show many features found in real earthquakes. As far as earthquake predictability [Pep94], Omori's law [Her02, Hel04], or the statistics of a network of epicenters [Pei04a, Pei04b] are concerned, the OFC model appears to be closer to reality than others. If α is chosen above 0.17, the avalanche size distribution agrees best with the empirical Gutenberg-Richter law (1.4) [Lis01a].

Second, the OFC model demonstrates that apparent power laws need not reflect a true scale invariance of the system. Although the system exhibits a self-similar geometrical structure, which can be described by power laws, and although the avalanche sizes within a patch are also power law distributed, the combination of both leads to a

global distribution of avalanche sizes that is not a power law. The actual lack of scale invariance can be expected to be true for many naturally driven systems. Due to the dynamics of the model, there occur avalanches of all sizes, at least in the relevant case of two dimensions. However, the mechanisms producing these avalanches are different on different scales. Large avalanches are mainly patch-wide avalanches, while smaller avalanches occur within patches during a series of foreshocks or aftershocks. Also, avalanches at different distance from the boundaries have different sizes. The observed "power laws" are thus *dirty* power laws [Dro02], which appear like power laws over a wide range of parameters and over a few decades on the avalanche size axis, while the "true" analytical form is no power law. A log-normal distribution as in (4.5) is known to be easily mistaken for a power law [Sor00].

Third, the lack of a true scale invariance is accompanied by a decreasing weight of avalanches larger than 1 with increasing system size. This indicates again that the avalanche size distribution of the model does not approach some asymptotic shape with increasing L, but that the weights of different types of avalanches shift with the system size. This effect has most clearly been seen in one dimension, where the distributions split into a α dependent part at small avalanche sizes and peaks at sizes of order of the system size.

Fourth, the extremely long transient times point to the possibility that some driven natural systems with avalanche-like dynamics are not in the stationary regime either.

Fifth, up to now, no other model exists, which combines self-organized critical properties with an internal dissipation mechanism beyond the open boundaries, and different to the dissipation of the Feder-Feder type, or the necessary dissipation in the forest fire models. Since the OFC model, which is the prime example for a SOC system with tunable dissipation, was shown not to obey a simple power law behavior, at least for the considered couplings, there remains an open question:

Can the OFC model still account for a dissipative system that exhibits self-organized criticality? As long as this question cannot be answered satisfactorily, and as long as no other model is proposed that features a controllable degree of dissipation, a local conservation law must be treated as a necessary ingredient in order to obtain self-organized criticality.

Appendix A

The numerics

A computer lets you make more mistakes faster then any other invention, with the possible exceptions of handguns and Tequila.
Mitch Ratcliffe

Obviously, the OFC model could not be explored without the use of computers and extensive numerical simulations. Usually, a simulation takes time, which just as usual is short, and precious, and must not be wasted. Efficient algorithms help to decrease the computational time. Especially suited to keep the record low for numerical investigation of the OFC model is a fast determination of the biggest site in the system. Except for the actual avalanches, which can to some extent also be tuned towards efficiency, the repeated search for the next triggering site consumes far the most computer time. In a square lattice of linear size L, the simple linear search, which compares each site once, needs of the order of $\mathcal{O}(L^2)$ computing steps to find the largest value z_m. Note that the uniform external energy input would also take of the order of $\mathcal{O}(L^2)$ floating point operations, since each site is increased by an amount $z_c - z_m$.

The second[1] run through the lattice can be avoided by *decreasing* the threshold z_c instead of increasing all the sites. The decrease of z_c to its new value $z_c' = z_m$ is accompanied by a parallel shift in the "zero" variable z_0 of the system by the same amount $z_c - z_m$ to $z_0' = z_m - 1$. The dynamic update rule accordingly changes to

$$z_u \to z_u' = z_0' \tag{A.1}$$

for any temporarily unstable and thus toppling site z_u, the toppling of which adds a package $\alpha(z_u - z_m + 1)$ to each neighboring site. This improved growth rule was suggested by Grassberger [Gra94], who also introduced the Grassberger algorithm, which reduces the search for the largest site to be proportional to the order of $\mathcal{O}(L)$ operations.

The new box algorithm to be explained below (in A.2) needs only of the order of $\mathcal{O}(\ln L)$ floating point operations before the next avalanche can start. However, the price to be paid is the necessary amount of storage, which has to be allocated for the overhead of meta data.

[1] The first one is the actual search for the largest site.

A.1 The Grassberger algorithm

This search routine was proposed by Grassberger in 1994 [Gra94]. Later it was improved by Ceva [Cev98]. Basically, it uses a meta structure, which groups the sites into several bins, according to their energy values. Such, only the bin with the largest values has to be searched for the largest site. The meta structure consists of two additional arrays, which are called `LIST` and `BOX`.

The algorithm is implemented by first mapping the coordinates (i, j) of each site onto a single integer variable k via $k = i + L \times j$. The unit interval of allowed energy values (not necessarily between 0 and 1, see the remarks above), is divided into M bins, each of which contains a number of sites, but some of the bins can also be empty. However, the total length of all the bins is fixed at L^2, which is just the number of sites in the system. All bins are stored in the same array, `LIST`, which is thus of size L^2. The second extra array, `BOX`, stores the starting position of each bin, and has M entries, the headers of the M bins. Note that the index structure in `LIST` does not correspond to the actual spatial order of sites, nor is it directly related to their energies. Instead, if the b-th bin contains the sites k_1 to k_n, with $k_1 < k_2 < \cdots < k_n$, the index of the largest site, k_n, is stored in $\texttt{BOX}(b)$, while $\texttt{LIST}(k_n)$ stores the index of the second largest site, and so on:

$$\begin{aligned} \texttt{BOX}(b) &= k_n \\ \texttt{LIST}(k_n) &= k_{n-1} \\ &\vdots \\ \texttt{LIST}(k_2) &= k_1 \\ \texttt{LIST}(k_1) &= 0 \quad , \end{aligned} \tag{A.2}$$

The last entry, $\texttt{LIST}(k_1) = 0$, is not a position, but signifies the end of the bin. Having M bins distributed over the array `LIST` requires M zero entries, which are lost to store the actual position of a site. However, the necessary information to access each site of the system is also stored in the M entries of `BOX`. In programming lingo, this structure is a called a *linked list*.

Now, if a site's energy changes during an avalanche, it has to be removed from the corresponding list and to be placed in a new bin. Let k_l be the site to be processed. The removal of the site's index from `LIST` would in principle be done by replacing

$$\texttt{LIST}(k_{l+1}) = \texttt{LIST}(k_l) \quad , \tag{A.3}$$

but the position of $\texttt{LIST}(k_{l+1})$ is not directly accessible. In this situation, the original algorithm had to follow the b-th bin from the beginning until a k was reached with $\texttt{LIST}(k) = k_l$, which is of the order $\mathcal{O}(L)$.

Ceva introduced a third array in order to reduce this search to a single access operation. `INVLIST` contained the necessary information,

$$\texttt{INVLIST}(k_l) = (k_{l+1}) \quad , \tag{A.4}$$

and the site k_l is taken from the b-th bin by performing

$$\texttt{LIST}(\texttt{INVLIST}(k_l)) = \texttt{LIST}(k_l) \quad . \tag{A.5}$$

Nevertheless, the removed site needs also to be sorted into the correct bin. Furthermore, the meta arrays also have to be kept up-to-date. Even if using all the information about

BOX, LIST, and INVLIST, this update takes again of the order of $\mathcal{O}(L)$ operations. Also, due to the tendency of the OFC systems to synchronize, the algorithm becomes less and less effective, the more sites are accumulated in a few bins only.

A.2 The Box algorithm

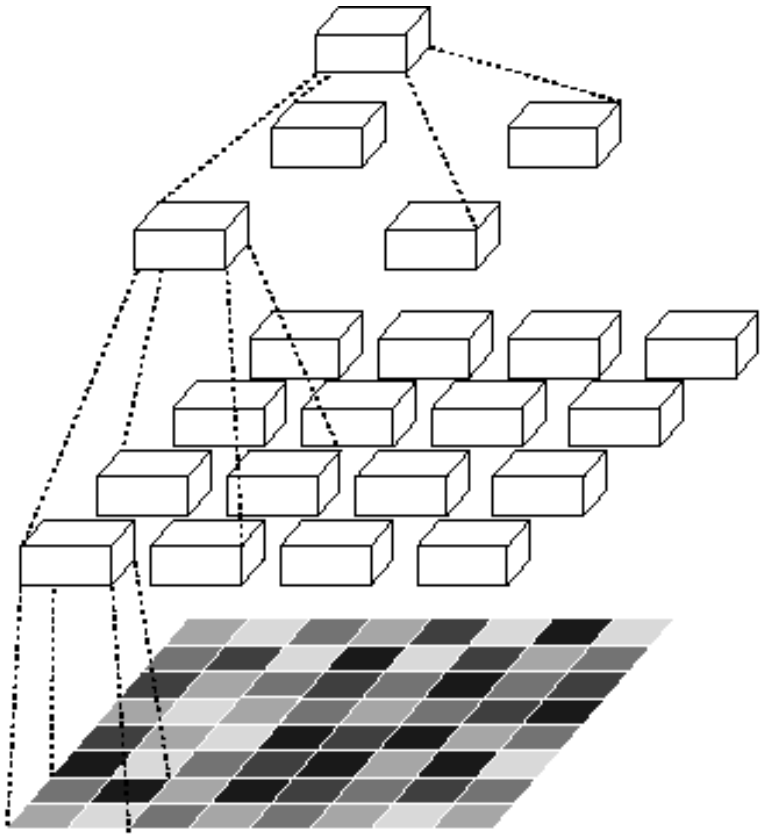

Figure A.1: Schematic view on the hierarchy of Boxes; the topmost Box controls 4 sub-Boxes, each of them in turn handles 4 other Boxes, and so on. Boxes on the lowest hyper level are linked to the real sites in the system. An avalanche, which affects only a few sites, results only in a small number of Boxes that have to be updated.

The new Box algorithm also uses a meta structure to store additional information about the sites' energies. A schematic setup of the structure is shown in figure A.1. The basic building block is a so-called Box (not to be mistaken with the BOX array above in the Grassberger algorithm), which governs 4 data types of the next lower level. These data types are either real sites for a Box on the lowest hyper level or 4 other Boxes on any other level. The biggest site in the system is determined by a hierarchical search, equivalent to a bisection in one dimension. Again, in programming lingo, this structure is called a *quadtree*.

The system size L is chosen to be a power of 2. The system as a whole is divided into 4 quadrants (a Box), each of which is again divided into 4 Boxes, etc., down to the

`Box` on the lowest level, which contains 4 lattice sites. Each `Box` knows the values of its 4 sub-structures (a site or a `Box`). The `Box` compares those for the largest value, and only this value and the coordinates of the corresponding site are passed to the next higher `Box`.

After initialization, the topmost `Box` returns the position of the site, which triggers the next avalanche. Once the avalanche is finished, the following update of the meta structure takes 4 comparison operations per hyper level. Since the number of hyper levels, l, is given by $l = \log_2 L$, the determination of the new largest site is of the order of $\mathcal{O}(\ln L)$.

This relation is valid as long as only a few sites within a small region have been affected by an avalanche, which spanned only an area of N^2 sites, and $N^2 \ll L^2$. The worst case is a system-wide avalanche, then all the `Box`es must be updated. Such an update is of the order of $\mathcal{O}(L^2)$, because the total number of `Box`es is $L^2 - 1$. Nevertheless, this update of polynomial order is acceptable for two reasons:

First, small avalanches, especially single topplings, occur far more often than any other avalanche (see the last chapters).

Second, the `Box` algorithm also uses the continual shift in the threshold z_c and in the zero variable $z_0 = z_c - 1$. When the zero reaches the absolute value -1, the whole system must be lifted to the initial unit interval $[0, 1]$. For sites having an absolute value smaller than this lower bound of -1 would decrease the precision of the simulations. For example, a value in the interval $[-100, -101]$ needs three digits to represent the integer part of the value, leaving only 12 decimal places for precision, in contrast to 15 decimal places as usual for a `double` variable. For `float` variables, the loss of precision is even worse. This overall lift is also of the order of $\mathcal{O}(L^2)$, since every site must be increased. In order to save time, the necessary lift is performed whenever an avalanche occurred, which is larger than some threshold (usually taken to be one fourth of the system), and the update takes proportional $\sim L^2$ operations, anyway.

A.3 The implementation

The `Box` algorithm was implemented in `C++` on a Debian `Linux` cluster using the `gnu g++-3.4` compiler with the help of Dipl.Phys. Torben Jabben.

The basic idea is to decouple the organization of the hyper structure from the dynamics in the OFC system. The latter is a two-dimensional lattice, and this structure was kept in the code, since an array in two dimensions allows a fast access operation on neighboring sites, which is a key feature in the OFC dynamics.

The program consists of 4 basic units: the actual OFC system, called `BaseArea`, built up from single `Site`s, the meta structure of `Box`es [2], and a class `Base` explained below.

For a OFC system of linear size $L = 2^l$, `BaseArea` was chosen to have an extension of $(L+2) \times (L+2)$ sites. Such, the integer coordinates of the sites were running from 1 to L (instead of from 0 to $L-1$), but the real reason for the extra sites is that avalanches can be simulated faster by avoiding boundary checks for each toppling. Thus, packages are added to all neighbors, irrespective of their position. The frame of

[2] In the real implementation, an extra `Double` was appended to the names to discriminate the data types from other possible implementations, as for example `Integer` or `Float` variables.

one site around the real lattice is accordingly constantly fed with energy [3], but a site from the frame never topples (see below).

The fourth basic unit, `Base`, is an abstract class, from which the other two classes `Site` and `Box` inherit common variables and, what is more important, their type. For the classes `Site` and `Box` it is not necessary to be of the same data type, but a common type has proven useful. Implemented in that way, there is no need to discriminate between physical sites and auxiliary units, and the coordinates of the largest site, as well as any other spatial information, can intrinsically be passed on through the meta levels by pointers of type `Base*`.

In the following, several properties of the used classes are explained in extracts. A complete documentation would go beyond the scope of the appendix. The sections below are meant as an introduction for the interested, and further information can be found in the program listings where remarks are added to the actual coding.

A.3.1 The `Base`

The `Base` data type has 5 `public` members and one virtual member function. The constructor initializes all variables to a default value, where `max_value` naturally is the actual value of a site or the largest value within a `Box`. Each unit knows about the level above via the pointer `Base* mama`. Only the topmost `Box` has a null pointer, which is used to stop the update routine (see below). `unsigned short int x` and `y` are the coordinates, and the `unsigned short` type is used to save storage.

```
class Base{
  public:
  Base(){
     touched=false;
     max_value=0.;
     x=0;
     y=0;
    };
  double max_value;
  Base* mama;
  unsigned short int x;
  unsigned short int y;
  bool touched;
  virtual void touch()=0;
 };
```

Table A.1: Abstract class `Base.hpp`, from which the classes `Site.hpp` and `Box.hpp` inherit their type and common variables.

The `bool`-valued variable `touched` is used in a twofold way: for real sites within the `BaseArea` array, it differs between physical sites and those sites, which are located in the boundary frame. Within a `Box` the `touched` variable is used to mark the particular `Box` as being affected by an avalanche.

[3] With energy *packages* only, the external input does not affect neither those sites in the frame nor the real sites, since the tracking of the threshold and the zero variable is used.

The function `touch()` is a `virtual` member, and as such must be implemented anew within inheriting classes. When called from a `Site`, `touch()` simply notifies the `Box` above, while within a `Box` it also pushes this `Box` into a stack, which is to be processed later during the `Update()` of the tree structure after an avalanche.

A.3.2 The `Site`

An object of type `Site` represents the basic unit the actual OFC lattice is built up from. While a site in the OFC model in principle consists only of a single energy value, the `Site`s used in the code have several extra features. For example, each `Site` knows its coordinates, which are used to find the position of the largest site in the lattice. Additionally, each `Site` knows, which `Box` it belongs to, since a `Site` must call its `Box` whenever the `Site` was affected by an avalanche.

Obviously, a `Site` stores the value of a site in the system, but it has additional member functions, which are used during the initialization or when this site takes part in an avalanche. The functions in detail are (see also table A.2):

`set`: called during the initialization: the variable `max_value` is set to s, and `touched` is turned from `false` to `true`, signifying a real site (not one within the frame)

`add`: a value a is added to the variable `max_value`. `touched` is temporarily set to `false`, which is used by the avalanche algorithm.

`topple`: `max_value` is set to z

`grow`: similar to `add`, a value g is added to the variable `max_value`. Additionally, the function `touch()` is called, which informs the `Box` on the next higher level.

`touch`: calls the above `Box mama`, and resets `touched` to true.

The check whether a site becomes unstable is not performed after each addition of a package, because a site can receive energy packages from more than one neighbor. The `add` function changes the `bool` variable `touched` temporarily to false, and the avalanche algorithm pushes each incremented `Site` into its corresponding stacks as long as `touch` is `true`. Due to the OFC dynamics, the system separates into two sub lattices, equivalent to the black and white sites of a checkerboard (see section 1.2.2). Two stacks are used , which contain either the "black" or the "white" sites. the `Site`s in the stacks are than processed alternately, which resets `touch` back to `true`. Thus, a site located in the outer frame is never pushed in a stack, and a site receiving multiple packages needs only a single check.

A.3.3 The `Box`

The `Box` class also inherits basic features from the `Base` class, but also defines the node of the quadtree. During the generation of the tree, each `Box` recursively sets up its sub nodes, until the whole tree structure as shown in figure A.1 is built up.

```
class Site : public Base {
  public:
  void set(double s);
  void add(double a);
  void topple(double z);
  void grow(double g);
  void touch();
 };
```

Table A.2: Class `Site.hpp`, which inherits from `Base.hpp` and has additional member functions. They are all related to the avalanche operator and to some extent explained in the text.

The first `Box` is called by the `BaseArea`. Only this topmost `Box` is visible and accessible to the outside (to `BaseArea`), and only the `SearchMax()` function is necessary, to obtain the largest site (its position and its current value).

Each `Box` knows its "mother"-`Box` through the pointer `mama` and has an array of 4 pointers to its "baby"-`Box`es, which on the lowest level point to 4 actual `Site`s in the `BaseArea`. The `static` variables are common to all instances of type `Box`, but they are stored only once in the topmost `Box`. They include the global variables of the whole tree, such as `levels`, which gives just the number of distinct meta levels, the actual `size` of the OFC system and two pointer `field` and `stacks`. The first one yields the connection to the `BaseArea`, while the second one contains several stacks, which are alternately filled and emptied with reference pointers of `Box`es during the avalanche. For each meta level there is one stack allocated to store pointers to those `Box`es, which have to be updated. Each `Site` that participates in an avalanche calls the function `touch()`, which puts the according `mama-Box` into the corresponding stack. The `Box`es in the stacks are processed successively after the avalanche, and while the first stack is cleared, the updated `Box`es call their `mama-Box`, if necessary, which in turn is stored in the second stack, and so on. The according call is the same `touch()` function, independent of whether a `Site` or another underlying `Box` does the call, but intrinsically, the call is processed differently for `Site`s and for `Box`es.

This update routine stops, when the topmost `Box` is reached, since their `mama` is a null pointer. The `push` and `pop`-functions of the stacks are called by `Update()`, which also compares the 4 sub-structures and thus determines the current largest value.

`Box()` is the constructor, which gets a series of variables: the current depth of the hierarchy level `l`; the current increment `dxy`, which is used to calculate the relative position of each sub-`Box` and which shrinks by a factor one half in each step from one meta level to the next lower one; the proper position (`x_pos` and `y_pos`) of the particular `Box`; a pointer to its `mama`; and finally a pointer to the `BaseArea`.

All these variables are internally processed, and all the functions are also encapsulated within the topmost `Box`. This `Box` is accessed by the `BaseArea` through two operations only:

First, the tree is generated by a call to the constructor, `<box> = new Box(...)`, which initializes the topmost `Box` using `InitFirstBox()`, which in turn generates iteratively the tree of `Box`es by calling repeatedly the `InitNextLevel()` function.

```
class Box : public Base {
public:
  Box(int l,int dxy,int x_pos,int y_pos, Box* m,
                                Array <Array <Site>>* f);
  double SearchMax();

  ~Box();
  void InitFirstBox(int l,int dxy,Array<Array<Site>>* f);
  void InitNextLevel(int l,int dxy,int x_pos,int y_pos,Box* m,
                                Array <Array <Site>>* f);
  void Update();
  void touch();

  Base* baby[4];
  int level;
  static int levels;
  static int size;
  static Array <Array<Site> >* field;
  static Array<stack<Box*> > stacks;
};
```

Table A.3: Class `Box.hpp`, which inherits from `Base.hpp` and has additional member functions. They are all related to the search of the largest site and to some extent explained in the text.

The second access is the `SearchMax()` routine, which yields all the information necessary for the `BaseArea` to start the next avalanche.

Having so much overhead requires a serious cleanup when the program should stop correctly after execution. This clearance is done by means of the destructor `~Box()`, which takes care that all `Box`es, which were generated during the simulation, are properly removed from the storage.

A.3.4 The `BaseArea`

The `BaseArea` is the only class accessed in the `main()` program. It is generated by the constructor `BaseArea(double l, double a)` where `l` is the linear size L and `a` is the value of the coupling α. The proper names are used within the code. The whole setup is initialized by the `Init()` function, which calls the `Box` and creates the random initial configuration of the system. Additionally, it prepares the arrays for the statistical evaluation of the simulation and handles other variables (a lot of counters and auxiliary arrays), but they are not explained here.

The stack `touched_sites` stores those sites, which took part in an avalanche, either receiving a package or having toppled, and whose `mama Box`es have to be updated. The `bool` variable `just_grown` is used to decide, whether it is necessary to lift the whole system back into the unit interval $[0, 1]$ (see the remarks above). This resetting is performed by the `Grow()` routine, which actually is *not* the external energy input of the OFC model. The latter is circumvented for the simulations by introducing `zero`

and `threshold`, the two variables to be tracked. The pointer `current_site` and the other variables are self explanatory, and `~BaseArea()` does the cleanup in the very end of the simulation.

Though a single avalanche can in principle be started from the `main()` program by calling the `Avalanche()` function, it makes more sense to simulate a series of avalanches. They are encapsulated within the `Earthquake(double top)` function where `top` determines how long an earthquake should last in terms of the number of total topplings. This instruction can only be approximately executed, since one does not know in advance how many topplings the next avalanche takes.

```
class BaseArea {
  public:
  BaseArea(int l, double a);
  ~BaseArea(){
    delete box;
  };
  void Init();
  void Grow();
  int Avalanche();
  void Earthquake(double t);

  Array <Array<Site> > area;
  Array <stack <Site*> > touched_sites;

  Box* box;
  Site* current_site;

  int L;
  double alpha;
  double zero;
  double threshold;
  int max_x;
  int max_y;
  bool just_grown;
}
```

Table A.4: Class `BaseArea.hpp` as explained in the text.

List of Figures

1.1 Schematic setup of the Burridge-Knopoff *train* model. In the original publication, all the blocks have the same mass m and springs with elastic constants k. Later work studied individual masses and springs. 12

1.2 Schematic setup of the Burridge-Knopoff *chain* model. All blocks are drawn along by the movement of the upper plate. 12

1.3 Detailed view of the block located at (i, j) and the surrounding blocks with their displacements, $d_{i\pm1,j\pm1}$, against the equilibrium position. 15

2.1 Return map for the uniformly driven system of two sites. Depending on the initial values, the system settles somewhere on the diagonal line of fixed points in the dashed square. 33

2.2 Return map for the system of two sites, where one site is driven slower than the other. The dashed diagonal line denotes the line of possible fixed points, cutting the graph at $z_2^* = 1 + \epsilon(1-\alpha)/(1+\alpha)$. 33

2.3 Poincaré map in the $z_l - z_r$ plane for the system of three sites and $z_m = 0$. Only the part for which $z_l \leq z_r$ is shown. The different regions with a specific sequence of topplings and phases of intermediate growth are separated and labeled from a to g. These regions are listed in detail in table 2.1. The fixed point line as derived below in equation (2.3) is indicated by a dashed line. . . 34

2.4 Period lengths for a system of 4 sites as a function of the coupling α, counted in two different measures: the number of topplings within a cycle (circles) and the number of avalanches (dots). Upper figure for a precision of 2^{-20}, lower figure for a precision of 2^{-10}. The solid line in both figures corresponds to $f(\alpha) = 4/\alpha$. 37

2.5 Average *absolute* size of packages $\bar{\alpha}$ as function of the coupling parameter α (solid line), averaged over hundred stationary systems of size $L = 128$ and 10^4 topplings per site; dashed line corresponds to the identity $f(\alpha) = \alpha$. 51

2.6 Average *relative* size of excess packages $(\bar{\alpha} - \alpha)/\alpha$ as a function of α for two different system sizes $L = 64$ (solid line) and $L = 128$ (dashed line). Statistics as in figure 2.5. 52

2.7 Toppling profile for a one-dimensional OFC system for $L = 30$ and $\alpha = 0.2$ as function of the site index i. Solid line with stars: numerical result obtained by averaging over 1000 different stationary systems for 10^4 topplings per site. Dashed line: Analytical solution (2.28) of the continuous approximation. Long dashed line with crosses: solution obtained by numerically inverting the matrix (2.26). 54

2.8 Random initial configuration and after 1400, 2800, 4200, and 5600 topplings per site in configuration space for a system with $L = 512$ and $\alpha = 0.2$ (from top left to bottom right). The two figures at the bottom represent stationary systems with different initial states, both after 5600 topplings per site. The synchronization proceeds into the system starting at the boundaries. Synchronized sites within the left (right) block need not take on the same energy value, as indicated by the bottom right figure. 56

2.9 $\Delta n(t)$ as defined in equation (2.33), the difference between the stationary size distribution of avalanches and the current size distribution as a function of time, measured in topplings per site (denoted as *tps*), averaged over 100 systems for $\alpha = 0.12$ and $L = 64$. Theoretically, the final value reached after about 10^6 topplings per site should vanish. The different lengths of the time intervals over which the distributions were obtained might be the reason for the non vanishing result around 10^{-9}. 57

2.10 Standard deviation σ^2 (top) and nearest-neighbor deviation σ_{nn} (bottom) as defined in equations (2.34) and (2.35) as a function of the system size L for a fixed coupling $\alpha = 0.35$. Data obtained by averaging over 1000 random initial configurations. Time measured in total number of topplings. 58

2.11 Standard deviation σ^2 (top) and nearest-neighbor deviation σ_{nn} (bottom) as defined in equations (2.34) and (2.35) as a function of the coupling α for a fixed system size $L = 200$. Data obtained by averaging over 1000 random initial configurations. Time measured in topplings per site. 59

2.12 Contour along the (arbitrary) value $\sigma^2 = 0.03$ to depict the dependence of the total number of topplings in the upper figure 2.10 on the system size L for fixed coupling $\alpha = 0.35$. Dashed line corresponds to $f(L) = 2\,L$. 60

2.13 Time (measured in topplings per site) needed to reach $\sigma^2 = 0.01$ for a system of $L = 200$ sites as a function of α, averaged over 1000 different random initial systems. The peaks are real and are not statistical fluctuations. The dashed lines are proportional to $f(\alpha) = A\exp(-14.8\alpha)$ with amplitudes $A = 2 \times 10^4$ and $A' = 2 \times 10^5$ respectively. 61

2.14 Time (measured in topplings per site) needed to generate the first avalanche of size ≥ 21 as function of α, averaged over 1000 different random initial states for systems of size $L = 50$. The straight dashed line corresponds to $f(\alpha) \propto \alpha^{-2.84}$. 62

2.15 Solid line: average size of avalanches triggered at site i; dashed line: average number of avalanches triggered at site i. Both data sets are plotted as function of the site index i, averaged over 10^4 different synchronized systems for $\alpha = 0.2$, $L = 100$. 66

2.16 Typical size distribution $n(s)$ of avalanches of size s, divided by the total number of topplings and the system size, averaged over 2140 systems. $L = 1000, \alpha = 0.2$. Note the larger weight for avalanches of about half the system size compared to avalanches with a size of around the system size. 67

2.17 Size distribution $n(s)$ of avalanches of size s divided by the total number of topplings for different values of L and a coupling of $\alpha = 0.15$, averaged over at least 3300 systems. Solid line: $L = 100$; dashed line: $L = 500$; dotted line: $L = 1000$. The low-size regime is independent of the system size, depends only on α, and is determined by the dynamics within the boundary layer. The relative weight for the avalanches of order $\mathcal{O}(L)$ decreases with increasing system size. 68

2.18 Size distribution $n(s)$ of avalanches of size s divided by the total number of topplings and the system size for different values of α and a system size $L = 1000$, averaged over at least 2000 systems. Solid line: $\alpha = 0.1$; dash-dotted line: $\alpha = 0.2$; dotted line: $\alpha = 0.3$; dashed line: $\alpha = 0.4$. Note the non vanishing weight for avalanches larger than the system size for $\alpha = 0.4$. . . . 69

2.19 Size distribution $n(s)$ of avalanches of size s divided by the total number of topplings and the system size for different precisions. $L = 500$ and $\alpha = 0.15$, averaged over at least 6300 systems. Solid line: precision 2^{-12}; dashed line: precision 2^{-20}; dotted line: precision 2^{-28}. 70

3.1 Configuration after 10^3, 10^4, 5×10^4, and 8.5×10^4 topplings per site in top view for a system with $L = 128$ and $\alpha = 0.09$ (from top left to bottom right). The darker a site, the lower the energy value z_{ij}. As in $d = 1$, the synchronization proceeds into the system starting at the boundaries. Instead of the synchronized blocks in one dimension, patches are formed, the size of which increases with distance to the boundaries. The disordered center of the system behaves similarly to one within periodic boundary conditions, until the patches invade more and more area of the system. 75

3.2 Snap shots of systems during the transient stage for a system size $L = 256$ and different values of the coupling. From left to right: $\alpha = 0.10$ after 2500 topplings per site; $\alpha = 0.15$ after 250 topplings per site; $\alpha = 0.20$ also after 250 topplings per site. 77

3.3 Snap shots of systems in the stationary state for a system size $L = 128$ and different values of the coupling. From left to right: $\alpha = 0.04$ after 1.34×10^9 topplings per site; $\alpha = 0.12$ after 8×10^3 topplings per site; $\alpha = 0.20$ after 200 topplings per site. 78

3.4 Time measured in topplings per site until the inner block vanishes for system sizes $L = 64$ (circles), $L = 128$ (stars), $L = 256$ (squares) and $L = 512$ (triangles) as function of α; the dashed lines correspond to the set of functions $T(\alpha, L) = \tilde{f}(\alpha) L^{\tilde{\mu}(\alpha)}$ as given below in equation (3.23) 79

3.5 The exponent $\tilde{\mu}(\alpha)$ as obtained from the data shown in figure 3.4. The dashed line corresponds to the function $E \exp(-e\alpha)$. Numerical values for the fit parameter E and e are given in table 3.1. 85

3.6 The function $t(\alpha) = \log \tilde{f}(\alpha)$ as obtained from the data shown in figure 3.4. The dashed line corresponds to the function $m\,\alpha + l + C\,\alpha^c$. Numerical values for the fit parameter m, l, C, c are given in table 3.1. 86

3.7 Correlation function $C_{i=10}(r)$ for $\alpha = 0.08$ for a distance $i = 10$ sites from the boundary at three different times (after 2570 (solid line), 5130 (dashed line), and 12490 (dotted line) topplings per site). 88

3.8 Correlation function $C(r)$ for $\alpha = 0.08$ for a distance $i = 20$ sites from the boundary at three different times (after 2570 (solid line), 5130 (dashed line), and 12490 (dotted line) topplings per site). 89

3.9 Correlation length ξ as function of the distance i to the boundary (measured in number of sites) for $\alpha = 0.12$ after 650 (dotted line), 1290 (dashed line) and 2570 (solid line) topplings per site. 90

3.10 Correlation length ξ as function of the distance i to the boundary (measured in number of sites) for $\alpha = 0.06, 0.09, 0.12$, and 0.15 (from bottom to top) at the largest times simulated for a given value of α (solid lines); the dashed lines correspond to lines of slope 1. 91

3.11 Schematic view of the system's structure: the width and height of patches increase with a power law in the distance to the boundary. Different generations of patches are coupled via n_c (as derived in equation (3.11)), the increase in the size of the patches is $P(\alpha)$ parallel to the boundary and $Q(\alpha)$ perpendicular to it, starting with a size $s_0 = p_0 q_0$. 92
3.12 Snap shots of systems in the stationary state for a coupling $\alpha = 0.11$ and different values of the system size: from left to right: $L = 128$ after 10^4 topplings per site; $L = 256$ after 102700 topplings per site; $L = 512$ after 592000 topplings per site. 93
3.13 Size distribution of avalanches for a system size $L = 64$ and $\alpha = 0.03, 0.08, 0.13, 0.18$, steeper curves correspond to smaller α (solid lines); the s axis extends up to the total number of sites within the system, 4096; the distributions are normalized on the total number of topplings; dashed lines correspond to $f(s) \sim s^{-\tau-\sigma \ln s}$. 94
3.14 Size distribution for system sizes $L = 64$ (solid line), $L = 128$ (dashed line), $L = 256$ (dotted line), and $L = 512$ (dash-dotted line) and coupling $\alpha = 0.09$; the distributions are divided by $n(2)$. 95
3.15 Size distribution for system sizes $L = 64$ (solid line), $L = 128$ (dashed line), $L = 256$ (dotted line), and $L = 512$ (dash-dotted line) and coupling $\alpha = 0.17$; the distributions are divided by $n(2)$. 96
3.16 The coefficients $\sigma(\alpha)$ (lower set of curves) and $\tau(\alpha)$ (upper set) as function of α as found by fitting the distributions $n(s)$ for $L = 64$ (solid line), $L = 128$ (dashed line), and $L = 256$ (long dashed line) for those values of α, for which the stationary state of the systems was reached. Dotted line indicates the value $\tau_0 = 1.8$. 99
3.17 The ratio $n(1)/n(2)$ obtained from the size distribution in figure 3.15 for $\alpha = 0.17$ as function of the system size L. The dashed line corresponds to $f(L) \sim L$. 100

A.1 Schematic view on the hierarchy of `Box`es; the topmost `Box` controls 4 sub-`Box`es, each of them in turn handles 4 other `Box`es, and so on. `Box`es on the lowest hyper level are linked to the real sites in the system. An avalanche, which affects only a few sites, results only in a small number of `Box`es that have to be updated. 109

List of Tables

1.1 Comparison between different (earthquake-) models. Data taken from [Bak87, Nak91, Zha89, Fed91, Ola92b]. 17

2.1 Scenarios in the Poincaré map, sorted by their toppling and growth sequences. The first column shows the different scenarios ($a-g$), presented in figure 2.3. Second column: range of configurations in state space for which each scenario is realized. Third column: resulting states after the second toppling of the center site and the ranges for the new z values. 35

2.2 Observed periods and their lengths measured in topplings and avalanches for $\alpha = 0.09$ and two different precisions, 2^{-10} (upper table) and 2^{-20} (lower table). Periods can be degenerate in the sense that the same number of topplings is split into different numbers of avalanches. The higher the precision, the more preferred are the long attractors. 39

3.1 Numerical values of the fit parameter for the the L-independent function $\tilde{f}(\alpha) \sim \exp(m\,\alpha + l + C\,\alpha^c)$ (left column) and for the exponent of L in figure 3.4, $\tilde{\mu}(\alpha) \sim E\exp(-e\,\alpha)$ (right column). 87

A.1 Abstract class `Base.hpp`, from which the classes `Site.hpp` and `Box.hpp` inherit their type and common variables. 111

A.2 Class `Site.hpp`, which inherits from `Base.hpp` and has additional member functions. They are all related to the avalanche operator and to some extent explained in the text. 113

A.3 Class `Box.hpp`, which inherits from `Base.hpp` and has additional member functions. They are all related to the search of the largest site and to some extent explained in the text. 114

A.4 Class `BaseArea.hpp` as explained in the text. 115

Bibliography

[Abe04] Abe, S. and Suzuki, N., Europhys. Lett. **65** 581 (2004).

[Alb02] Albert, R. and Barabási, A.L., Rev. Mod. Phys. **74** 47 (2002).

[All96] Alley, M., *The Craft of Scientific Writing* (Springer, New York, Berlin, Heidelberg, 1996).

[Als88] Alstrøm, P., Phys. Rev. A. **38** 4905 (1988).

[Bac05] Bach, M., *Die Auswirkung von Unordnung im dissipativen Olami-Feder-Christensen Erdbebenmodell*, Bachelorthesis, Institut für Festkörperphysik, Technische Universität Darmstadt, Deutschland (2005).

[Bak87] Bak, P., Tang, C., and Wiesenfeld, K., Phys. Rev. Lett. **59** 381 (1987).

[Bak90a] Bak, P., Chen, K., and Tang, C., Phys. Lett. A **147** 297 (1990).

[Bak90b] Bak, P. and Tang, C., Phys. Lett. A **147** 297 (1990).

[Bak96] Bak, P., *How nature works: The science of self-organized criticality* (Copernicus Press, New York, 1996).

[Bar99] Barabási, A.L. and Albert, R., Science **286** 506 (1999).

[Bla00] Blanchard, P., Cessac, B., and Krueger, T., J. Stat. Phys. **98** 375 (2000).

[Bot95] Bottani, S., Phys. Rev. Lett. **74** 4189 (1995).

[Bot97] Bottani, S. and Delamotte, B., Physica D **103** 430 (1997).

[Bro97] Broeker, H. and Grassberger, P., Phys. Rev. E **56** 3944 (1997).

[Bur67] Burridge, R. and Knopoff, L., Bull. Seismol. Soc. Am. **57** 341 (1967).

[Car89a] Carlson, J. and Langer, J., Phys. Rev. Lett. **62** 2632 (1989).

[Car89b] Carlson, J. and Langer, J., Phys. Rev. A **40** 6470 (1989).

[Cev95] Ceva, H., Phys. Rev. E **52** 154 (1995).

[Cev98] Ceva, H., Phys. Lett. A **245** 413 (1998).

[Cha97] Chabanol, M. and Hakim, V., Phys. Rev. E **56** R2343 (1997).

[Che89] Chen, K. and Bak, P., Phys. Lett. A **140** 299 (1989).

[Che90] Chen, K., Bak, P., and Jensen, H.J., Phys. Lett. A **149** 207 (1990).

[Che91] Chen, K., Bak, P., and Obukhov, S., Phys. Rev. A **43** 625 (1991).

[Chr92a] Christensen, K., *Self-Organization in Models of Sandpile, Earthquakes and Flashing Fireflies*, Ph.D. thesis, Institute of Physics and Astronomy, University of Aarhus, Denmark (1992).

[Chr92b] Christensen, K. and Olami, Z., Phys. Rev. A **46** 1829 (1992).

[Chr92c] Christensen, K. and Olami, Z., J. Geophys. Res. **97** 8729 (1992).

[Chr92d] Christensen, K., Olami, Z., and Bak, P., Phys. Rev. Lett. **68** 2417 (1992).

[Chr93] Christensen, K., Phys. Rev. Lett. **71** 1289 (1993).

[Chr01] Christensen, K., Hamon, D., Jensen, H.J., and Lise, S., Phys. Rev. Lett. **87** 039801 (2001).

[Cla05] Clancy, I. and Corcoran, D., Phys. Rev. E **71** 046124 (2005).

[Cor95] Corral, A., Pérez, C., Diaz-Guilera, A., and Arenas, A., Phys. Rev. Lett. **74** 118 (1995).

[Cor97] Corral, A., Pérez, C., and Diaz-Guilera, A., Phys. Rev. Lett. **78** 1492 (1997).

[Cri92] Crisanti, A., Jensen, M.H., and Vulpiani, A., Phys. Rev. A, Rapid Communication **46** R7363 (1992).

[deC00] deCarvalho, J.X. and Prado, C.P.C., Phys. Rev. Lett. **84** 4006 (2000).

[deC01] deCarvalho, J.X. and Prado, C.P.C., Phys. Rev. Lett. **87** 039802 (2001).

[Dha89] Dhar, D. and Ramaswamy, R., Phys. Rev. Lett. **63** 1659 (1989).

[Dha99] Dhar, D., Physica A **270** 69 (1999).

[Dro92] Drossel, B. and Schwabl, F., Phys. Rev. Lett. **69** 1629 (1992).

[Dro02] Drossel, B., Phys. Rev. Lett. **89** 238701 (2002).

[dV92] deSousa Vieira, M., Phys. Rev. A **46** 6288 (1992).

[dV99] deSousa Vieira, M., Phys. Rev. Lett. **82** 201 (1999).

[Ebe98] Ebeling, W., Freund, J., and Schweitzer, F., *Komplexe Strukturen: Entropie und Information* (Teubner, Wiesbaden, 1998).

[Fed91] Feder, H. and Feder, J., Phys. Rev. Lett. **66** 2669 (1991).

[Fel57] Feller, W., *An Introduction to Probability Theory and its Applications* (Wiley, New York, 1957), vol. 1.

[Fii93] Fiig, T. and Jensen, H.J., J. Stat. Phys. **71** 653 (1993).

[Fre96] Frette, V., Christensen, K., Malthe-Sørenssen, A., Feder, J., Jøssang, T., and Meakin, P., Nature **379** 49 (1996).

[Gai06] Gaite, J. and Domínguez, A., URL: http://arxiv.org/abs/astro-ph/0610886 (2006).

[Gra94] Grassberger, P., Phys. Rev. E **49** 2436 (1994).

[Gri90] Grinstein, G., Lee, D.H., and Sachdev, S., Phys. Rev. Lett. **64** 1927 (1990).

[Gut41] Gutenberg, B. and Richter, C.F., Geol. Soc. Am. **34** Special Papers (1941).

[Gut42] Gutenberg, B. and Richter, C.F., Bull. Seism. Soc. Am. **32** 163 (1942).

[Gut44] Gutenberg, B. and Richter, C.F., Bull. Seism. Soc. Am. **34** 185 (1944).

[Gut54] Gutenberg, B. and C.F.Richter, *Seismicity of the earth and associated phenomena* (Princeton University Press, Princeton, New Jersey, 1954).

[Gut56] Gutenberg, B. and Richter, C.F., Bull. Seism. Soc. Am. **46** 105 (1956).

[Har63] Harris, T.E., *The Theory of Branching Processes* (Springer, Berlin, Heidelberg, 1963).

[Hel90] Held, G.A., Solina, D.H., Solina, H., Keane, D.T., Haag, W.J., Horn, P.M., and Grinstein, G., Phys. Rev. Lett. **65** 1120 (1990).

[Hel03] Helmstetter, A., Phys. Rev. Lett. **91** 058501 (2003).

[Hel04] Helmstetter, A., Hergarten, S., and Sornette, D., Phys. Rev. E **70** 046120 (2004).

[Her02] Hergarten, S. and Neugebauer, H., Phys. Rev. Lett. **88** 238501 (2002).

[Hes] Hessisches Landesmuseum Darmstadt, Abteilung Geologie, permanent exhibition, visited Apr. 22, 2007.

[Hwa89] Hwa, T. and Kardar, M., Phys. Rev. Lett. **62** 1813 (1989).

[Ján93] Jánosi, I. and Kertész, J., Physica A **200** 179 (1993).

[Jen90] Jensen, H.J., Phys. Rev. Lett. **64** 3103 (1990).

[Jen98] Jensen, H.J., *Self-Organized Criticality* (Cambridge University Press, Cambridge, Great Britain, 1998).

[Kad89] Kadanoff, L.P., Nagel, S.R., Wu, L., and Zhou, S., Phys. Rev. A **39** 6524 (1989).

[Kei95] Keisuke, I., Phys. Rev. E **52** 3232 (1995).

[Kim06] Kimbal, J.C. and Frisch, H.L., URL: http://arxiv.org/abs/cond-mat/0606454 (2006).

[Kin99] Kinouchi, O. and Prado, C., Phys. Rev. E **59** 4964 (1999).

[Kle93] Klein, W. and Rundle, J., Phys. Rev. Lett. **71** 1288 (1993).

[Li] Li, W., $1/f$-noise, URL: http://www.nslij-genetics.org/wli/1fnoise/index.html and references therein, site checked Nov. 2, 2006.

[Lis96] Lise, S. and Jensen, H.J., Phys. Rev. Lett. **76** 2326 (1996).

[Lis01a] Lise, S. and Paczuski, M., Phys. Rev. E **63** 036111 (2001).

[Lis01b] Lise, S. and Paczuski, M., Phys. Rev. E **64** 046111 (2001).

[Lis02a] Lise, S., J. Phys. A **35** 4641 (2002).

[Lis02b] Lise, S. and Paczuski, M., Phys. Rev. Lett. **88** 228301 (2002).

[Luc] Lucas, C., Self-organizing systems (SOS) FAQ, URL: http://www.calresco.org/sos/sosfaq.htm, site checked Nov. 15, 2006.

[Man90] Manna, S., Kiss, L., and Kertész, J., J. Stat. Phys. **61** 923 (1990).

[Man91a] Manna, S., J. Phys. A **24** L363 (1991).

[Man91b] Manna, S., Physica A **179** 249 (1991).

[Mid95] Middleton, A. and Tang, C., Phys. Rev. Lett. **74** 742 (1995).

[Mil02] Miller, G. and Boulter, C., Phys. Rev. E **66** 016123 (2002).

[Mil03a] Miller, G. and Boulter, C., Phys. Rev. E **67** 046114 (2003).

[Mil03b] Miller, G. and Boulter, C., Phys. Rev. E **68** 056108 (2003).

[Mir90] Mirollo, R.E. and Strogatz, S., SIAM J. Appl. Math **50** 1645 (1990).

[Mis94] Mishra, R.K., Maaß, D., and Zwierlein, E. (Editors), *On Self-Organization* (Springer, Berlin, Heidelberg, 1994).

[Mou96] Mousseau, N., Phys. Rev. Lett. **77** 968 (1996).

[MS99] Malthe-Sørenssen, A., Feder, J., Christensen, K., Frette, V., Jøssang, T., and Meakin, P., Phys. Rev. Lett. **83** 764 (1999).

[Nak90] Nakanishi, H., Phys. Rev. A **41** 7086 (1990).

[Nak91] Nakanishi, H., Phys. Rev. A **43** 6613 (1991).

[New96] Newman, M.E.J. and Sneppen, K., Phys. Rev. E **54** 6226 (1996).

[New04] Newman, M.E., URL: http://arxiv.org/abs/cond-mat/0412004 (2004).

[NZ] NIEDERÖSTERREICHISCHER-ZIVILSCHUTZVERBAND, Erdbeben - was tun?, URL: http://www.noezsv.at/wastun/erdbeben/erdbeben.htm, site checked Nov. 2, 2006.

[Ola92a] Olami, Z. and Christensen, K., Phys. Rev. A. **46** R1720 (1992).

[Ola92b] Olami, Z., Feder, H.J.S., and Christensen, K., Phys. Rev. Lett. **68** 1244 (1992).

[Omo94] Omori, F., J. Coll. Sci. Imp. Univ. Tokyo **7** 111 (1894).

[Pac96] Paczuski, M., Maslov, S., and Bak, P., Phys. Rev. E. **53** 414 (1996).

[Pei04a] Peixoto, T.P. and Prado, C., Phys. Rev. E **69** R025101 (2004).

[Pei04b] Peixoto, T.P. and Prado, C., Physica A **342** 171 (2004).

[Pep94] Pepke, S. and Carlson, J., Phys. Rev. E **50** 236 (1994).

[Pes75] Peskin, C.S., *Mathematical Aspects of Heart Physiology* (Courant Institute of Mathematical Sciences, New York University, New York, USA, 1975).

[Pin98] Pinho, S., Prado, C., and Kinouchi, O., Physica A **257** 488 (1998).

[Plo93] Plourde, B., Nori, F., and Bretz, M., Phys. Rev. Lett. **71** 2749 (1993).

[Ram06] Ramos, O., Altshuler, E., and Måløy, K., Phys. Rev. Lett. **96** 098501 (2006).

[Ric35] Richter, C., Bull. Seism. Soc. Am. **25** 1 (1935).

[Sne93] Sneppen, K. and Bak, P., Phys. Rev. Lett. **71** 4083 (1993).

[Soc93] Socolar, J., Grinstein, G., and Jayaprakash, C., Phys. Rev. E **47** 2366 (1993).

[Sor92] Sornette, D., J. Phys. I **2** 2065 (1992).

[Sor95] Sornette, D., Johansen, A., and Dornic, I., J. Phys. I France **5** 325 (1995).

[Sor00] Sornette, D., *Critical Phenomena in Natural Sciences* (Springer, Berlin, Heidelberg, 2000).

[SR00] Sinha-Ray, P. and Jensen, H.J., Phys. Rev. E **62** 3215 (2000).

[Tan88] Tang, C. and Bak, P., Phys. Rev. Lett. **60** 2347 (1988).

[Tuk88] Tukwell, H.C., *Introduction to Theoretical Neurobiology* (Cambridge University Press, Cambridge, Great Britain, 1988).

[Tur92] Turcotte, D.L., *Fractals and chaos in geology and geophysics* (Cambridge University Press, Cambridge, Great Britain, 1992).

[Ves98] Vespignani, A. and Zapperi, S., Phys. Rev. E **57** 6345 (1998).

[Wil83] Wilkinson, D. and Willemsen, J.F., J. Phys. A **16** 3365 (1983).

[Wis05] Wissel, F. and Drossel, B., New Journal of Physics **7** 5 (2005).

[Wis06] Wissel, F. and Drossel, B., Phys. Rev. E **74** 066109 (2006).

[Zap95] Zapperi, S., Lauritsen, K., and Stanley, H., Phys. Rev. Lett. **22** 4071 (1995).

[Zha89] Zhang, Y., Phys. Rev. Lett. **63** 470 (1989).

Acknowledgement

I don't know the secret to success, but the secret to failure is trying to please everybody.
Bill Cosby

First, this thesis would not have been written without the money from the Deutsche Forschungsgesellschaft (DFG), which supported the work under Contract No Dr300/3-1 and Dr300/3-2.

Well, besides that, some real people have been involved as well. The first to be mentioned is Barbara "Scheffin" Drossel, who not only convinced the DFG to spend some money on this project. She also spent numerous hours with me, always willing to help and providing hints. Her doors were always open, and not because I had a copy key to her office. I am very thankful for her incredible intuition and guiding, since she often had to apply the brakes and kept me in the right direction. I also appreciate all the support and the occasions to improve, the visit to Imperial College and the preparation for the Spring conferences, just to name a few. Not to forget the wagonload lot of gummi bears. And she *really* takes care for her sheaps, I did not even have to ask.

And here's a list of people who gave a helping hand, plates of cookies, and did the whole lot of administration, besides keeping the moods up: special thanks to Hella "Hello" Breitfeld, Heike Hardt, and Barbara Knell.

The best brains are lost in the wilderness of literature. Not that I would claim to belong to that group, but I am lost, anyway. Ruth Laeri, Magda Rudolph, and Melanie Schenkel spent a lot of time to procure those ancient papers. Without the professional help of the library, I would not even have started writing yet.

Probably I would still try to fix the programs, but Torben "Zuschauerbett" Jabben provided an excellent guidance to avoid the pitfalls of coding. His insight into the nerd stuff still amazes me. Of course, he could rely on the basics, which I was taught by Frithjof Anders, another grandmaster of coding.

Several people had a great impact on me during my studies. Ahead of all, Norbert "Scheffe" Grewe, who taught me more than physics, besides being a Godfather of condensed matter theory. He granted me asylum, when I deserted the AG Grewe after my Diploma.

The largest influence, however, had those guys I spent most of my time with (which implies for them having the best opportunities to goof on me, to keep me down, and to spend time on other valuable activities):

Frank "Frollein" Böhm, Torben "Kacknerd" Jabben, Eberhard "my first MiFo Ebbi, Ebbi, Ebbi, Pateng" Jakobi, Peter "Dr." Krafft, Tamara "sag's in deutsch" Mihaljev, Basti "Karlsohn" Schmitt, and this ominous gang of $\dot{\Phi}$, with the additional help of Manuel "Bachelor" Bach, Thomas "mit dem Scheiss bin ich fertig" Stemmler, Falco

"Kraftkugel" Strenzle. Florian "FloTeich" Teichert, Beata "Raman" Walasek, Sebastian "Andrew Lloyd" Weber, and Michael "Mischaal" Wahlig.

In their efforts to trouble me, they could always rely on the members of the Institut für Festkörperphysik. The AG Benner, AG Drossel, AG Grewe, AG Feile, and AG Porto are responsible for the friendly atmosphere and that going to the office did not mean going to work.

A special mentioning of Frithjof Anders (again), Timm Plefka, and Horst Turschner is appropriate. They introduced me into the art of teaching.

Mariana Kirchbach gave me new enthusiasm after the Vordiplom. And she also gave me a new point of view.

During my visit at Imperial, I felt so welcome, and this trip really gave me a new upswing, both undoubtedly was due to Kim Christensen, and Henrik Jensen, and their family of students, especially Vera Pancaldi.

I also want to express my gratitude to Jürgen Berges, Gerhard Birkl, Joachim Enders, Rudolf Feile, Robert Roth, and Markus Porto. They all agreed very, very short-termed to take part in my final examination. And special thanks for special hints to Jürgen Berges.

I am also really grateful for a particular group of people. They deserve their own paragraph: many thanks to all the assistants, who took care for the proof reading. Becky Stuffins-Bauer gave a first look on the first drafts, Khamsay and Friday Savathphoune offered their help without really knowing me, and a great deal of corrections was done by Jody Bartholomew. She did not only help me with the grammar, but spent much time on getting me further assistants. Especially, I want to thank Heike Schwehn for the epilogue, and Jana Kaiser for precious advice and a very helpful book on the craft of writing. All of a sudden, in times of great despair, I got the unexpected help of Ian Menz-McNicol. He turned out to be the best proof reader I could have gotten.

So I have come a long way. I don't think I could have gone that road without the help of many. Thanks to the Hollandts (and the Hollandt home group), especially to Jörg for listening to the talk and for lending his bike. Just as well I want to thank my regular home group, Meister Haase, Knut Pippin, Rüdiger, Christian, Netti und A-lena for support and friendship.

This is the adequate position to mention Basti "Schmittlack" Schmitt once more, probably the best Muffgenosse in the whole Muff. He is a constant companion, but also the source of a constant sorrow for all his impertinence.

There is no doubt about this: the thesis would never be finished without my Mum and Mama Bahlke, who attended the little ones, provided additional help in word and deed whenever needed, and took care of the fridge. Dad and Papa Bahlke also deserve to be mentioned, not at last, because they had to cope with the lack of the first two. I can't express my thanks to my family appropriately.

Most of all, I need Kathrin. I am forever thankful for her aid and patience, and I am still deeply impressed by her caring and how she manages being sanftig. Without her, nothing would make sense at all.

There is one more for whom I am thankful, Jesus Christ, who carried me through the last 33 years.

Finally, a happy message to Mäuse, Räuber, and Stift: It's over.

Lebenslauf

Felix Michael Wissel,
geboren am 31.07.1974 in Alzenau i. Ufr.
verheiratet mit Kathrin Bahlke seit 3.3.1999
Kinder:
Mia, 27. April 2000
Finn, 17. August 2002
Matilda, 2. Oktober 2005

1981-1985	Besuch der Brentano Grundschule in Kleinostheim
1985-1987	Besuch des Kronberggymnasiums in Aschaffenburg
1987-1988	Besuch des Riemenschneidergymnasiums in Würzburg
1988-1990	Besuch des Johannes-Butzbach-Gymnasiums in Miltenberg
1990-1992	Besuch des Kronberggymnasiums in Aschaffenburg
1992-1994	Besuch des Karl-Theodor-v.-Dalberg-Gymnasium in Aschaffenburg
1994	Abitur am Karl-Theodor-v.-Dalberg-Gymnasium in Aschaffenburg
1994-1995	Zivildienst beim Bayerischen Roten Kreuz in Aschaffenburg
1995-2002	Physikstudium an der TU Darmstadt
1998-1999	Physikstudium am Trinity College Dublin
2001-2002	Diplomarbeit in der AG Grewe am Institut f. Festkörperphysik, TU Darmstadt
2002	Abschluss des Studiums mit Diplom an der TU Darmstadt
2002-2007	Wissenschaftlicher Mitarbeiter und Beginn der Dissertation in der AG Drossel am Institut f. Festkörperphysik,TU Darmstadt

Erklärung an Eides statt

Hiermit erkäre ich, dass ich die vorliegende Dissertation selbständig verfasst, keine anderen als die angegebenen Hilfsmittel verwendet und bisher noch keinen Promotionsversuch unternommen habe.

Darmstadt, im Mai 2007